CHOLESTEROL ACCESSIBILITY IN PLASMA MEMBRANES

APPROVED BY SUPERVISORY COMMITTEE

_____
Arun Radhakrishnan, Ph. D.

_____
Neal Alto, Ph. D.

_____
Jose Rizo-Rey, Ph. D.

_____
Paul Blount, Ph. D.

DEDICATION

To my late grandfather, Dr. Venkat Reddy who instilled in me the importance of determination, hard work and honesty

CHOLESTEROL ACCESSIBILITY IN PLASMA MEMBRANES

by

SHREYA ENDAPALLY

DISSERTATION

Presented to the Faculty of the Graduate School of Biomedical Sciences

The University of Texas Southwestern Medical Center at Dallas

In Partial Fulfillment of the Requirements

For the Degree of

DOCTOR OF PHILOSOPHY

The University of Texas Southwestern Medical Center at Dallas

Dallas, Texas

May, 2019

CHOLESTEROL ACCESSIBILTY IN PLASMA MEMBRANES

SHREYA ENDAPALLY, Ph.D.

The University of Texas Southwestern Medical Center at Dallas, 2019

ARUN RADHAKRISHNAN, Ph.D.

Cholesterol levels in mammalian cells are tightly regulated to lie within narrow limits. This regulation is achieved by employing multiple feedback mechanisms to regulate both synthesis and uptake of cholesterol. Most of a cell's cholesterol (~80 % of total) is in the plasma membrane (PM), but the protein machinery that senses and regulates cellular cholesterol resides in the endoplasmic reticulum (ER) membrane, which contains a very small fraction (~1% of total) of a cell's cholesterol. A carefully regulated lipid transport pathway between PM and ER allows cholesterol sensors in ER to monitor the cholesterol content of cholesterol-rich PM. This transport depends on the interactions of cholesterol with various phospholipids that control its accessibility for transport to the ER. Cholesterol in PM is organized into three different pools. One pool is accessible for transport to the ER, a second pool is sequestered by sphingomyelin (SM) and can be released by treatment with sphingomyelinase, and a third pool remains sequestered even after sphingomyelinase treatment. Here, I describe our work in developing and characterizing tools to study these different pools.

The three pools were identified using bacterial toxins called cholesterol dependent cytolysins (CDCs) which selectively bind to the accessible pool of cholesterol. One example of these toxins is Anthrolysin O (ALO). To better understand the dynamics of accessible cholesterol sensing at a molecular level, we developed a stable construct of the cholesterol sensing domain of ALO (ALOD4) and performed NMR and other biophysical studies using cholesterol containing model membranes. We were able to identify residues that are significantly affected by the interaction of ALOD4 to membranes.

We also developed a highly specific sensor for the SM-sequestered pool of cholesterol. This sensor is derived from a fungal toxin, Ostreolysin A (OlyA). Using X-ray crystallography, we studied the interaction of OlyA with SM and cholesterol at the atomic level. This structural analysis combined with detailed mutagenesis led us to a single point mutation in OlyA that abolishes its cholesterol specificity while retaining SM specificity. Comparing the X-ray structures of these two versions of lipid-bound OlyA combined with ligand docking simulations revealed two distinct conformations of SM: one in complex with cholesterol and one free from cholesterol. Studies in live cells using OlyA and ALOD4 show that the pool of SM/cholesterol complexes in plasma membrane is maintained at a constant level across a large range of cholesterol concentrations.

The development of new tools for specific forms of cholesterol (ALOD4 and OlyA) has allowed us to evaluate long-standing hypotheses regarding lipid organization in PMs and has also shed new light on lipid dynamics in the context of cellular signaling.

ACKNOWLEDGEMENTS

I take this opportunity to thank all the people who helped me in the course of this work. First and foremost, I would like to thank my mentor, Arun Radhakrishnan for the training, guidance and encouragement throughout all these years. I learnt to think, write and speak like a scientist from observing and working with you. Your passion and curiosity for science is infectious and makes work much more fun.

I would also like to thank all the members of the Radhakrishnan lab for making it a collaborative environment that made coming to work every day enjoyable. Technical assistance by Donna Frias was absolutely critical for this work. Donna, your patience and diligence always amazed me. Daphne Rye, not only did you help so much in the course of this work, your presence always brightens my day. Austin Gay, thank you for showing me the ropes when I first joined the lab and for all the support later on. Kristen Johnson, thank you for all the helpful discussions about science, career and life and for all the exciting ongoing work on OlyA. Daniel Kober, thank you for being a helpful resource of structural biology knowledge and for all the scientific discussions. Bilkish Bajaj and Danya Vasquez, thank you for all the technical help, for listening to my rants and for providing some comic relief in the lab.

My thesis committee members: Neal Alto, Jose Rizo-Rey and Paul Blount, have always been helpful with suggestions and guidance throughout this work. A lot of this work could not have been possible without the help from our collaborators. I would like to thank the Rizo-Rey lab, especially Eric Prinslow, for welcoming me into their lab for performing the NMR experiments. Jose and Eric, thank you so much for your time and patience in teaching me NMR. I would like to thank Diana Tomchick and Helen Aronovich for all the help in the crystallography core. Diana, you have been so generous with your time, thank you for your suggestions and for

teaching me X-ray crystallography. Magdalena Grzemska, thank you for your help with the docking experiments. I thank the Alto lab, especially Michael Abrams, for work on the ongoing Listeria project. I would also like to thank all the members of the department of Molecular Genetics who were always ready to provide help, advice or reagents.

Friends and family who have supported me throughout my life, I thank you. To my parents, who sacrificed so much to get me to where I am. To my sister Pooja, who stubbornly believes I can do anything! To my friend, Madhu, who has patiently been on the receiving end of my rants for 10 years now and continues to support me. Lastly and most importantly, I would like to thank my husband, Souparno, for patiently being my rock these past few years. Thank you for being my late night lab company, for listening to my practice talks, for the comfort food and drinks on bad days, and for celebrating even the smallest of victories with me.

TABLE OF CONTENTS

Abstract..... v

Acknowledgements.....vii

Table of Contents..... ix

Prior Publications..... x

List of Figures and Tables..... xi

List of Abbreviations..... xiv

Introduction..... 1

Chapter 1 – Structural Basis to Accessible Cholesterol Sensing by ALOD4

Introduction..... 10

Materials and Methods..... 12

Results..... 21

Figures..... 28

Discussion..... 44

Chapter 2 – Molecular Discrimination between Two Conformations of Sphingomyelin in Membranes

Introduction..... 45

Materials and Methods..... 46

Results..... 58

Figures..... 74

Discussion..... 99

Chapter 3 – Monitoring Different Pools of Cholesterol in Plasma Membranes

Introduction..... 101

Materials and Methods..... 102

Results..... 105

Figures..... 109

Discussion..... 115

Conclusion and Perspective..... 116

Bibiliography..... 124

PRIOR PUBLICATIONS

Endapally, S. Frias, D. Grzemska, M. Gay, A. Tomchick, D. Radhakrishnan, A. (2019) Molecular discrimination between two conformations of sphingomyelin in plasma membranes. Cell 176(5):1040-1053.e17

Endapally, S. Infante, R. Radhakrishnan, A. (2019) Monitoring and modulating intracellular cholesterol trafficking using ALOD4, a cholesterol binding protein. Methods Mol. Biol. 1949:153-163

LIST OF FIGURES AND TABLES

INTRODUCTION

FIGURE 1: Cholesterol biosynthesis..... 9

CHAPTER 1

FIGURE 1-1: Measuring insertion depth of ALO in cholesterol-containing membranes..... 28

FIGURE 1-2: Chemical modification of ALOD4..... 30

FIGURE 1-3: ^{1}H-^{15}N HSQC spectra of ALOD4..... 32

FIGURE 1-4: ALOD4 binding to cholesterol dissolved in ethanol..... 33

FIGURE 1-5: Effect of detergents on stability of ALOD4..... 34

FIGURE 1-6: Binding of ALOD4 to C12E8 bicelles..... 35

FIGURE 1-7: HSQC of ALOD4 binding to C12E8 bicelles..... 36

FIGURE 1-8: ALOD4 construct with increased stability..... 37

FIGURE 1-9: ^{1}H-^{15}N HSQC spectra of cALOD4..... 38

FIGURE 1-10: cALOD4 binding to cholesterol containing nanodiscs..... 39

FIGURE 1-11: 2D-HSQC of cALOD4 binding to nanodiscs..... 40

FIGURE 1-12: Backbone assignment of cALOD4..... 41

FIGURE 1-13: Structural analysis of ALOD4 binding to nanodiscs..... 42

CHAPTER 2

TABLE 1: Data collection and refinement statistics for OlyA..... 72

FIGURE 2-1: Identification of a sensor for sphingomyelin-cholesterol complexes.....74

FIGURE 2-2: OlyA senses sphingomyelin-cholesterol complexes in membranes..... 76

FIGURE 2-3: Purification of OlyA(WT) for crystallography, structure of OlyA(WT) and dot blot assay with OlyA(WT) 79

FIGURE 2-4: Structural analysis of SM binding by wild-type OlyA..... 81

FIGURE 2-5: Effect of mutations on OlyA's PlyB-mediated hemolytic activity..... 83

FIGURE 2-6: Effect of mutation of E69 on OlyA's lipid specificity and purification of OlyA(E69A) for crystallization..... 84

FIGURE 2-7. Structural analysis of SM binding by OlyA(E69A) 86

FIGURE 2-8: Comparison of affinities and phospholipid specificities of OlyA(WT) and OlyA(E69A) 87

FIGURE 2-9: Phospholipid and sterol specificity, and temperature dependence of OlyA..... 89

FIGURE 2-10: Docking simulations for binding of SM to OlyA(WT) and OlyA(E69A) and chemical modification assays..... 92

FIGURE 2-11: Top 10 scoring poses for binding of SM to OlyA(WT) and OlyA(E69A) 94

FIGURE 2-12: Sphingomyelin binding pockets occur in structurally similar locations in OlyA(WT), OlyA(E69A), and Stn..... 95

FIGURE 2-13: Recovery of cholesterol specificity on OlyA(E69A) 97

CHAPTER 3

FIGURE 3-1: Fluorescent labeling of OlyA proteins..... 109

FIGURE 3-2: Time course, dose and lipid mobility dependence of binding of fluorescently-labeled OlyA to CHO-K1 cells..... 110

FIGURE 3-3: Organization of SM and cholesterol in PMs of CHO-K1 cells..... 112

FIGURE 3-4: SM-cholesterol complexes in PMs of different cell lines..... 114

CONCLUSION AND PERSPECTIVE

FIGURE C-1: SCAP and ALOFL share identical sterol structural specificity..... 120

FIGURE C-2: Sensors for different pools of PM cholesterol..... 121

FIGURE C-3: OlyA can be used to switch cholesterol between accessible and inaccessible states..... 122

LIST OF ABBREVIATIONS

ALO, Anthrolysin O

bHLH-Zip, basic helix-loop-helix-leucine zipper

C12E8, Octaethylene Glycol Monododecyl Ether

CDC, Cholesterol Dependent Cytolysin

CHAPS, 3-((3-cholamidopropyl) dimethylammonio)-1-propanesulfonate

CHO, Chinese Hamster Ovary

D4, Domain 4

D7PC, 1,2-diheptanoyl-d26-sn-glycero-3-phosphocholine

DMSO, dimethyl sulfoxide

DOPC, 1,2-dioleoyl-sn-glycero-3-phosphocholine

DTT, dithiothreitol

Eqt, Equinatoxin II

ER, endoplasmic reticulum

FCS, fetal calf serum

FH, familial hypercholesterolemia

FL, full length

FRAP, fluorescence recovery after photobleaching

HDL, high density lipoprotein

HMG-CoA, 3-hydroxy-3-methylglutaryl CoA

HSQC, heteronuclear single quantum coherence

IDL, intermediate density lipoproteins

IPTG, isopropyl-1-thio-β-d-galactopyranoside

LAL, lysosomal acid lipase

LDL, low density lipoproteins

LDLR, LDL-receptor

LLO, Listeriolysin O

Lys, Lysenin

MDCK, Madin-Darby Canine Kidney cells

NP-40, Nonidet P-40 (nonyl phenoxypolyethoxylethanol)

NPC, Niemann-Pick disease type C

OG, n-Octyl-β-D-Glucopyranoside

OlyA, Osterolysin A

PFO, Perfringolysin O

PlyB, Pleurotolysin B

PM, plasma membrane

POC, phosphocholine

S1P, site-1 protease

S2P, site-2 protease

SCAP, SREBP cleavage activating protein

SDS-PAGE - sodium dodecyl sulfate polyacrylamide gel electrophoresis

SM, Sphingomyelin

SMase, Sphingomyelinase

SRE, sterol regulatory element

SREBP, sterol regulatory element binding protein

TCEP, tris (2-carboxyethyl) phosphine (TCEP)

TEV, Tobacco etch virus

TR-DHPE, Texas Red 1,2-dihexadecanoyl-sn-glycero-3-phosphoethanolamine

TROSY, transverse relaxation-optimized spectroscopy

VLDL, very low density lipoproteins

WT, wild type

INTRODUCTION

Cholesterol was first isolated in 1790 as a waxy, crystalline substance present in human gallstones and has been extensively studied for the last two centuries. Brown and Goldstein described cholesterol as 'the most highly decorated small molecule in biology' in their 1985 Nobel Prize Lecture. Cholesterol is essential for mammalian cell survival and has many physiological roles to play in a cell. It is a critical structural component of cell membranes and helps regulate membrane fluidity, stability and passive permeability [29, 104]. Cholesterol is also a precursor to a number of steroid hormones and bile acids [93, 110]. Levels of cholesterol in membrane affect transmembrane protein folding, stability and function [26, 131]. Lipidation with cholesterol is necessary for membrane anchoring and function of hedgehog proteins, a family of proteins that are essential for development [95, 107]. All of these and many more reasons are why cholesterol is an essential lipid in mammalian cells and it is one of the most intensely regulated molecules in biology [22].

Misregulation of cholesterol can lead to many disease states, the most prominent of which is atherosclerosis [53]. It is characterized by formation of plaques because of improper removal of cholesterol from cells and can most certainly lead to cardiovascular disease, the primary cause of death worldwide. While not as prevalent as atherosclerosis, there are a large number of diseases caused by genetic defects in intracellular cholesterol transport [63]. In fact, much of our knowledge about intracellular cholesterol trafficking comes from studying key proteins that have been discovered by identifying gene defects that underlie human disorders of cholesterol transport.

More than 80 years ago, Rudolf Schoenheimer first showed evidence of cholesterol balance in mice. He found that mice that were fed a diet low in cholesterol synthesized their own cholesterol, while those fed a diet high in cholesterol did not [115] . Along with the demonstration

that mammals can synthesize their own cholesterol, this was the first example of a biosynthetic pathway that undergoes end-product feedback inhibition. Following this, the research in the next two decades delineated the complicated 30-step biosynthetic pathway that converts 2-carbon acetate to a 27-carbon cholesterol (Fig 1) [11]. 3-hydroxy-3-methylglutaryl CoA (HMG-CoA) reductase was identified as the rate-limiting enzyme of this biosynthetic pathway [23]. The question then was: how does dietary cholesterol from the mouse intestine enter the bloodstream and reach other cells to inhibit HMG-CoA reductase?

As a hydrophobic molecule, the hydroxyl group of dietary cholesterol is esterified with long chain fatty acids and transported across the blood stream packaged into lipoproteins. The core of lipoprotein particles is composed of triglycerides and cholesterol esters while the surface is a monolayer of phospholipids and free cholesterol and the whole particle is stabilized by a protein [30]. There are five different kinds of lipoproteins: chylomicrons, very low density lipoproteins (VLDL), low density lipoproteins (LDL), intermediate density lipoproteins (IDL), and high density lipoproteins (HDL). Of these, the LDL particles are the most abundant in the blood stream and are the major means of delivering cholesterol to peripheral cells [50]. Also, accumulation of LDL particles is the major cause for atherosclerosis [53]. While packaging of cholesterol into lipoproteins like LDL solves the problem of its insolubility, the question still remained: how do the cholesteryl esters enter the cell and ultimately inhibit cholesterol synthesis?

An answer to this question came from efforts by the Brown and Goldstein lab to understand familial hypercholesterolemia (FH), a genetic disease characterized by elevated levels of cholesterol-rich LDL in plasma and premature myocardial infarctions [52]. Their studies not only led to the discovery of LDL-receptor (LDLR) but this was also the first experimental evidence for receptor mediated endocytic pathway in mammalian cells [20]. While cells in normal patients can take up LDL via the LDLR, FH homozygotes lack a functional LDLR and cannot take up LDL,

which explains the presence of high levels of LDL in the plasma of FH patients. Steps following endocytosis were revealed using studies with mutant fibroblasts derived from a patient with an autosomal recessive cholesteryl ester storage disorder [6, 24]. After LDL is internalized into the lysosomes, cholesteryl esters are hydrolyzed by lysosomal acid lipase (LAL) into free cholesterol [55]. The question of how this highly hydrophobic free cholesterol is transported from inside of the aqueous lysosome, through the lysosomal membrane to the cytoplasm and other membranes was answered using studies of Niemann-Pick disease type C (NPC), which is a rare autosomal-recessive disorder resulting from mutations in genes encoding two proteins, NPC1 or NPC2 [40, 129]. NPC1 is a polytopic membrane protein that spans the lysosomal membrane and NPC2 is a soluble protein enriched in lysosomes [33, 89]. NPC2 binds to free cholesterol hydrolyzed from LDL and engages in a "hydrophobic handoff" to the membrane bound NPC1 to transfer cholesterol to the cytoplasm while preventing crystallization of insoluble free cholesterol inside of the aqueous lysosomal lumen [69, 139]. This cholesterol can now go on to inhibit cholesterol biosynthesis and lower the number of surface LDLRs in normal cells [19]. On the other hand, NPC patient derived cells can hydrolyze cholesteryl esters, but the free cholesterol remains trapped in lysosomes [129]. How does free cholesterol released from endocytosed LDL in normal cells go on to shut down endogenous cholesterol synthesis and also cutoff the uptake of external cholesterol?

Studies demonstrated a sterol-dependent reduction in rates of transcription of LDLR and HMG-CoA reductase leading to the isolation of a hypothesized group of sterol-regulated transcription factors, sterol regulatory element binding proteins (SREBPs) [76, 140, 147]. SREBPs are endoplasmic reticulum (ER) membrane proteins that contain a basic helix-loop-helix-leucine zipper (bHLH-Zip) domain in the N-terminus that can bind to DNA and activate transcription [141]. Activation of SREBPs in the absence of sterols requires for the ER-bound full length SREBP to be transported to the Golgi where it is proteolytically cleaved by two proteases S1P and

S2P [111]. The resulting soluble and active SREBP with the bHLH-Zip domain can then be transported to the nucleus to activate genes encoding all the proteins for cholesterol biosynthesis and the LDLR gene. How is SREBP transported to the Golgi for activation in a sterol-regulated manner?

Isolation of SREBP cleavage activating protein (SCAP), another ER membrane protein, using a sterol-resistant mutant cell line answered this question [61]. SCAP is a polytypic membrane protein with eight transmembrane helices on the N-terminus and a cytosolic C-terminal domain that contains repeats of a sequence termed WD40 that is known to mediate protein-protein interactions [91]. The WD40 domain binds to the C-terminus of SREBP and this interaction is required for SREBP translocation and activation [112]. When cholesterol levels are low, a six amino acid sequence (MELADL) on the loop 6 region of SCAP binds to Sec23/24 and the SCAP/SREBP complex is incorporated into CopII vesicles for transport to the Golgi [39, 132]. When cholesterol levels are high, SCAP binds to cholesterol and undergoes a conformational change which induces its binding to another ER membrane protein, INSIG. This conformational change renders the MELADL sequence inaccessible to Sec23/24 and the transport of SCAP/SREBP complex to Golgi is blocked [133]. SREBP no longer gets cleaved for activation and the transcription of cholesterol synthesis and uptake genes are blocked until cholesterol homeostasis is achieved. Hence, SCAP is a key protein in the cholesterol regulatory machinery and acts as a cholesterol sensor. How sensitive is SCAP to levels of cholesterol in the ER? To answer this question, SREBP activation was monitored in cells treated with various cholesterol depleting and enriching agents. At the same time, ER membranes were purified, and their cholesterol content was measured. Surprisingly, the response to cholesterol was distinctly non-linear and switch-like [100]. When ER cholesterol was just above 5 mole %, SREBP-2 was completely inactivated, while it was activated at just below 5 mole %.

While elucidation of SCAP/SREBP pathway provided a molecular explanation for the cholesterol feedback mechanism first observed by Schoenheimer in 1933, many open questions remained. When cellular cholesterol is low, the number of LDLRs on the cell surface increase and more LDL is endocytosed. The free cholesterol released from lysosomes needs to be transported to the rest of the cell including the plasma membrane (PM) and ER. How is cholesterol transported to the PM and ER? Does the cholesterol go to the PM first and then to the ER or vice-versa? Both routes of transport have been proposed over the years [74, 90, 144]. Also, while PMs contain 80% of cell's total cholesterol [71, 73], the cholesterol regulating SCAP/SREBP system resides in the ER which contains only 1% of cell's total cholesterol [72]. How does the ER communicate with the PM to regulate cholesterol levels in that membrane? Also, how does SCAP sense such small changes in ER cholesterol in an almost all-or-none fashion? While an exact answer to these questions is not yet clear, use of cholesterol-dependent cytolysins (CDCs) as tools to study organization of cholesterol in plasma membranes has given an insight.

CDCs are a family of soluble pore-forming toxins secreted by gram-positive bacteria [137]. There are 28 members in this family of proteins and are secreted by bacteria belonging to the genera of *Bacillus, Listeria*, *Lysinibacillus*, *Paenibacillus*, *Brevibacillus*, *Streptococcus*, *Clostridium*, *Gardnerella*, *Arcanobacterium*, and *Lactobacillus* [58]. As the name suggests, CDCs specifically bind to cholesterol containing membranes and form large oligomeric pores [137]. Most CDCs have a cleavable signal sequence which aids in their secretion by the bacteria into the extracellular space. Since bacterial membranes do not contain cholesterol, CDCs may have evolved as a defense mechanism to target cholesterol-containing mammalian cell membranes without targeting themselves.

Perfringolysin O (PFO) is secreted by *Bacillus perfringens* and is one of the most well studied members of the CDC family [136]. The crystal structure of the water-soluble monomeric

form of PFO reveals four distinct domains [108]. The C-terminal Domain 4 (D4) is responsible for targeting and specific binding to cholesterol-containing membranes [105]. Extensive structural analysis has been used to study the conformational changes in the domains 1-3 that follow PFOD4 binding to cholesterol containing membranes and end in formation of a large oligomeric pore comprising of 40-60 PFO monomers [59, 66, 106, 119, 120]. However, less is known about the initial interaction between PFOD4 and cholesterol. This is mainly due to the lack of a structure of PFO bound to cholesterol. Nevertheless, biochemical studies do provide some information about the nature of this interaction.

While membrane cholesterol is required for the function of CDCs, this cholesterol dependence is not linear. In model liposomes made of cholesterol and phospholipids, PFO binding is observed only after cholesterol levels are above a certain threshold [32, 45, 130]. There is little or no binding to membranes containing cholesterol below the threshold. This kind of sigmoidal response could be attributed to cooperativity induced by PFO oligomer formation. While that is partly the case, binding studies with purified PFOD4, which can bind to cholesterol containing membranes but cannot form oligomers, also showed similar threshold dependence to cholesterol concentration in the model liposomes [48]. The cholesterol threshold for PFOD4 binding ranged from 20 mole% to 50 mole% depending on the phospholipid present. This suggests that the sigmoidal response of PFO is also dependent on interactions of cholesterol with its phospholipid neighbors [48]. In other words, it is dependent on the "accessibility" of membrane cholesterol to PFO.

The sigmoidal response observed above in model liposomes also holds true in more complex membranes derived from mammalian cells but with different thresholds for cholesterol. Binding of PFO to purified PMs has a threshold of 35 mole% cholesterol [32]. On the other hand, PFO binds to purified ER membranes after concentration of cholesterol exceeds only 5 mole%

[130]. Interestingly, 5 mole% is also the concentration of ER cholesterol at which SCAP is retained in the ER and SREBP activation is inhibited [100], suggesting a similar binding mechanism between these two very different proteins that depends on cholesterol accessibility.

As mentioned above, PM cholesterol is accessible to PFO only after its concentration exceeds 35 mole%. Also, SREBP is active only when the concentration of cholesterol in PMs is below 35 mole% [31]. Cholesterol above 35 mole% is not only accessible to PFO but also for potential transport to ER for binding to SCAP and inhibiting SREBP activation. One in three lipids in the PM membrane is still cholesterol when the cholesterol concentration is just below 35 mole%. How is this cholesterol rendered inaccessible?

Studies in live cells using a ^{125}I-labeled mutant form of PFO, hereafter referred to as ^{125}I-PFO*, that still binds accessible cholesterol on PM but does not form pores at 4°C, shed some light on this question [32]. ^{125}I-PFO* binding was used to define three different pools of cholesterol on PMs of fibroblasts [31]. The first pool of cholesterol is the "accessible pool" of cholesterol described above, that is available for binding to PFO as well as for transport to the ER to shutdown SREBP. The second pool of cholesterol is a "sphingomyelin-sequestered pool" of cholesterol that is inaccessible to PFO or for transport to ER until it is released by treatment of cells with sphingomyelinase (SMase) which cleaves sphingomyelin (SM) to ceramide. The third and last pool of cholesterol is inaccessible even after SMase treatment and is labeled as "essential pool" of cholesterol because this is the minimum amount of cholesterol required for cellular survival. Cells carefully control the accessibility of PM cholesterol to allow for regulated communication between PM and ER [31, 64]. This ensures that cholesterol uptake and synthesis is not prematurely shut down before the cell's cholesterol needs are met.

This poses more questions. How do cells maintain these three pools of cholesterol in plasma membranes? How do cells sense the accessible cholesterol in PM and regulate its movement between PM and ER? Monitoring and modulating these different pools of cholesterol in live cells could provide answers to these questions. Here, I present my work in developing and characterizing tools to monitor different pools of cholesterol on PMs.

FIGURE 1

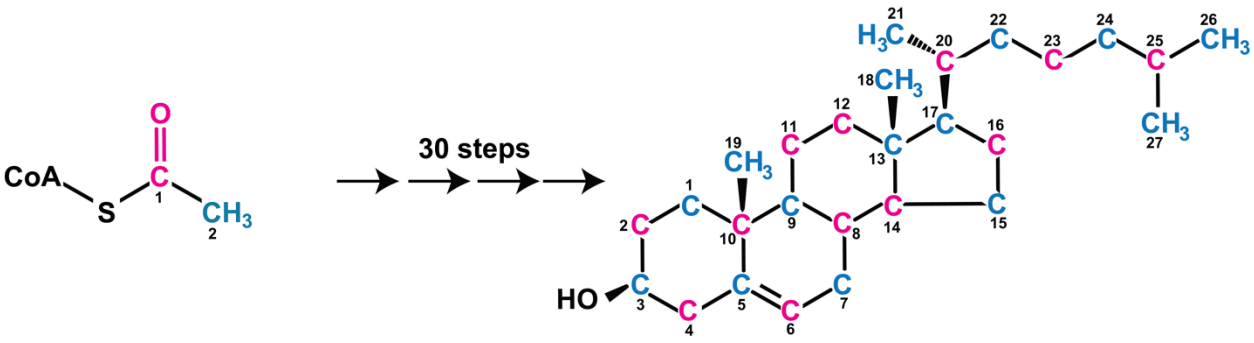

FIGURE 1: Cholesterol biosynthesis. All 27 carbon atoms in cholesterol are derived from the 2-carbon acetate in a 30-step biosynthetic pathway. Carbon atoms derived from the methyl group are labeled in blue and the carbon atoms derived from carboxyl group are labeled in pink. Figure adapted from [7].

CHAPTER 1

STRUCTURAL BASIS TO ACCESSIBLE CHOLESTEROL SENSING BY ALOD4

INTRODUCTION

Cholesterol levels in mammalian cells are tightly regulated by a network of proteins in ER membrane [22] This regulation is achieved by a feedback mechanism involving sensing of cellular membrane cholesterol and transcriptionally regulating genes for both cholesterol synthesis and the LDL receptor gene for cholesterol uptake [20, 54]. When cholesterol levels are low, ER-bound transcription factors called SREBPs are activated. This activation requires translocation of SREBPs from ER to Golgi, where SREBP undergoes proteolytic cleavage and the active transcription factor domain is released to the nucleus to turn on the target genes and increase cholesterol levels [21]. SCAP, another ER membrane protein binds to SREBPs and is essential for ER to Golgi transport of SREBP and for feedback regulation of cholesterol levels [61]. When cholesterol levels rise above optimal levels, SCAP directly binds to cholesterol and is retained in the ER by forming complexes with Insigs [103, 146]. This prevents the ER to Golgi translocation and subsequent activation of SREBPs. As a result, transcription of cholesterol biosynthetic and uptake genes declines, and cholesterol levels return to resting value.

This feedback response by SCAP is switch-like and is sensitive to very small changes in ER membrane cholesterol. Small increases in ER cholesterol above a threshold of 5 mole% of ER lipids are sensed by SCAP and result in complete inactivation of SREBP [100]. The molecular mechanism of how SCAP senses such small changes in ER cholesterol is not understood. It can be attributed to both the cooperativity mediated by interactions of SCAP with other proteins in this

system and the interaction of cholesterol with phospholipids in the membrane that contributes to its accessibility to SCAP [130]. Differentiating between these two mechanisms of SCAP and studying the interaction of SCAP with membrane cholesterol is challenging, partly due to difficulties in purification and reconstitution of this large, polytopic, oligomeric membrane protein.

Fortunately, a more convenient model has been recently described. A large family of bacterial toxins, called CDCs, bind to membranes containing cholesterol and forms large oligomeric pores [137]. PFO, one of the most well studied members of this family, has been shown to bind to cholesterol containing membranes only after cholesterol concentrations reach a certain threshold that depends on the other phospholipids in the membrane [32, 45, 48, 57, 130]. In other words, PFO binding depends on the accessibility of cholesterol in the membrane. PFO and SCAP share two remarkable similarities. PFO binds to ER membranes only when cholesterol concentration increases above a threshold of 5 mole%, the same threshold that retains SCAP in the ER and inactivates SREBP [130]. Also, PFO shares identical sterol structural specificity as SCAP. Both Scap and PFO bind to cholesterol, dihydrocholesterol, desmosterol, and β-sitosterol, but not to epicholesterol, lanosterol, 19-hydroxy-cholesterol, or 25-hydroxy-cholesterol [101, 130]. This suggests that PFO, a soluble bacterial protein, and SCAP, a mammalian membrane protein, may sense accessible cholesterol through a similar mechanism. Being soluble proteins that can be easily purified in large quantities, PFO and other CDCs are a convenient model system to study accessible cholesterol sensing [48].

Of the 28 CDCs discovered thus far, there are high-resolution crystal structures of six members of this family [16, 43, 68, 97, 108, 143]. There are no structures of the cholesterol-bound form of any of the members of the CDC family. Extensive biophysical studies using PFO have revealed many details of the CDC oligomer and pore formation following recognition of

cholesterol in membranes [59, 66, 106, 119, 120]. Unfortunately, none of these elegant studies explain PFO's threshold sensitivity or structural specificity for cholesterol. The C-terminal domain 4 of PFO (PFOD4) is necessary and sufficient for binding to membrane cholesterol but cannot form oligomers or a pore [41, 105]. By decoupling oligomerization from membrane binding using PFOD4, it was shown that the switch-like response to cholesterol is defined by accessibility of membrane cholesterol which is dependent on the lipid composition of the membrane [48].

The goal of this study is to understand the molecular mechanism of cholesterol sensing by CDCs. Here, we use another member of the CDC family, Anthrolysin O (ALO), that is secreted by *Bacillus anthracis* [118]. It has similar domain architecture and cholesterol threshold dependence as PFO [16, 108]. Crystal structure of the soluble form of ALOFL has been solved and is shown in Figure 1-1a [16]. The C-terminal D4 of ALO (ALOD4) is shaded yellow. Similar to PFOD4, purified ALOD4 is necessary and sufficient for binding to membrane cholesterol without oligomerization after the cholesterol concentration exceeds a threshold [28, 48]. Here, we investigated the molecular details of ALOD4-cholesterol interactions using various biophysical and biochemical techniques.

MATERIALS AND METHODS

Materials: We obtained all phospholipids from Avanti Polar Lipids; Texas Red 1,2-dihexadecanoyl-sn-glycero-3-phosphoethanolamine (TR-DHPE), and isopropyl-1-thio-β-d-galactopyranoside (IPTG) from Invitrogen; deuterated dimethyl sulfoxide (DMSO), deuterated ethanol, cholesterol, $^{2}H,^{12}C$-labeled glucose and tris (2-carboxyethyl) phosphine (TCEP) from Sigma-Aldrich; epicholesterol from Steraloids; Octaethylene Glycol Monododecyl Ether (C12E8) from Anatrace; mPEG maleimide 5kDa (mPEG-MAL-5000) from Nanocs Inc; ^{15}N-labeled ammonium chloride and ^{13}C-labeled glucose from Cambridge Isotope Laboratories.

Buffers and media: Buffer A contains 50 mM Tris-HCl (pH 7.5), 150 mM NaCl and 1 mM TCEP. Buffer B contains 40 mM Tris-HCl (pH-8) and 300 mM NaCl. Buffer C is buffer B with 1% (w/v) Triton-X 100. Buffer D contains 20 mM Tris-HCl (pH 7.4), 100 mM NaCL and 0.5 mM EDTA. Buffer E contains 25 mM HEPES-KOH (pH 7.5), 125 mM KCl and 1% sodium cholate. Buffer F contains 25 mM Tris-HCl (pH 7.5) and 1 M NaCl. Buffer F contains 50 mM Tris-HCl (pH 7.5), 150 mM NaCl and 1 mM DTT. Buffer G contains 50 mM Tris-HCl (pH 7.5), 150 mM NaCl, 4mM TCEP and 2 mM DTT. 1 L of M9 minimal media contains 6.8 g of Na_2HPO_4, 3 g of KH_2PO_4, 500 mg of NaCl, 1 g of NH_4Cl, 3g of glucose, 11 mg of $CaCl_2$, 246 mg $MgSO_4$, 10 mg biotin and 10 mg thiamine.

Expression Plasmids: The gene encoding signal-peptide deficient ALO from *Bacillus Anthracis* (amino acids 35-512) was synthesized by Genscript, Inc. and cloned into the pRSET B expression vector along with an NH_2-terminal hexahistidine tag followed by an enterokinase cleavage site. Using this plasmid as a template, we generated a derivative where the sole cysteine of ALOD4 (C472) was mutated to alanine and a new cysteine was introduced at the NH_2 terminus (K46C) using site-directed mutagenesis (QuikChange II XL Site Directed Mutagenesis Kit, Agilent). This plasmid is hereafter referred to as pALOFL. Using ALOFL as a template, a plasmid encoding domain 4 of ALO (amino acids 404-512) was generated and the serine at amino acid 404 was mutated to cysteine (S404C). This plasmid is hereafter referred to as pALOD4. pALOFL and pALOD4 were described previously [48]. For some studies, we used a version of ALOD4 where the S404 and C472 were intact and there were no other mutations. This plasmid is hereafter referred to as pALOD4WT. For some NMR studies, we generated a derivative of pALOD4WT with a Tobacco etch virus (TEV) protease cleavage site (ENLYFQG) following the NH_2-terminal hexahistidine tags. This plasmid is hereafter referred to as pTEVALOD4. pGEX-4T1 expression plasmid encoding TEV protease with a NH_2-terminal hexahistidine tag (pTEV) was kindly

provided to us by Jing Yang (University of Texas Southwestern Medical Center). pET28a expression vector encoding ApoA1 with a NH_2-terminal hexahistidine tag (pApoA1) was kindly provided to us by Dr. Jose Rizo-Rey (University of Texas Southwestern Medical Center). This construct was described previously [17]. Mutations in all constructs were generated by site-directed mutagenesis using a QuickChange II XL Site-Directed Mutagenesis Kit (Agilent). The integrity of each plasmid was verified by DNA sequencing of its entire open reading frame.

Overexpression of Recombinant Proteins: All the above described plasmids with the exception of pApoA1 were transformed into *Escherichia coli* BL21 (DE3) pLysS competent cells (Invitrogen). pApoA1 was transformed into *Escherichia coli* BL21 (DE3) competent cells (Invitrogen). For recombinant protein production, a single colony from a freshly transformed plate was grown in Luria Broth media (Research Products International) containing 100 μg/ml ampicillin (50 μg/ml kanamycin for pApoA1). ALOFL overexpression was induced at OD_{600} = 0.8 with 0.5 mM IPTG at 30°C for 16 hours. TEV overexpression was induced at OD_{600} = 0.8 with 1 mM IPTG at 37°C for 3 hours. ApoA1 overexpression was induced at OD_{600} = 1.5 with 1 mM IPTG at 37°C for 4 hours. Overexpression of ALOD4, ALOD4WT and TEVALOD4 was induced at OD_{600} = 0.8 with 1 mM IPTG at 18°C for 16 hours. In all the above cases, following overexpression, cells were harvested by centrifugation at 3220xg for 10 min at 4°C. Cell pellets were stored at -80°C after flash freezing in liquid nitrogen.

For generating isotope-labeled versions of ALOD4 proteins for use in NMR spectroscopy, M9 minimal media was used in place of Luria Broth and the same protocol as above was followed for overexpression. For generating ^{15}N-labeled proteins, M9 media with $^{15}NH_4Cl$ as the sole nitrogen source was used. For generating ^{13}C, ^{15}N labeled proteins, M9 minimal medium was used with $^{15}NH_4Cl$ and $^{13}C_6$-glucose as the sole nitrogen and carbon sources. For generating ^{2}H, ^{15}N,

ILV-$^{13}CH_3$ labeled proteins, M9 media was prepared using 99.9% D_2O with $^{15}NH_4Cl$ and $^{2}H,^{12}C$-glucose as the sole nitrogen and carbon sources. ^{13}C methyl-labeling was achieved by adding [3,3-$^{2}H_2$] ^{13}C-methyl alpha-ketobutyric acid (80 mg/L) and [3-^{2}H] ^{13}C- dimethyl alpha-ketoisovaleric acid (80 mg/L) (Cambridge Isotope Laboratories) to the deuterated protein cultures 30 minutes prior to IPTG induction.

Purification of Recombinant Proteins: For ALOFL, ALOD4, ALOD4WT, TEVALOD4, and TEV purification, we followed protocols previously described with a few modifications [48]. A cell pellet from a 1L bacterial culture was resuspended in 20 ml of buffer A containing 1 mg/ml lysozyme, 0.4 mg/ml PMSF, and 1 protease inhibitor cocktail tablet (Complete Mini, EDTA-free, Roche). The cell suspension was homogenized using a Dounce homogenizer and incubated at 4°C for 3 hours for lysozyme disruption. Lysozyme disrupted cells were subjected to lysis by a tip sonicator (Branson, Inc) and then subjected to centrifugation at 220,000 x g for 1h. The resulting supernatant was loaded on to a prepacked 1-ml HisTrap-HP Ni column (ALOFL and TEV) or 5-ml HisTrap-HP Ni column (ALOD4, ALOD4WT and TEVALOD4). Columns were washed with 10 column volumes of buffer A containing 50 mM imidazole, and bound proteins were eluted with either buffer A containing 300 mM imidazole (ALOFL and TEV) or with buffer A containing a linear gradient of 50-300 mM imidazole (ALOD4, ALOD4WT and TEVALOD4). For TEV, the eluted fractions with the protein were pooled, concentrated, and then diluted with buffer A to lower the imidazole concentration to 35-55 mM. After addition of glycerol (20% v/v final concentration), aliquots of His_6-TEV were flash frozen in liquid nitrogen and stored at -80°C. For ALOFL, ALOD4WT and TEVALOD4, the eluted fractions with the proteins were pooled and concentrated using an Amicon Ultra centrifugal filter (Millipore; 30,000 MWCO for ALOFL, and 10,000 MWCO for TEVALOD4). For ALOD4, the eluted fractions with the protein were pooled and concentrated using ion-exchange chromatography (1-ml HiTrap Q HP anion exchange

column, GE healthcare). All concentrated proteins were further purified by gel filtration chromatography on a Tricon 10/300 Superdex 200 column equilibrated with buffer A. Protein-rich fractions were pooled, concentrated to 1-10 mg/ml, and stored at 4°C until use. Protein concentrations were measured using a Nanodrop instrument (Thermo Fisher Scientific).

After purification, TEVALOD4 was subjected to cleavage by TEV protease. In each cleavage reaction, 500 µg of ALOD4 proteins were incubated with 50 µg of TEV at 4°C. After 16 h, the cleavage reaction was loaded onto a prepacked 5-ml HisTrap-HP Ni column, and cleaved ALOD4 was collected in the flow through. Cleaved ALOD4 was concentrated in a 3,000 MWCO concentrator and subjected to gel filtration chromatography using a Superdex 200 column pre-equilibrated with Buffer A. Protein-rich fractions were pooled, concentrated to 1-10 mg/ml (3,000 MWCO concentrator) and stored at 4°C until use. The cleaved form of ALOD4 is hereafter referred to as cALOD4.

ApoA1 was purified as described previously with a few modifications [17]. A cell pellet from a 1 L bacterial culture was resuspended in 25 ml of buffer C containing 0.4 mg/ml PMSF and 1 protease inhibitor cocktail tablet. The cell suspension was homogenized using a Dounce homogenizer and then subjected to lysis by a tip sonicator. Lysed cells were subjected to centrifugation at 50,000xg for 1 hour. The resulting supernatant was incubated with nickel-nitrilotriacetic acid (Ni-NTA) agarose beads (Qiagen) for 1.5 hours following which unbound proteins were separated from beads using a gravity column. The beads were washed with 20 column volumes each of buffer C, buffer B containing 50mM sodium cholate and 20mM imidazole, and buffer B containing 50 mM imidazole. Bound ApoA1 was eluted with buffer B containing 500 mM imidazole. Eluted fractions with protein were pooled and dialyzed (10,000 MWCO Slide-A-Lyser, Thermo Scientific) against Buffer D. Dialyzed protein was then

concentrated using an Amicon Ultra centrifugal filter (10,000 MWCO) to 3.5-5mg/ml. Aliquots of concentrated protein were flash frozen in liquid nitrogen and stored at -80°C.

Detergent stability assay: Reaction mixtures (50 µl of Buffer F) containing 100 µM ALOD4 and indicated amounts (units of critical micellar concentration) of detergents were setup in 1.7 ml microcentrifuge tubes. After incubation at room temperature for 1 hour, the reactions were subjected to centrifugation at 100,000xg for 30 min. The resulting supernatants were collected and protein concentrations were quantified using BCA protein assay (Pierce). The critical micellar concentrations (cmc) of the detergents used here are as follows: 1,2-diheptanoyl-d26-sn-glycero-3-phosphocholine (D7PC) – 1.4 mM; 3-((3-cholamidopropyl) dimethylammonio)-1-propanesulfonate (CHAPS) – 8 mM; n-Octyl-β-D-Glucopyranoside (OG) – 20 mM; nonyl phenoxypolyethoxylethanol (NP-40) – 150 µM; Octaethylene Glycol Monododecyl Ether (C12E8) – 90 µM.

Preparation of Liposomes: Liposomes were prepared as described previously [48]. Mixtures containing the indicated proportions of phospholipids and sterols in chloroform along with a trace amount (< 0.2 mole%) of a fluorescently labeled phospholipid (TR-DHPE) were evaporated to dryness under a steady stream of nitrogen gas and stored under vacuum for at least 16 hours. The dried lipid mixtures were hydrated by adding buffer A to the desired final lipid concentration, agitated on a vortexer for 1 hour, and subjected to 3 freeze-thaw cycles (1 cycle = 60 seconds in a liquid nitrogen bath, 3 minutes in a room temperature water bath). The resulting lipid dispersions were placed in a water bath at 37°C and subjected to sonication for 15 min followed by a 15 min pause for cooling (2 cycles). Finally, the lipid mixtures were extruded through a polycarbonate filter (100 nm pore size) 11 times to yield homogeneous unilamellar liposomes. Liposomes were stored at 4°C and used within a week.

Preparation of Bicelles: Bicelles were prepared based on a protocol described previously with a few modifications [5]. Octaethylene Glycol Monododecyl Ether (C12E8) was used for stabilization of bicelles. Bicelles were prepared on a 20 mg/ml basis with detergent:total lipid ratio of 7. Mixtures of indicated phospholipids and sterols in chloroform along with a trace amount (< 0.2 mole%) of a fluorescently labeled phospholipid (TR-DHPE) were evaporated to dryness under a steady stream of nitrogen gas and stored under vacuum for at least 16 hours. Appropriate amounts of detergent in buffer A were added to the dried lipid mixtures and the tubes were rotated for 16 hours at 37°C. The detergent lipid mixtures were then subjected to 15 freeze-thaw-vortex cycles (1 cycle = 60 seconds in a liquid nitrogen bath, 10 minutes in a 37°C water bath, 6 min on a vortexer). Bicelles were stored at 4°C and used within a week. Approximate molecular weight of the above bicelles is 550kDa and the final concentration of bicelles is 36 mM.

Preparation of Nanodiscs: Nanodiscs were prepared by adapting protocols as described previously [37]. 3250 nanomole lipid mixtures containing the indicated proportions of phospholipids and sterols in chloroform were evaporated to dryness under a steady stream of nitrogen gas and stored under vacuum for at least 16 hours. Dried lipid mixtures were reconstituted in 250 µl of Buffer E, agitated on a vortexer for 30 min, and subjected to 10 freeze-thaw cycles as described above. Purified recombinant ApoA1 was added to the reconstituted lipids to yield a lipid to ApoA1 ratio of 55:1. The mixture was supplemented with additional sodium cholate to a final detergent concentration of 1% and incubated at room temperature for 30 min. Nanodisc self-assembly was initiated by removing the detergent from the mixture. For this, the mixture was loaded onto 1ml of packed resin equilibrated with Buffer F. Detergent free nanodiscs were collected and loaded on a Tricon 10/300 Superdex 200 gel filtration chromatography column equilibrated with buffer A. Protein-rich fractions were pooled and concentrated using an Amicon

Ultra centrifugal filter (30,000 MWCO). Nanodisc concentrations were measured using a Nanodrop instrument (Each nanodisc is stabilized by 2 ApoA1 proteins).

Tryptophan Fluorescence assay: Reaction mixtures (200 µL of Buffer F) containing 600 µM liposomes and 4.4 µM of ALOFL or ALOD4 were set up in 1.5 mL Eppendorf tubes. After incubation for 1 h at room temperature, a portion of each reaction mixture (100 µl) was transferred to a 96-well plate (black, flat-bottom, non-binding; Greiner Bio-One), and intrinsic tryptophan fluorescence was measured using a micro-plate reader (Tecan) (excitation wavelength, 290 nm; emission wavelength, 340 nm; band pass, 5 nm for each).

Gel-shift assay: In some tryptophan fluorescence assay experiments with ALOFL, a portion of each reaction mixture (20 µL) was mixed with SDS loading buffer, heated for 10 min at 37°C, and subjected to 10% SDS-PAGE. Proteins were visualized with Coomassie Brilliant Blue R-250 stain (Bio-Rad).

mPEG-maleimide modification of ALOD4: For isolation of liposome-bound ALOD4, we used liposomes containing 1 mole% 18:1 Biotinyl CAP PE for quick separation of bound and unbound ALOD4 using magnetic streptavidin beads (NanoLink™ Streptavidin Magnetic Beads 1.0 µm). Reaction mixtures (100 µL of buffer A) containing 600 µM liposomes (50 mole % cholesterol, 49 mole % DOPC and 1mole % Biotinyl CAP PE) and 5 µg of ALOD4 or ALOD4WT were set up in 1.7 mL low-retention microcentrifuge tubes. After incubation for 1 h at room temperature, a portion of each reaction mixture (80 µl) was first used to confirm ALOD4 binding using change in Tryptophan fluorescence as described above. After this, the 80 µl reaction mixture was added to 200 µg washed magnetic streptavidin beads. Preliminary experiments indicated that this amount of streptavidin beads was sufficient to capture all the added liposomes. After incubation for 30 min at room temperature, the reaction mixtures were subjected to magnetic pull-

down (DynaMag™-2 magnet). The beads, containing bound liposomes and proteins were washed once with 200 µL buffer A and resuspended in 120 µL buffer A. mPEG modification reaction mixtures, in a final volume of 100 µL of buffer A, containing either resuspended pellets from the above step (40 µL) or 1 µg of soluble ALOD4, and the indicated amounts of mPEG-MAL-5000 were incubated in 1.7 ml low-retention microcentrifuge tubes at room temperature. After 30 min, reactions were quenched by addition of 10mM DTT (1 M stock). Aliquots of the reaction mixtures (10 µL) were mixed with 5x loading buffer, heated at 95°C for 10 min, and subjected to 15% SDS-PAGE. The electrophoresed proteins were transferred to nitrocellulose membranes using the Bio-Rad Trans Blot Turbo system. These membranes were subjected to immunoblot staining with anti-His antibody (1:1000 dilution). Bound antibodies were visualized by chemiluminescence (Super Signal Substrate; Thermo Fisher) by using a 1:5000 dilution of donkey anti-mouse IgG conjugated to horseradish peroxidase (Jackson ImmunoResearch, West Grove, PA). Filters were exposed to Phoenix Blue X-Ray Film (F-BX810; Phoenix Research Products, Pleasanton, CA) at room temperature for 1-30 s.

Assay for interaction of ALOD4 with bicelles: Reaction mixtures (300 µL of Buffer F) containing 24 mM of indicated bicelles and 133 µM ALOD4 were setup in 1.5 ml Eppendorf tubes. After incubation for 3 hours at room temperature, the reactions were loaded on to a Tricon 10/300 Superdex 200 gel filtration chromatography column equilibrated with buffer F and 500 µL fractions were collected. 100 µl of each fraction was transferred to a 96-well plate (black, flat-bottom, non-binding; Greiner Bio-One), and fluorescence from bicelles (Texas Red) was measured using a micro-plate reader (Tecan) (excitation wavelength, 595 nm; emission wavelength, 617 nm; band pass, 5 nm for each). 40 µl of each fraction was used to measure protein concentration using BCA protein assay.

NMR spectroscopy: Varian INOVA spectrometers equipped with cold probes were used to perform all NMR experiments at room temperature. ^{1}H-^{15}N HSQC spectra were obtained on a Varian INOVA spectrometer operating at 600 MHz. ^{1}H-^{15}N TROSY-HSQC spectra were obtained on a Varian INOVA spectrometer operating at 800 MHz. 400 μM ^{15}N, ^{13}C cALOD4 was used for backbone assignments, obtained with gradient-enhanced 3D CBCA(CO)NH, HNCACB and HNCO experiments on Varian INOVA spectrometer equipped operating at 600 MHz [88]. The protein conditions for all spectra are indicated in the figure legends. NMRpipe [36] was used to process data, and NMRView [65] was used to analyze data.

Secondary structure prediction of ALOD4: We obtained the average predicted values for random coil backbone chemical shifts for individual amino acids from the Biological Magnetic Resonance Data Bank (BMRB). We used a secondary structure prediction method as described before [142]. Using the Cα and Cβ values of each amino acid on ALOD4 from our triple resonance experiments, we calculated ΔCα ($C\alpha_{ALOD4}$- $C\alpha_{randomcoil}$) and ΔCβ ($C\beta_{ALOD4}$- $C\beta_{randomcoil}$). Four or more continuous residues having $\Delta C\alpha>0$ and $\Delta C\beta<0$ were assigned as a helix and three or more continuous residues having $\Delta C\alpha<0$ and $\Delta C\beta>0$ were assigned as a beta sheet and residues not following a pattern were assigned as random coil.

RESULTS

Measuring insertion depth of ALO in cholesterol-containing membranes: We first sought to understand the depth of insertion of ALOFL in cholesterol-containing membranes. ALOFL contains six tryptophan (Trp) residues, five of which are in D4 (Fig 1-1a, Trp shown as red sticks). It has previously been shown that binding of ALOFL to membranes containing cholesterol results in a 2-3 fold increase in its intrinsic Trp fluorescence [48]. We measured depth-dependent tryptophan fluorescence quenching [70] using phospholipids containing nitroxide spin labels

(doxyl) attached at various positions on the acyl chain (Fig 1-1b, positions shown as green circles). We used model liposomes containing 10 mole % doxyl labeled lipids and increasing mole fraction of cholesterol on a DOPC background and measured the intrinsic Trp fluorescence of ALOFL upon binding. When liposomes contained no doxyl labeled lipids, Trp fluorescence increased by ~2.5 fold in a sigmoidal fashion as has been observed before (Fig 1-1 d). The presence of 5-doxyl PC and 7-doxyl PC led to a complete decrease in Trp fluorescence and the presence 10-doxyl PC led to a partial decrease in Trp fluorescence (Fig 1-1 d). Presence of 12-doxyl PC and 14-doxyl PC did not show a significant change in Trp fluorescence (Fig 1-1 d). This depth dependent decrease in Trp fluorescence is not due to loss of binding of ALOFL to doxyl containing liposomes. ALOFL forms SDS-resistant oligomers upon binding to cholesterol containing membranes and these oligomers migrate with slower electrophoretic mobility during SDS-PAGE [48]. ALOFL forms SDS-resistant oligomers in membranes containing 50 mole % cholesterol and this ability is not affected by the presence of doxyl-labeled lipids (Fig 1-1 e). Purified ALOD4 which is sufficient for membrane cholesterol binding also shows an increase in intrinsic Trp fluorescence upon membrane binding [48]. We measured the depth dependent quenching of Trp fluorescence using ALOD4 and observed a similar trend as seen with ALOFL (Fig 1-1 f). Disappointingly, ALOD4 does not form SDS-resistant oligomers like ALOFL [48] and we could not confirm binding of ALOD4 to doxyl-containing liposomes. A summary of the depth-dependent Trp fluorescence quenching is shown in Fig 1-1 g.

Doxyl-dependent quenching requires contact between the spin label and Trp residue [56]. The model liposomes used above are bilayer membranes. It is not clear from the above experiments if the quenching by doxyl groups at 5, 7 and 10 is from the lipids on the outer leaflet or the inner leaflet. In other words, there can be two possibilities for the binding of ALOD4 to cholesterol-containing membranes (Fig 1-2 a). To differentiate between these two models, we assayed for the

membrane proximity of a sole cysteine residue at two different locations when bound to cholesterol containing membranes. The ALOD4 construct we have been using so far has been modified such that the sole cysteine at position 472 is mutated to alanine and the NH_2 terminal (position 404) serine is mutated to cysteine (Fig 1-2 b). For this experiment, in addition to ALOD4, we also used the ALOD4WT construct that has the C472 and S404 residues intact (Fig 1-2 c). We probed for accessibility of the cysteines in these two versions of ALOD4 using mPEG-MAL-5000, a high molecular weight membrane-impermeable reagent that forms a covalent bond with exposed cysteines and causes proteins to migrate with higher molecular weight on SDS-PAGE [75]. When in solution, we observed mPEG-MAL-5000 modification of both ALOD4 (S404C C472A) and ALOD4WT (S404 C472) (Fig 1-2 d, e top panels). However, when bound to cholesterol containing liposomes, mPEG-MAL-5000 did not react with ALOD4WT (Fig 1-2 d, bottom panel). In contrast, liposome-bound ALOD4 was still modified by mPEG-MAL-5000 (Fig 1-2 e, bottom panel). These results suggest that in a membrane bound form of ALOD4, amino acid at position 472 is inaccessible but the amino acid at position 404 is still accessible. In other words, these results support binding model 1 over binding model 2 (Fig 1-2 a).

Model Membranes for studying ALOD4 binding using NMR spectroscopy: While the above biochemical studies shed some light on the depth of binding of ALOD4 to membranes, the molecular mechanism of threshold dependence and cholesterol binding is still not clear. Although the crystal structure of ALOFL has been solved (Fig 1-1 a), we were unable to get crystals with bound cholesterol, despite many efforts. So, we turned to NMR spectroscopy which can provide details of protein-lipid interactions in solution. For this purpose, we first overexpressed and purified ^{15}N-labeled version of ALOD4 and obtained a 2D ^{1}H-^{15}N heteronuclear single quantum coherence (HSQC) spectrum. As shown in Figure 1-3, ^{15}N-ALOD4 gave a well dispersed HSQC spectrum where each peak refers to a single backbone or side-chain amide group. We next wanted

to see the effect of the presence of cholesterol on the protein. We incubated ^{15}N-ALOD4 with cholesterol dissolved in either DMSO or ethanol and obtained a 2D ^{1}H-^{15}N HSQC spectrum. While we observed cross-peak shifts in the HSQC spectrum in the presence of cholesterol, most of these shifts were a solvent effect from ethanol (Fig 1-4). We were unable to isolate the effect of cholesterol from the solvents. To remove solvent-dependent effects, we decided to use model bilayer membranes containing cholesterol.

We previously used model liposomes containing cholesterol for biochemical characterization of ALOD4 binding. Liposomes are 100 nm in diameter and binding of ALOD4 to liposomes would result in much slower tumbling rates of the complex and broadening of ALOD4 peak signals. To get around this problem, we decided to use bicelles which are small bilayer-like membranes, 5 nm in diameter, that are stabilized with a detergent [113]. The small size of bicelles has made them an attractive tool to use in NMR spectroscopy because of their fast tumbling rates [98].

Bicelles are normally stabilized using lipid-like zwitterionic detergents like D7PC [77]. When we made bicelles using D7PC, we saw a cholesterol-independent precipitation of ALOD4 in the presence of bicelles. We then performed a stability test of ALOD4 in the presence of increasing concentrations of D7PC and observed a detergent dependent decrease in stability (Fig 1-5 a). We then tested a panel of different detergents to find one that did not decrease the stability of ALOD4. We observed a detergent dependent decrease in ALOD4 stability using bile acid salts like CHAPS and sugar-based detergents like OG, but not with polyoxyethylene containing NP40 (Fig 1-5 a). ALOD4 was stable even at higher concentrations of NP40 that are required in bicelles (Fig 1-5 b). Another polyoxyethylene containing detergent, C12E8, also did not precipitate

ALOD4 at high concentrations (Fig 1-5 b). Hereafter, we made bicelles stabilized by C12E8 for use in NMR studies with ALOD4.

Before proceeding to NMR studies using bicelles, we first confirmed binding of ALOD4 to C12E8 bicelles in a cholesterol dependent manner. For this purpose, we made bicelles containing either 100 % DOPC or 60 mole % DOPC and 40 mole % cholesterol using the protocol described in methods. These bicelles also contained a small fraction of a fluorescently-labeled lipid (TR-DHPE) for easy detection. ALOD4 and bicelles elute at different volumes on a size exclusion chromatography column when loaded separately. When pre-incubated with 100% DOPC bicelles, most of ALOD4 still eluted separately from bicelles (Fig 1-6 a). On the other hand, when ALOD4 is incubated with 40% cholesterol bicelles, a fraction of ALOD4 eluted along with bicelles (Fig 1-6 b). This suggests that ALOD4 specifically binds to cholesterol-containing bicelles. We next incubated ^{15}N-ALOD4 with bicelles and observed the effect using NMR spectroscopy. When we acquired ^{1}H-^{15}N HSQC spectra of ^{15}N-ALOD4 with bicelles, we observed a cholesterol-independent broadening of signals in the presence of bicelles and could not proceed into further structural characterization (Fig 1-7).

At this point, we considered the possibility that the ALOD4 construct used in the above studies is not very stable and this could limit our scope in obtaining NMR data with membrane-bound protein. So, we engineered a more stable ALOD4 construct containing WT cysteine at position 472 and inserted a Tobacco-Etch virus (TEV) cleavage site for efficient removal of the NH_2 terminal His_6 tag (Fig 1-8 a). The resulting cleaved ALOD4, hereafter referred to as cALOD4, contained an eight amino acid overhang followed by the ALOD4 sequence. When we tested the binding of cALOD4 to liposomes containing cholesterol by tryptophan fluorescence assay, we observed a sigmoidal response to cholesterol concentration similar to that seen with ALOD4

(Figure 1-8 b). We did not observe any binding to epicholesterol-containing liposomes, as has been observed before with ALOD4 [48]. Similar to ^{15}N-ALOD4, ^{15}N-cALOD4 also resulted in a well dispersed ^{1}H-^{15}N HSQC spectrum and the cross-peaks were more uniform in intensity as compared to cross-peaks from ^{15}N-ALOD4 (Fig 1-9).

Nanodiscs are another form of model membranes widely used in NMR spectroscopy [99]. They are disc-like bilayer membranes about 5-10 nm in diameter and are stabilized by membrane scaffolding proteins like ApoA1. Just like bicelles, they are characterized with a fast tumbling rate due to their small size [99]. By adapting published protocols [37], we were able to make nanodiscs containing up to 42 mole % cholesterol. We next incubated ^{15}N-cALOD4 with cholesterol-containing nanodiscs at different concentrations and acquired 1D ^{1}H-^{15}N HSQC spectra (Fig 1-10). We observed a nanodisc-dependent broadening of cALOD4 signal. We were encouraged to see that this broadening was not complete and hence it might be possible to get some molecular insight into this binding. To improve sensitivity and get higher intensity peaks in our experiments, we used the approach of transverse relaxation-optimized spectroscopy (TROSY) [94]. We produced ^{2}H, ^{15}N, ILV-$^{13}CH_3$ labeled cALOD4 using protocols described in methods and acquired 2D TROSY ^{1}H-^{15}N HSQC spectra of protein bound to cholesterol containing nanodiscs. The signals obtained from cALOD4 bound to nanodiscs were much broader compared to those obtained from cALOD4 in solution. We were encouraged by selective broadening of some peaks more than others suggesting their role in the interaction of ALOD4 to membranes (Fig 1-11, circles). We also observed shifting of some cross-peaks (Fig 1-11, arrows). In total, we observed significant changes in 33 cross-peaks (Fig 1-11) in the presence of nanodiscs.

Backbone Assignment of ALOD4: To get a molecular understanding of this binding, we next worked towards backbone assignment of ALOD4. We overexpressed and purified ^{13}C and

^{15}N labeled cALOD4 using protocols described in methods, concentrated the protein to 400 μM and used it to obtain high-quality triple resonance data (HNCO, CBCA(CO)NH and HNCACB) of sufficient quality to assign the backbone resonances. The resonances for the corresponding cross-peak assignments (Fig 1-12 a) from the ^{1}H-^{15}N HSQC spectrum are observable for all residues of ALOD4 (Fig 1-12 b).

Analysis of ALOD4 binding to cholesterol nanodiscs: The crystal structure of ALOFL has been solved [16] (Fig 1-1 a), but the crystal structure of ALOD4 has not been solved. We used the Cα and Cβ values from our triple resonance experiments, and performed a secondary structure prediction to generate a structural model of ALOD4 [142]. As shown in Fig 1-13 a, ~83% of ALOD4 retains the secondary structure obtained from ALOFL. Hereafter, we used the structure of domain 4 from the crystal structure of ALOFL for our analysis.

We next used our backbone assignments of ALOD4 and the 2D ^{1}H-^{15}N HSQC spectra of ALOD4 bound to nanodiscs to find residues whose peaks shift or broaden in the presence of nanodiscs. We mapped these residues to their positions on domain 4 from the ALOFL crystal structure (Fig 1-13b). A close up of the two loops that have the most significant changes is shown (Fig 1-13c).

FIGURE 1-1

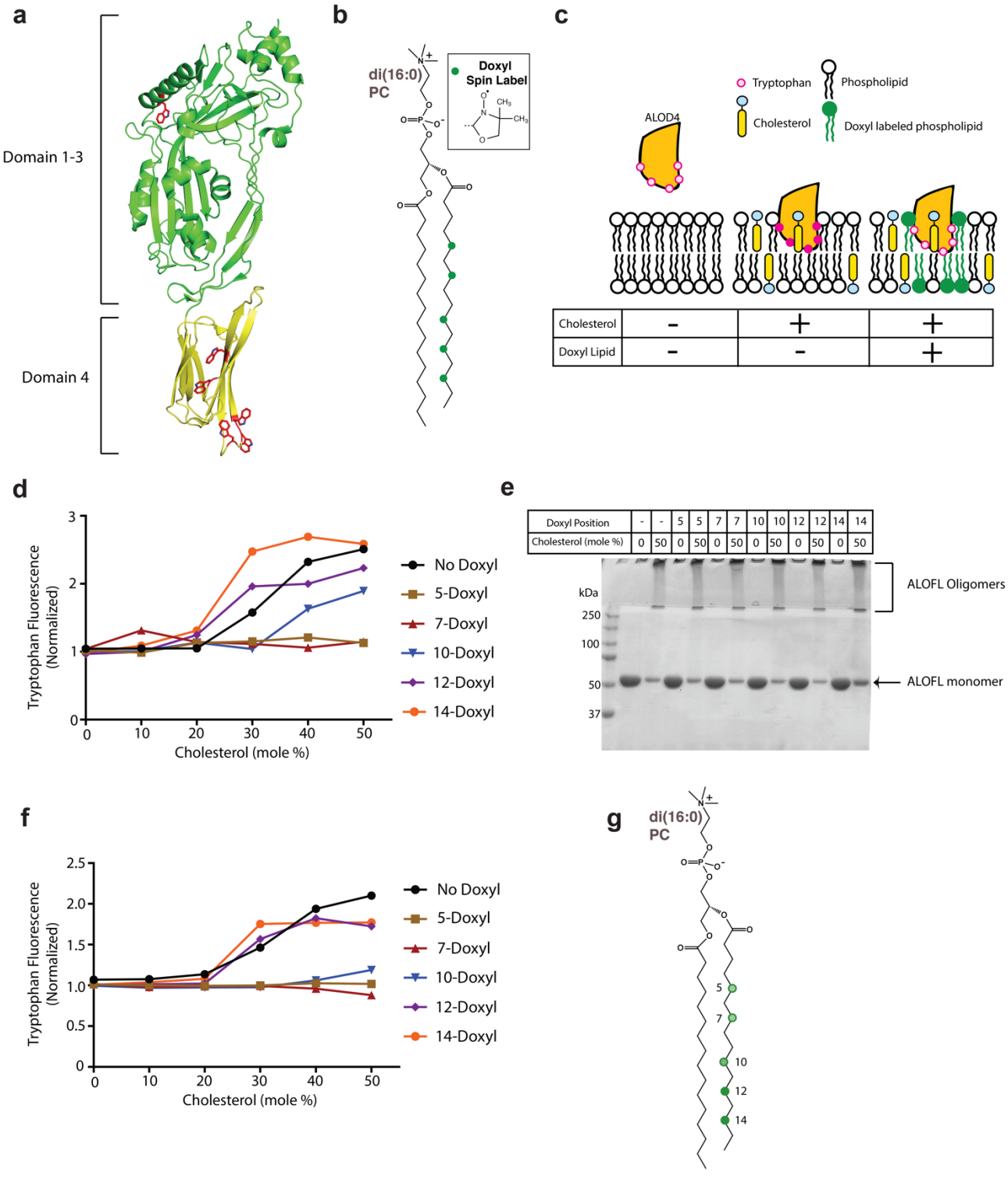
a
Domain 1-3
Domain 4
b
di(16:0)
PC
Doxyl
Spin Label
c
Tryptophan
Phospholipid
Cholesterol
Doxyl labeled phospholipid
ALOD4
Cholesterol - + +
Doxyl Lipid - - +
d
Tryptophan Fluorescence (Normalized)
Cholesterol (mole %)
No Doxyl
5-Doxyl
7-Doxyl
10-Doxyl
12-Doxyl
14-Doxyl
e
Doxyl Position - - 5 5 7 7 10 10 12 12 14 14
Cholesterol (mole %) 0 50 0 50 0 50 0 50 0 50 0 50
kDa
250
100
50
37
ALOFL Oligomers
ALOFL monomer
f
Tryptophan Fluorescence (Normalized)
Cholesterol (mole %)
No Doxyl
5-Doxyl
7-Doxyl
10-Doxyl
12-Doxyl
14-Doxyl
g
di(16:0)
PC
5
7
10
12
14

FIGURE 1-1: Measuring insertion depth of ALO in cholesterol-containing membranes. a, Overall crystal structure of ALOFL (pdb-3cqf) is shown as a cartoon. NH_2-terminal domains 1-3 are shown in green and the COOH-terminal domain 4 is shown in yellow. Tryptophan side-chains are shown as red sticks. **b,** Chemical structure of 16:0 doxyl labeled phospholipids. Structure of doxyl group is shown in the box on the right. Positions of doxyl groups used in this study are indicated as green circles. **c,** Schematic of depth-dependent tryptophan fluorescence quenching of ALO. **d, f,** Doxyl dependent quenching of ALOFL and ALOD4. Liposomes containing 10 mole% of the indicated doxyl lipids were prepared as described in methods. Reaction mixtures (200 µL of Buffer F) containing 600 µM liposomes and 4.4 µM of ALOFL **(d)** or ALOD4 **(f)** were set up in 1.5 mL Eppendorf tubes. After incubation for 1 h at room temperature, tryptophan fluorescence measurements were carried out as described in methods. Values shown are averages of duplicate assays **e,** Oligomerization of ALO after binding to cholesterol-containing membranes. Aliquots (20 µl) of the reaction mixtures from **d** containing ALOFL bound to membranes containing 0 mole% or 50 mole% cholesterol were subjected to SDS-PAGE. Proteins were visualized with Coomassie Brilliant Blue R-250 stain. **g,** Schematic representation of depth dependent quenching results from **d** and **f**. The doxyl positions are indicated as green circles and the degree of quenching by each doxyl groups is depicted by the intensity of green color (high quenching – light green, low quenching – dark green).

FIGURE 1-2

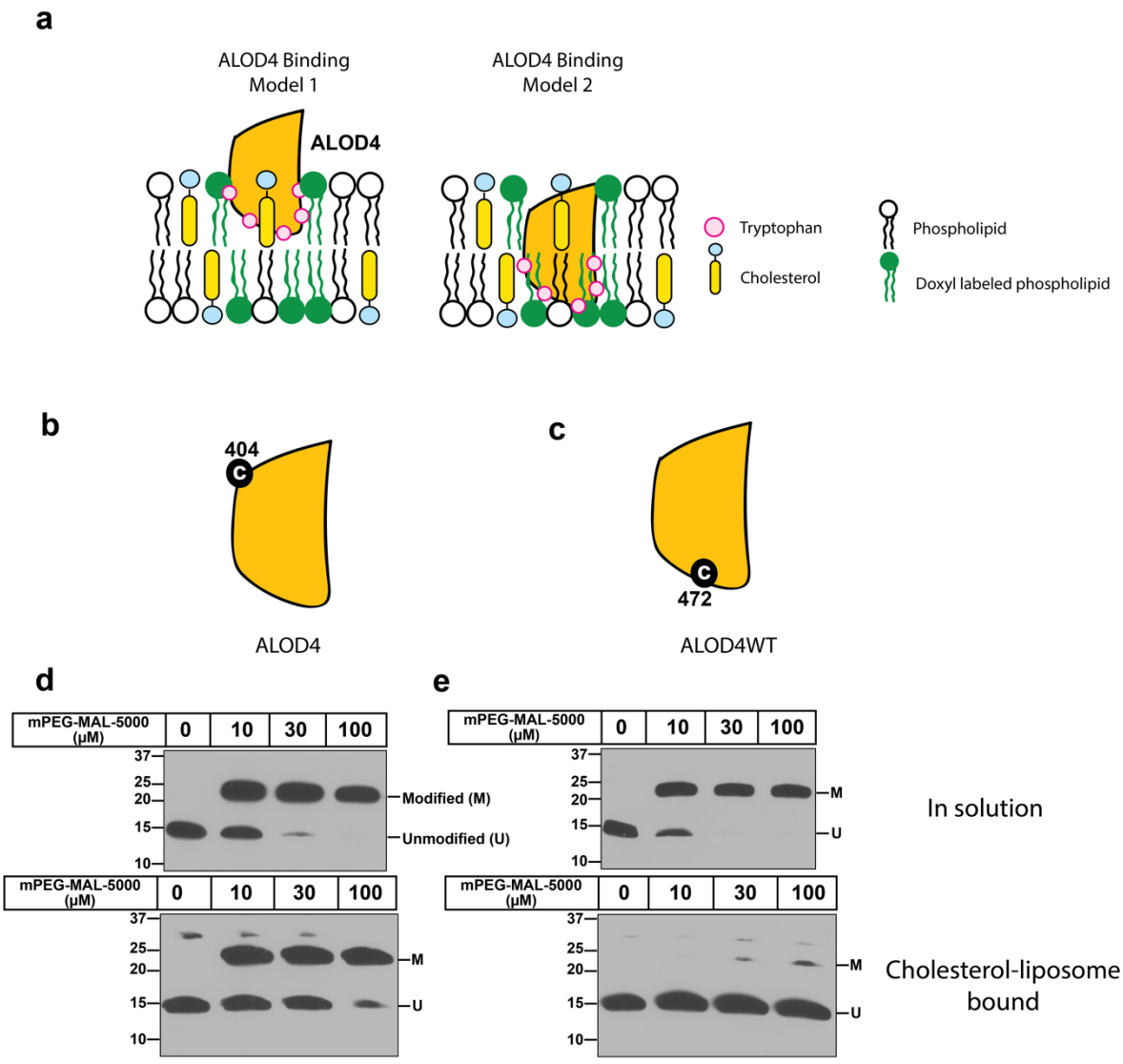

FIGURE 1-2: Chemical modification of ALOD4. a, Schematic representation of two models for binding of ALOD4 to cholesterol containing membranes as concluded from **Figure 1-1**. **b,** mPEG maleimide modification of ALOD4. Reaction mixtures (100 µL of buffer A) containing 600 µM liposomes (50 mole % cholesterol, 49 mole % DOPC and 1mole % Biotinyl CAP PE) and 5 µg of ALOD4 or ALOD4WT were set up in 1.7 mL low-retention microcentrifuge tubes. After incubation for 1 h at room temperature, liposome-bound ALOD4 or ALOD4WT were isolated

using streptavidin beads as described in methods and incubated with indicated amounts of mPEG-MAL-5000. mPEG modification was studied using immunoblot analysis. M – ALOD4 modified by mPEG, U – unmodified ALOD4.

FIGURE 1-3

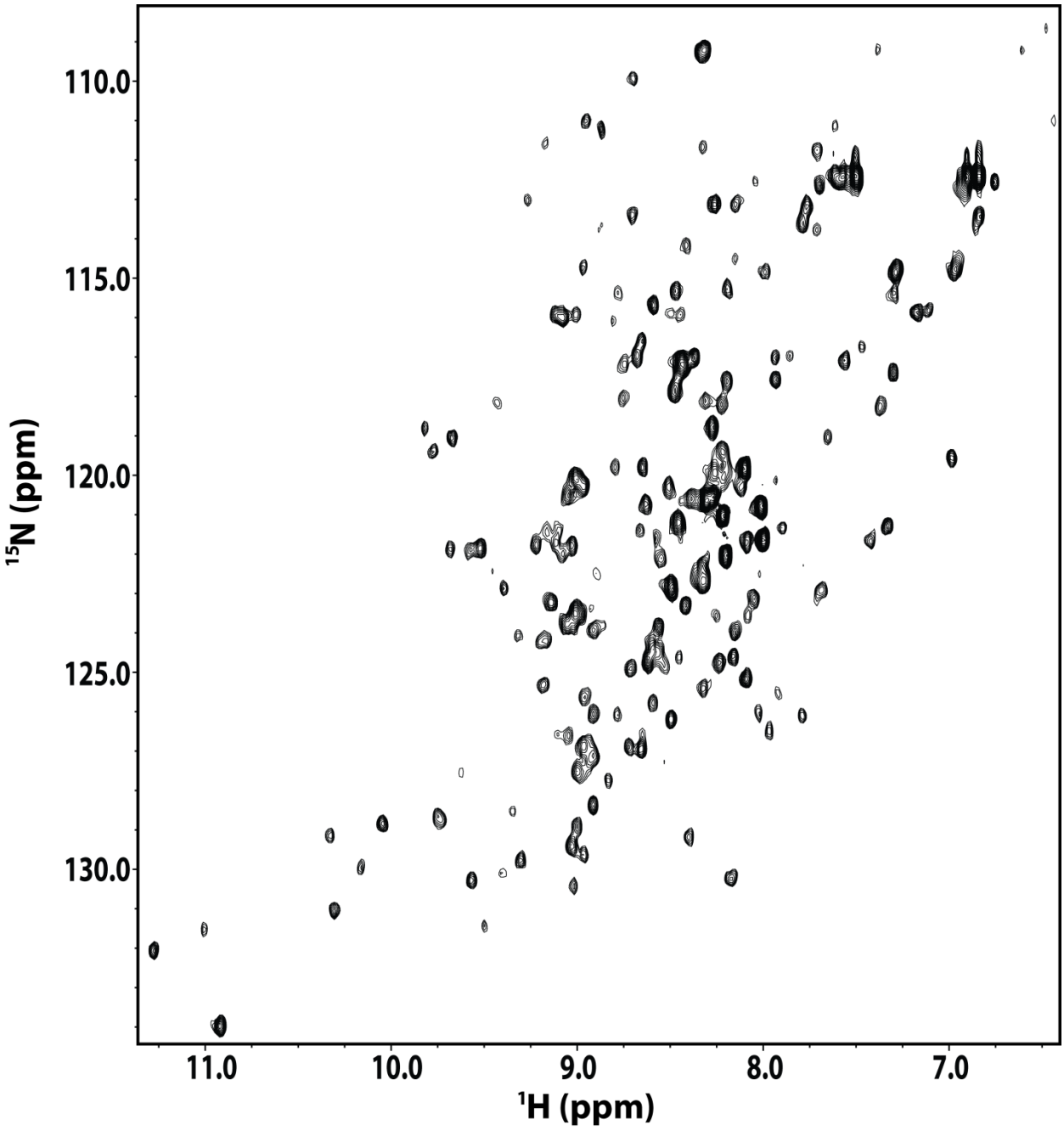

FIGURE 1-3: ^{1}H-^{15}N HSQC spectra of ALOD4. 2D ^{1}H-^{15}N HSQC spectra 50 μM of ^{15}N-ALOD4 in Buffer F containing 7% D_2O.

FIGURE 1-4

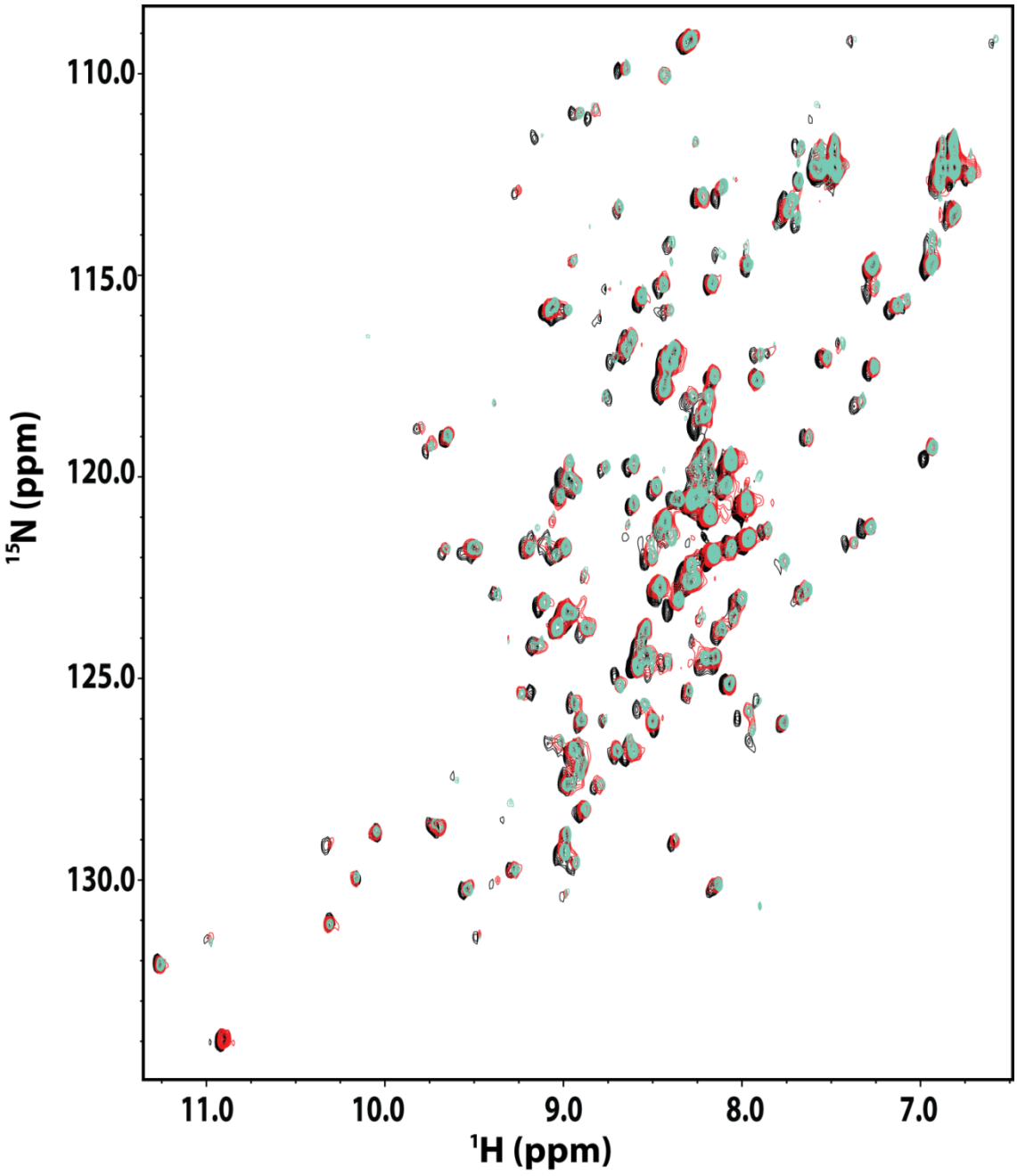

FIGURE 1-4: ALOD4 binding to cholesterol dissolved in ethanol. 2D ^{1}H-^{15}N HSQC spectra of 35 µM ^{15}N-ALOD4 in the absence (black), presence of 1.25 mM cholesterol/deuterated(d6)-ethanol (red) (final d6 ethanol concentration – 5%), or presence of 5% d6-ethanol without sterols (cyan). All spectra were obtained in the presence of 15% D_2O.

FIGURE 1-5

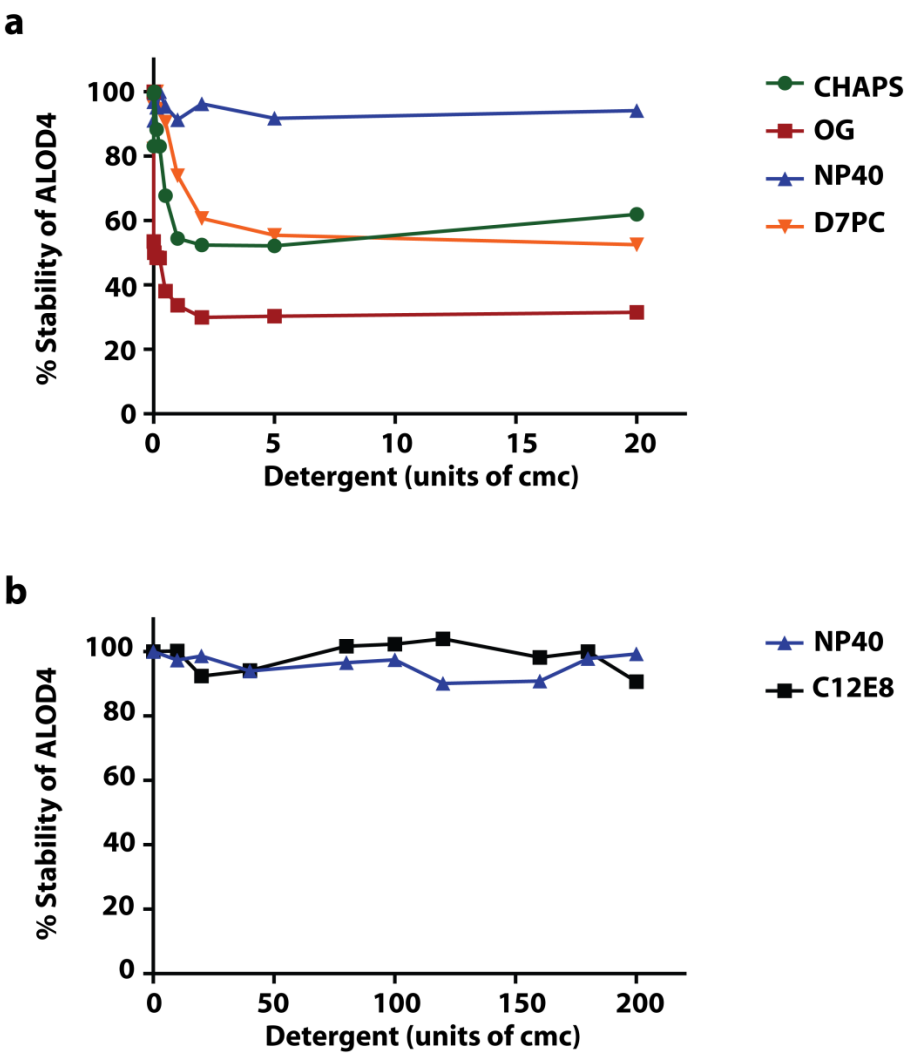

FIGURE 1-5: Effect of detergents on stability of ALOD4. a,b - Reaction mixtures (50 µl of Buffer F) containing 100 µM ALOD4 and indicated amounts of detergents were setup in 1.7 ml microcentrifuge tubes. After incubation at room temperature for 1 hour, the reactions were subjected to centrifugation at 100,000xg for 30 min and protein concentrations of supernatants were quantified as described in methods. The measured concentration of ALOD4 with no detergent treatment was set to 100% and all other values were normalized to this concentration. Values shown are averages of duplicate assays.

FIGURE 1-6

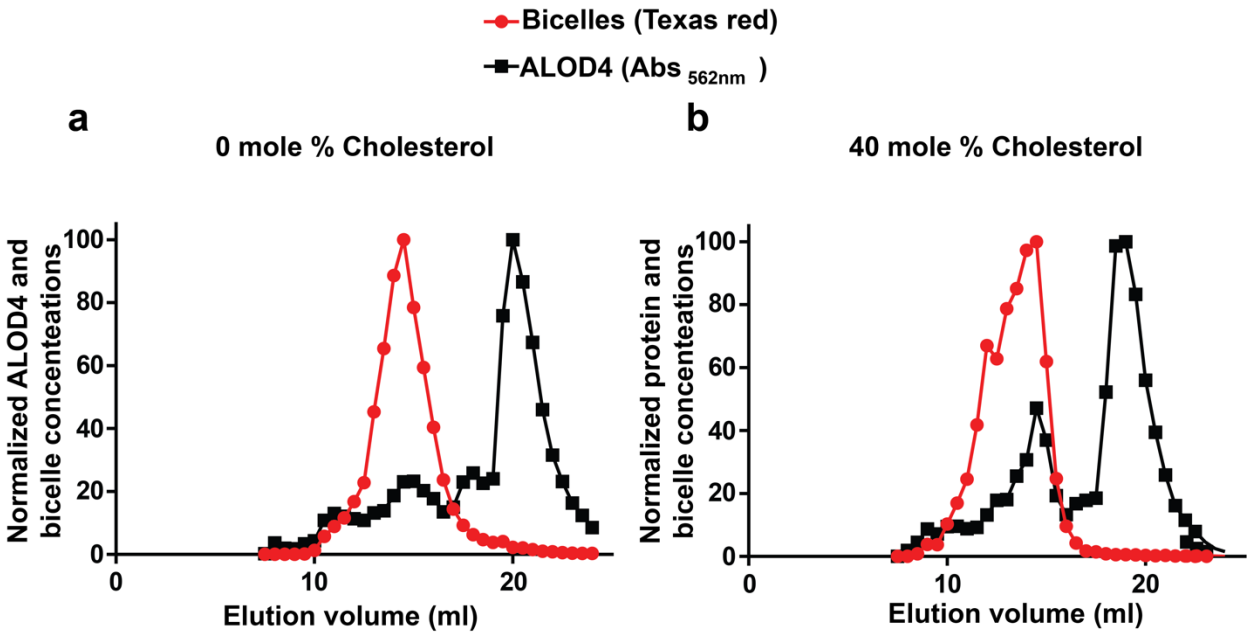

FIGURE 1-6: Binding of ALOD4 to C12E8 bicelles. Reaction mixtures (300 µL of Buffer F) containing 24 mM of indicated bicelles containing a small fraction of TR-DHPE and 133 µM ALOD4 were setup in 1.5 ml Eppendorf tubes. After incubation for 3 hours at room temperature, the reactions were loaded on to a Tricon 10/300 Superdex 200 gel filtration chromatography column equilibrated with buffer F and 500 µL fractions were collected. Concentration of bicelles and ALOD4 were measured using texas red fluorescence (A_{595nm}) and BCA assay (A_{562nm}) respectively. All the fluorescence values were normalized between 0 and 100.

FIGURE 1-7

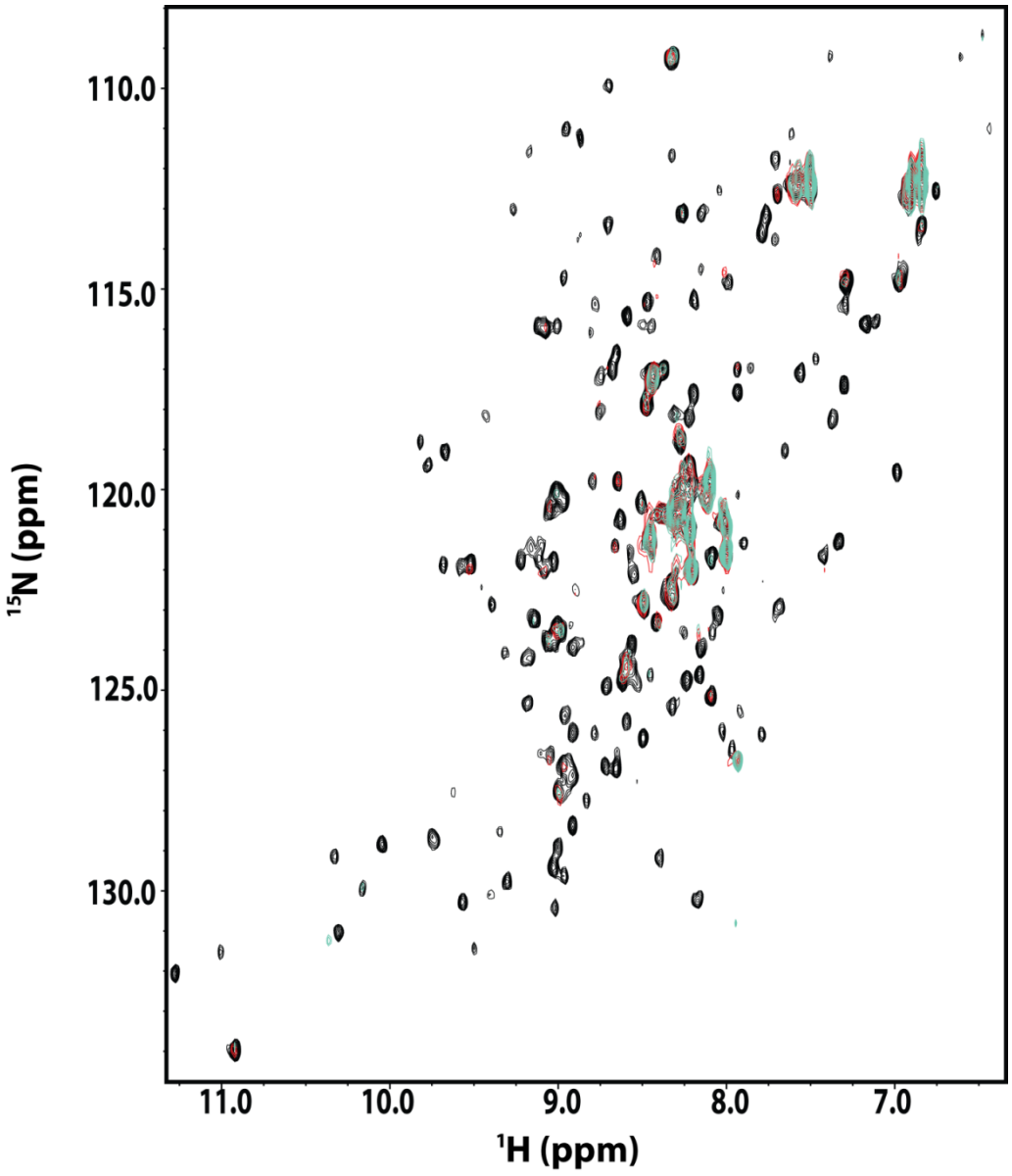

FIGURE 1-7: NMR of ALOD4 binding to C12E8 bicelles. 2D ^{1}H-^{15}N HSQC spectra of reaction mixtures (in buffer F) containing 35 μM of ^{15}N-ALOD4 in the absence (black), or presence of 21.5 mM C12E8 bicelles with 0 mole% (red) or 40 mole% cholesterol (cyan). All spectra were obtained in the presence of 7% D_2O.

FIGURE 1-8

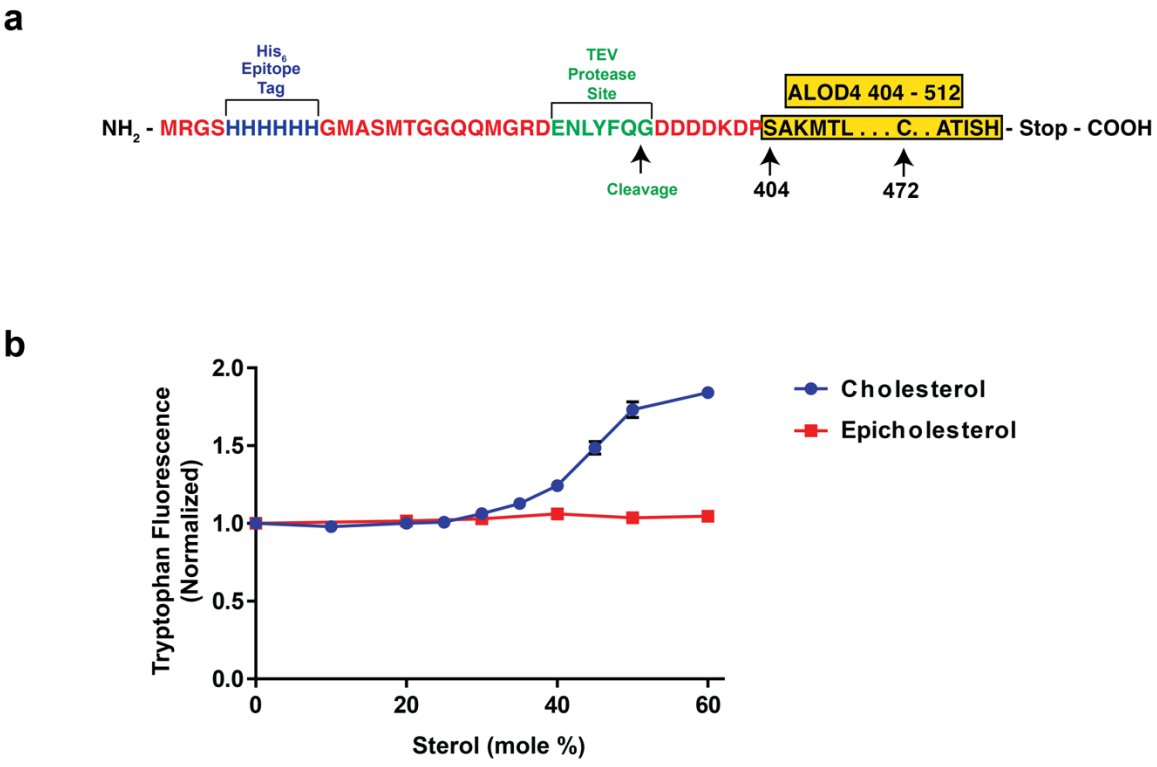

FIGURE 1-8: ALOD4 construct with increased stability. a, Schematic of TEVALOD4 construct Starting at the NH2-terminus, pTEVALOD4 contains a His_6 epitope tag, a 14 amino acid linker, a TEV protease cleavage site, a 7 amino acid overhang and ALOD4WT (aa 404-512). The TEV protease cleaved form ALOD4 is referred to as cALOD4 **b,** cALOD4 binding to liposomes. Liposomes containing DOPC and indicated mole % of cholesterol or epicholesterol were prepared as described. Reaction mixtures (200 µL of Buffer F) containing 600 µM liposomes and 4.4 µM of cALOD4 were set up in 1.5 mL Eppendorf tubes. After incubation for 1 h at room temperature, tryptophan fluorescence measurements were carried out as described in methods. Values shown are averages of triplicate assays.

FIGURE 1-9

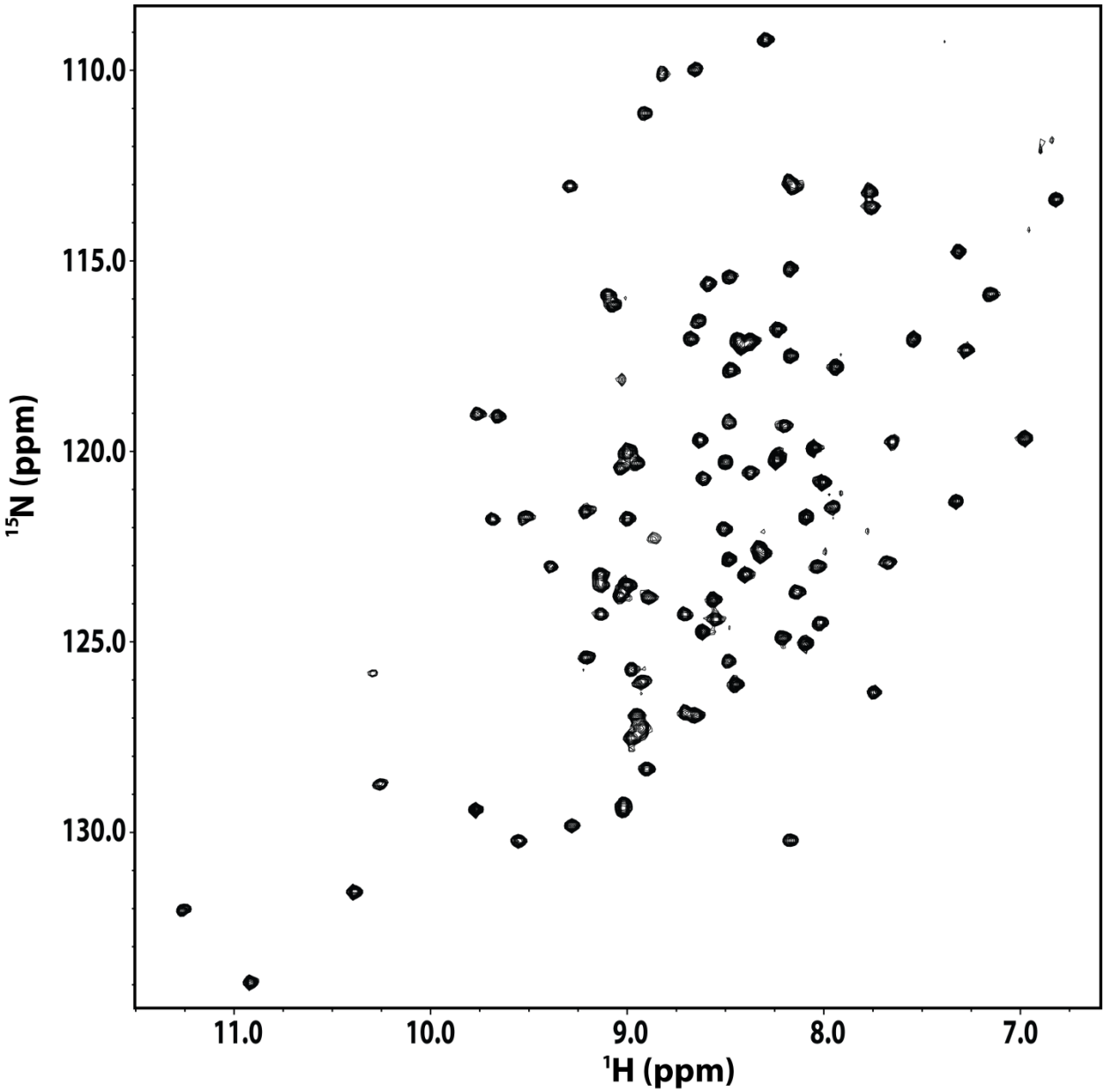

FIGURE 1-9: ^{1}H-^{15}N HSQC spectra of cALOD4. 2D ^{1}H-^{15}N HSQC spectra 50 µM of ^{15}N-cALOD4 in Buffer G containing 7% D_2O.

FIGURE 1-10

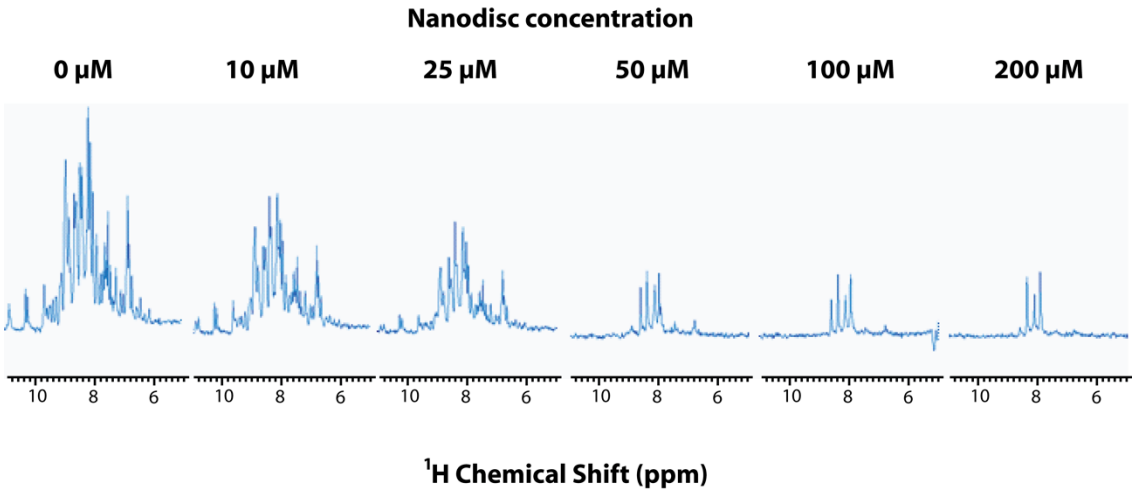

FIGURE 1-10: cALOD4 binding to cholesterol containing nanodiscs. 1D ^{1}H-^{15}N HSQC spectra of reaction mixtures (in Buffer G) containing 10 µM of ^{15}N-cALOD4 in the absence or presence of indicated amounts of nanodiscs with 42 mole% cholesterol. All spectra were obtained in the presence of 7% D_2O.

FIGURE 1-11

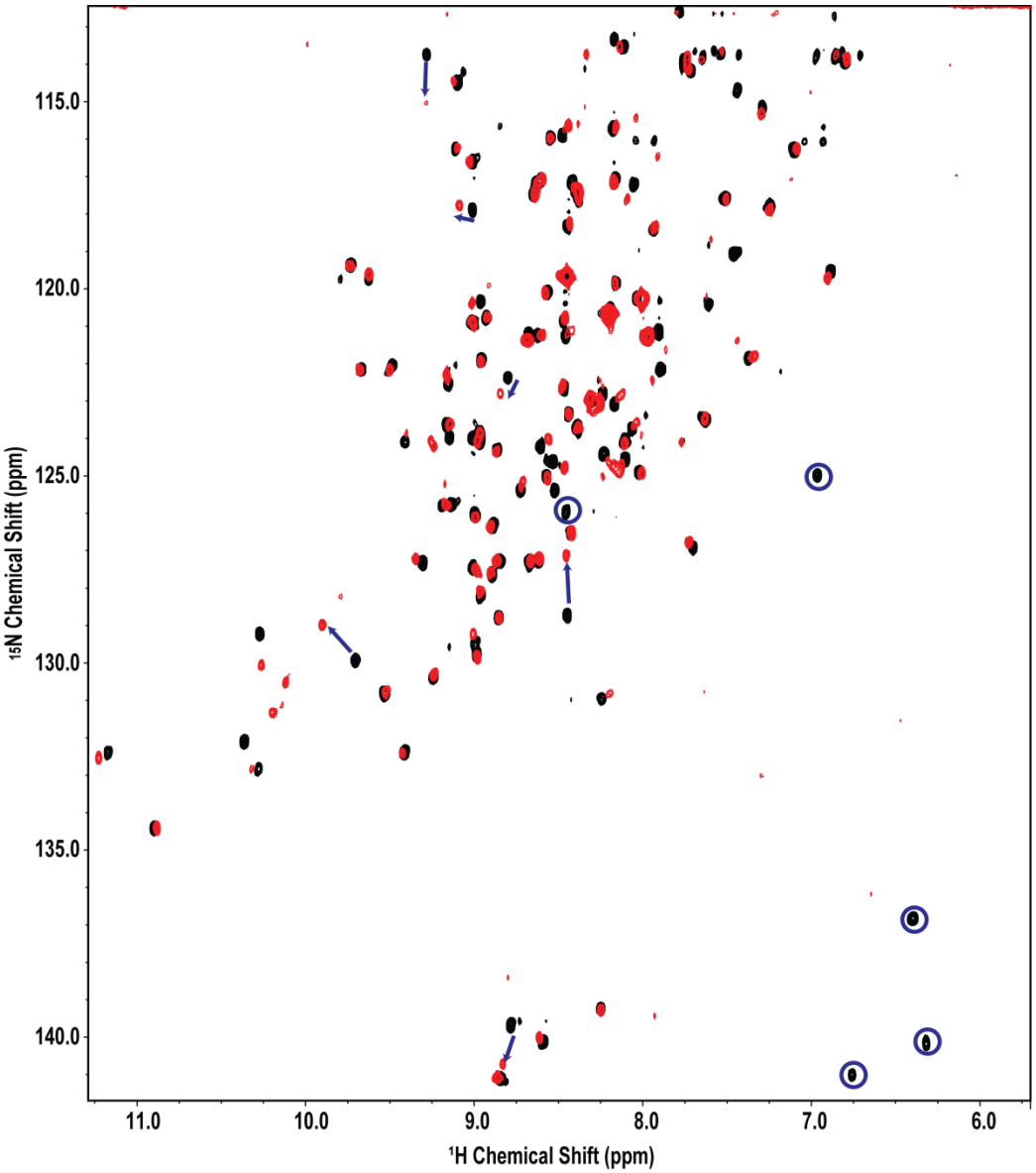

FIGURE 1-11: 2D-HSQC of cALOD4 binding to nanodiscs. 2D ^{1}H-^{15}N TROSY HSQC spectra of reactions mixtures (in buffer G) containing 50 µM of ^{2}H, ^{15}N, ILV-$^{13}CH_3$ labeled-cALOD4 in the absence or presence of 100 µM nanodiscs containing 42 mole% cholesterol. Some peaks that shift in the presence of nanodiscs are shown with arrows and some peaks that broaden in the presence of nanodisc are circled. All spectra were obtained in the presence of 7% D_2O

FIGURE 1-12

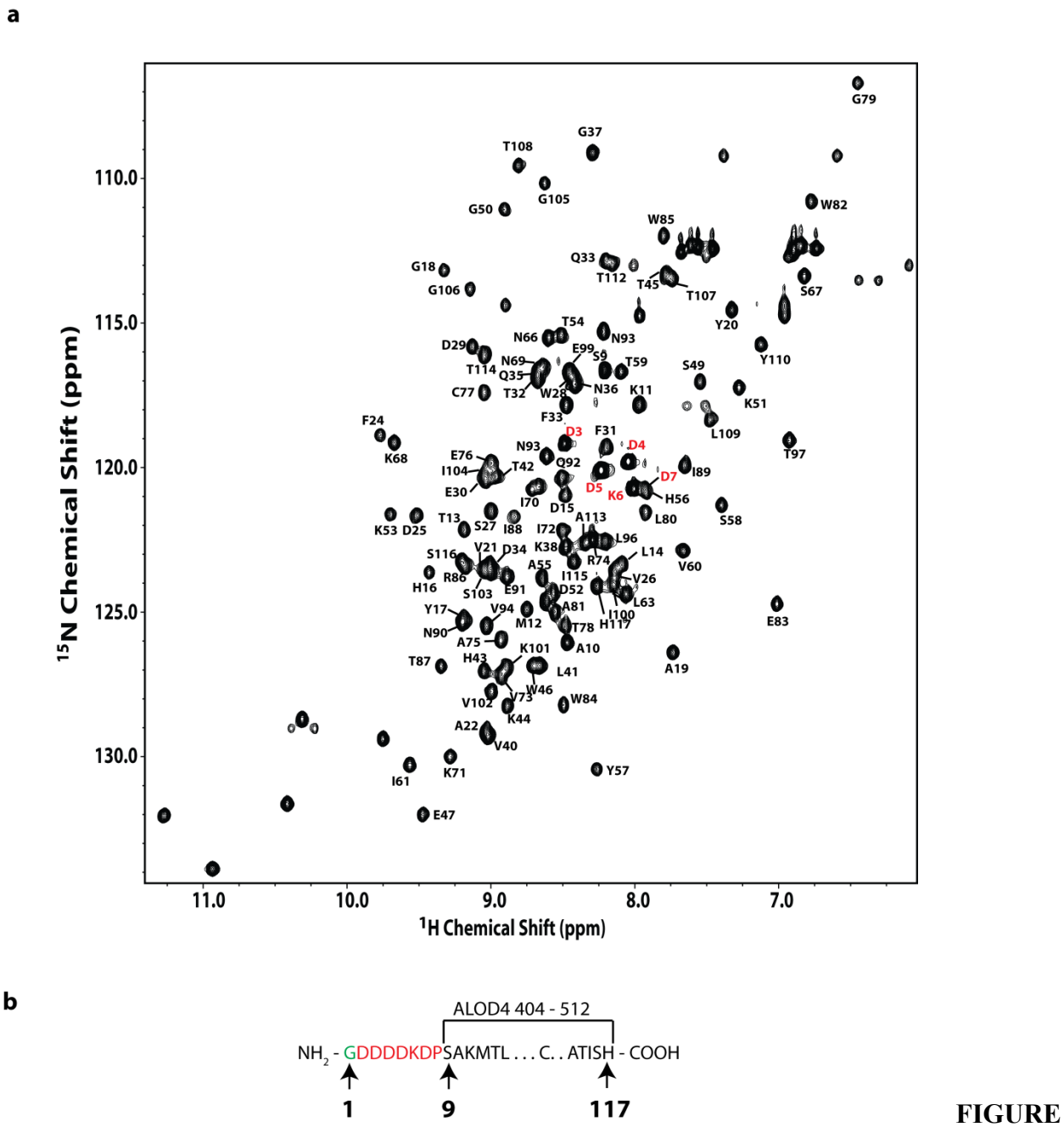

FIGURE 1-12: Backbone assignment of cALOD4. a, 2D ^{1}H-^{15}N HSQC spectra 50 µM of ^{15}N-cALOD4 in buffer G with backbone assignments. N-terminal residues from the expression plasmid are labeled in red. **b,** Numbering scheme for the backbone assignment of cALOD4 in **a**.

FIGURE 1-13

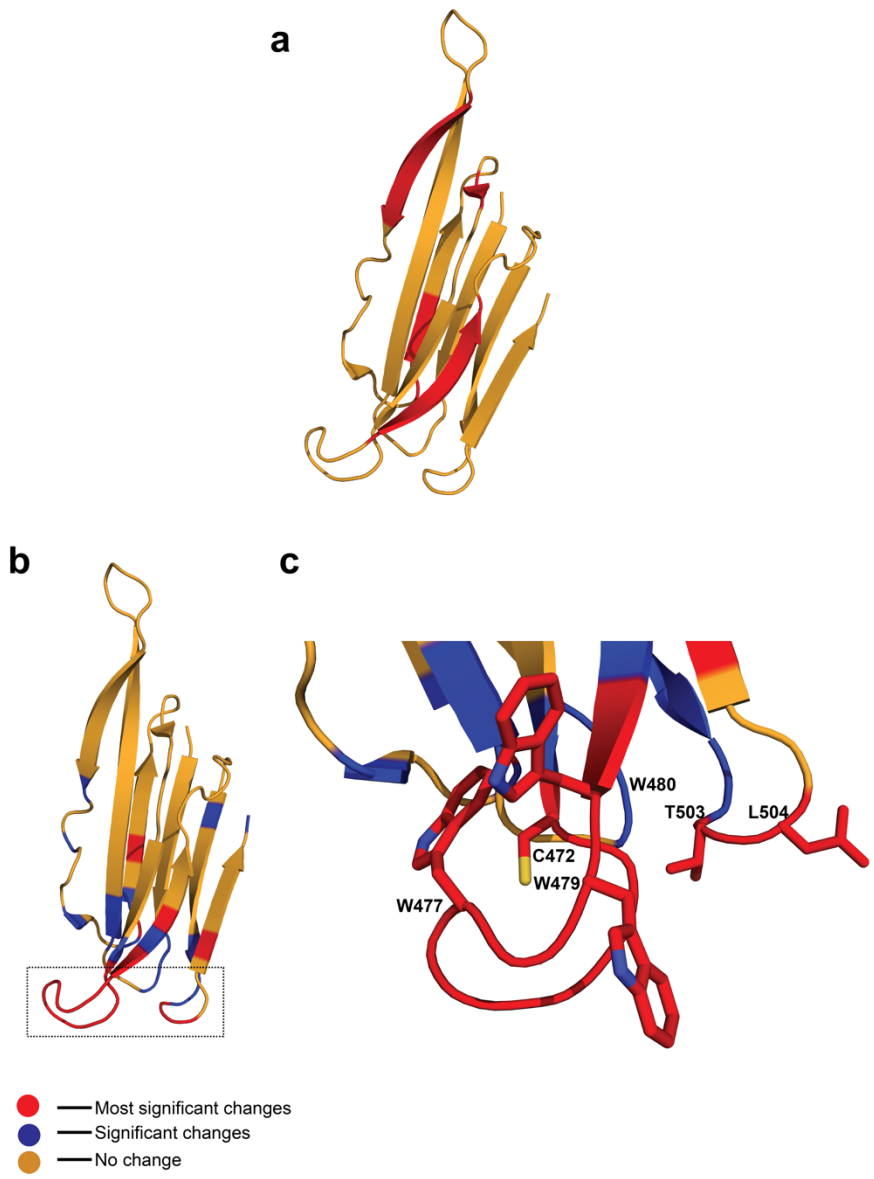

FIGURE 1-13: Structural analysis of ALOD4 binding to nanodiscs. a, Secondary structure prediction of ALOD4. COOH-terminal domain 4 from ALOFL crystal structure (pdb:3cqf) is shown as a cartoon. Secondary structure prediction of ALOD4 was performed using triple resonance data. The regions of ALOD4 predicted to have the same secondary structure as domain 4 from ALOFL are colored yellow and the rest of the domain is colored red. The red region is

predicted to be random coil in ALOD4 from the triple resonance data. **b,** COOH-terminal domain 4 from ALOFL crystal structure (pdb:3cqf) is shown as a yellow cartoon. Amino acids whose ^{1}H-^{15}N TROSY-HSQC cross peaks show significant changes (broadening and/or shifts) in the presence of cholesterol-containing nanodiscs are shown in red (most significant) and blue (significant). **c,** Close up view of the region of ALOD4 with the most changes in the presence of cholesterol-containing nanodiscs (boxed region in **b**).

DISCUSSION

This study provides some molecular insight into ALOD4 binding to cholesterol-containing membranes. Depth-dependent tryptophan quenching studies combined with accessibility of cysteine at two different positions on ALOD4 provided us an insight into the depth of insertion of ALOD4 into membranes containing cholesterol (Fig 1-1 and 1-2). We made use of nanodisc technology [37] to make cholesterol-containing model bilayer membranes that are suitable for use in NMR spectroscopy [99]. We studied the binding of ALOD4 to cholesterol-containing nanodiscs and mapped the residues of ALOD4 that are significantly affected by this interaction (Fig 1-14 b). It is worth noting that the two loops with the most significant changes (Fig 1-14 c) (undecapeptide (E_{471}CTGLAWEWWR$_{481}$) and hexapeptide (G_{501}TTLYP$_{506}$)) are the most highly conserved regions in almost all the CDCs [66]. Mutation of the hexapeptide loop to AAAAAA completely abolishes binding of ALOD4 to cholesterol-containing membranes suggesting its role in the interaction of ALOD4 with cholesterol [41, 48].

There are no high-resolution structures of CDCs bound to cholesterol. Structure of ALOFL without any bound ligand does not reveal any obvious binding pockets for cholesterol [16]. We were unable to isolate and crystallize ALOFL or ALOD4 bound to cholesterol in solution, partly due to the high insolubility of cholesterol. The NMR studies here are a small step towards a structural understanding of ALOD4 binding to cholesterol-containing membranes. Nanodiscs containing doxyl spin-labeled phospholipids (Fig 1-1 b) can be used for paramagnetic relaxation enhancement studies to provide further insight into residues important for this binding [116]. Side–chain assignment of ALOD4 combined with HMQC studies using ^{2}H, ^{15}N, ILV-$^{13}CH_3$ labeled ALOD4 can also provide a more detailed molecular understanding of this binding. In combination, these studies could provide a model for ALOD4 binding to membrane cholesterol.

CHAPTER 2

MOLECULAR DISCRIMINATION BETWEEN TWO CONFORMATIONS OF SPHINGOMYELIN IN MEMBRANES

INTRODUCTION

A special relationship between sphingomyelin (SM) and cholesterol in the PMs of animal cells has been proposed to modulate many cellular signaling processes [117, 121-123]. One such process is cholesterol homeostasis, which ensures optimal cholesterol levels in cellular membranes by precise regulation of its synthesis and uptake [22]. This link between SM and cholesterol homeostasis was initially revealed in a pair of studies where i) SM addition to cells increased cholesterol synthesis [47], and ii) SM removal from PMs of cells by treatment with sphingomyelinase (SMase), an enzyme that degrades SM, reduced cholesterol synthesis [127]. Both of these effects were explained by a model where SM sequesters cholesterol in PMs, preventing cholesterol transport to ER membranes to shut down activation of SREBPs [114, 128]. Depletion of SM by SMase released some sequestered PM cholesterol, which then was free for transport to ER to shut down activation of SREBPs. More recently, we have quantified pools of PM cholesterol using two soluble bacterial toxins, Perfringolysin O (PFO) and Anthrolysin O (ALO), which bind PM cholesterol when it is accessible at the membrane surface but not when it is rendered inaccessible due to sequestration by SM and other phospholipids [25, 31, 48]. We found that PM cholesterol is accessible to toxins only after the cholesterol concentration surpasses a threshold of 30-35 mole% of PM lipids [32]. Cholesterol in excess of this threshold is transported to ER to signal that the cholesterol requirements of the cell have been met and to terminate SREBP activation [31, 64]. About half of the inaccessible cholesterol, ~15 mole% of PM lipids, is

sequestered by sphingomyelin (SM), and can be liberated by treating cells with SMase. The remaining inaccessible PM cholesterol is sequestered by other membrane factors. While our understanding of the role of accessible PM cholesterol has steadily improved, we know little about how inaccessible cholesterol is sequestered. Here, we focus on acquiring a molecular understanding of how SM sequesters PM cholesterol to make it inaccessible to sensors and cellular signaling processes.

MATERIALS AND METHODS

Materials: We obtained all phospholipids from Avanti Polar Lipids; Texas Red 1,2-dihexadecanoyl-sn-glycero-3-phosphoethanolamine (TR-DHPE), Alexa Fluor C5 maleimide and isopropyl-1-thio-β-d-galactopyranoside (IPTG) from Invitrogen; cholesterol, ergosterol, sitosterol, lanosterol, and tris (2-carboxyethyl) phosphine (TCEP) from Sigma-Aldrich; epicholesterol, 25-hydroxy cholesterol and dihydrocholesterol from Steraloids; mPEG maleimide 5kDa (mPEG-MAL-5000) from Nanocs Inc; Osmium tetraoxide from Electron Microscopy Sciences.

Buffers: Buffer A contains 50 mM Tris-HCl (pH 7.5), 150 mM NaCl and 1 mM TCEP. Buffer B is buffer A supplemented with 1% (w/v) SDS. Buffer C contains 50mM Tris (pH-8.0), 1% Triton-X-100, 1% Sodium oxycholate, 100mM NaCl, 5mM MgCl2. Buffer D contains 50mM Tris (pH-8.0) and 1mM EDTA. Buffer E is Buffer D with 0.5% Triton-X 100 and 100mM NaCl. Buffer F contains 50mM Tris (pH 8.5), 10mM β-mercaptoethanol and 8M urea. Buffer G contains 50mM Tris (pH 8.5), 150mM NaCl, 0.1mM EDTA and 5% glycerol.

Expression plasmids: The gene encoding lysenin from *Eisinia fetida* (amino acids 1-297) with a COOH-terminal hexahistidine tag and flanking BamHI and EcoRI restriction sites was synthesized by GenScript (Piscataway, NJ) with a codon sequence optimized for efficient bacterial

overexpression and provided to us in the pUC57 cloning vector. This lysenin gene was excised and ligated into the pRSET B expression vector, and this construct is hereafter referred to as pLys-His_6. Expression plasmids encoding equinatoxin II from *Actinia equina* with a NH_2-terminal hexahistidine tag in the pET8c vector (pHis_6-Eqt) and ostreolysin A (OlyA) from *Pleurotus ostreatus* with a COOH-terminal hexahistidine tag in the pET21c+ vector were kindly provided to us by Dr. Kristina Sepcic (University of Ljubljana, Slovenia) [124]. Using OlyA as template, we generated a derivative where the two native cysteines of OlyA were mutated to serines and a new cysteine was introduced at the COOH-terminus (C62S C94S S151C), hereafter designated as pOlyA-His_6. For crystallographic studies, we generated a derivative of OlyA where its two native cysteines were mutated to serines (C62S C94S), the COOH terminal His_6 tag was removed, and a NH_2-terminal His_6 tag was introduced followed by a Tobacco etch virus (TEV) protease cleavage site (ENLYFQG), hereafter designated as pHis_6-TEV-OlyA. An expression plasmid encoding pleurotolysin B (PlyB) from *Pleurotus ostreatus* in the pET3a vector was kindly provided to us by Dr. Michelle Dunstone (Monash University, Australia) [78]. Using PlyB as template, we generated a derivative where an octahistidine tag was appended to the NH_2-terminus, hereafter designated as pHis_8-PlyB. pALOFL, pALOD4 and pTEV used in this study are described in Chapter 1. Mutations in all constructs were generated by site-directed mutagenesis using a QuickChange II XL Site-Directed Mutagenesis Kit (Agilent). The integrity of each plasmid was verified by DNA sequencing of its entire open reading frame.

Overexpression of recombinant proteins: All plasmids were transformed into *Escherichia coli* BL21 (DE3) pLysS competent cells (Invitrogen). For recombinant protein production, a single colony from a freshly transformed plate was grown in Luria Broth media (Research Products International) containing 100 µg/ml ampicillin. ALOFL, TEV and ALOD4 overexpression was induced was induced as described in Chapter 1. Lys-His_6 overexpression was induced at OD_{600}

=0.8 with 1 mM IPTG at 22°C for 20 hours. His_6-Eqt overexpression was induced at OD_{600}=0.8 with 1 mM IPTG at 37°C for 3 h. Overexpression of OlyA-His_6 and His_6-TEV-OlyA was induced at OD_{600} with 1 mM IPTG at 18°C for 16 h. His_8-PlyB overexpression was induced at OD_{600}=0.4 with 1 mM IPTG at 37°C for 4 h. Following overexpression, cells were harvested by centrifugation at 3220xg for 10 min at 4°C. Cell pellets were stored at -80°C after flash freezing in liquid nitrogen.

Purification of recombinant proteins: ALOFL, ALOD4 and TEV were purified as described in Chapter 1. For Lys-His_6, His_6-Eqt, OlyA-His_6 and His_6-TEV-OlyA purification, cell pellet from a 1L bacterial culture was resuspended in 20 ml of buffer A containing 1 mg/ml lysozyme, 0.4 mg/ml PMSF, and 1 protease inhibitor cocktail tablet (Complete Mini, EDTA-free, Roche). The cell suspension was homogenized using a Dounce homogenizer and incubated at 4°C for 3 hours for lysozyme disruption. Lysozyme disrupted cells were subjected to lysis by a tip sonicator (Branson, Inc) and then subjected to centrifugation at 25,000xg (20,000xg for His_6-Eqt) for 1h. The resulting supernatant was loaded on to a prepacked 1-ml HisTrap-HP Ni column. Columns were washed with 10 column volumes of buffer A containing 50 mM imidazole, and bound proteins were eluted with either buffer A containing 300 mM imidazole (His_6-Eqt) or with buffer A containing a linear gradient of 50-300 mM imidazole (Lys-His_6, OlyA-His_6 and His_6-TEV-OlyA). The eluted fractions with the proteins were pooled and concentrated using an Amicon Ultra centrifugal filter (Millipore; 10,000 MWCO) and further purified by gel filtration chromatography on a Tricon 10/300 Superdex 200 column equilibrated with buffer A. Protein-rich fractions were pooled, concentrated to 1-10 mg/ml, and stored at 4°C until use. Protein concentrations were measured using a Nanodrop instrument.

After purification, His_6-TEV-OlyA was subjected to cleavage by TEV protease. In each cleavage reaction, 500 µg of His_6-TEV-OlyA was incubated with 50 µg of His6-TEV at 4°C. After 16 h, the cleavage reaction was loaded onto a prepacked 1-ml HisTrap-HP Ni column, and cleaved OlyA was collected in the flow through. OlyA was concentrated in a 3,000 MWCO concentrator and subjected to gel filtration chromatography using a Superdex 200 column pre-equilibrated with Buffer A. Protein-rich fractions were pooled and concentrated to 40-50 mg/ml for crystallization studies.

His_8-PlyB was purified using a refolding protocol described previously [78]. Cell pellet from a 1L bacterial culture was resuspended in 20 ml of buffer C containing 1 mg/ml lysozyme, 0.4 mg/ml PMSF, and 1 protease inhibitor cocktail tablet. The cell suspension was homogenized using a Dounce homogenizer and incubated at room temperature for 30 min after which the cells were lysed using a tip sonicator. The lysed cell suspension was subjected to centrifugation at 15,000xg for 30 min. The inclusion body pellet was resuspended in buffer E and centrifuged at 15,000xg for 15 min. This pellet wash step was repeated until the inclusion body appeared white (typically takes 20-25 washes). Finally, the white pellet was washed with buffer D using the above method. The washed pellet was resuspended in 25 ml of buffer F and added dropwise over 16 hours into 1L of refolding buffer G. The refolded protein solution was incubated with nickel-nitrilotriacetic acid (Ni-NTA) agarose beads (Qiagen) for 6 hours following which unbound proteins were separated from beads using a gravity column. 1.5 hours following which unbound proteins were separated from beads using a gravity column. The beads were washed with 10 column volumes buffer F containing 50mM imidazole. Bound PlyB was eluted with buffer F containing 500 mM imidazole. The eluted fractions with the proteins were pooled and concentrated using an Amicon Ultra centrifugal filter (Millipore; 30,000 MWCO) and further purified by gel

filtration chromatography on a Tricon 10/300 Superdex 200 column equilibrated with buffer F. Protein-rich fractions were pooled, concentrated to 1-2 mg/ml, and stored at 4°C until use.

OlyA labeling: After purification, some aliquots of OlyA-His_6 were labeled with Alexa Fluor 488 C5-maleimide dye as described previously [48]. In a typical 300 µL labeling reaction, 20 nmoles of protein was incubated with 200 nmoles of Alexa Fluor 488 C5-maleimide. After incubation for 16 hours at 4°C, the reaction was quenched by addition of DTT to a final concentration of 10 mM. Free dye was separated from labeled OlyA-His_6 by passing the reaction mixture over a hand-packed nickel column (~1 ml), and eluting labeled OlyA-His_6 using buffer A containing 300 mM imidazole. The eluted fluorescently-labeled OlyA-His_6 (fOlyA) was then subjected to gel filtration chromatography on a Superdex 200 column pre-equilibrated with buffer A. Protein labeling was verified by SDS-PAGE followed by imaging using a BioSpectrum scanner (Analytik Jena, Germany).

Liposome preparation: Liposomes were prepared as described previously [130]. Mixtures containing the indicated proportions of phospholipids and sterols in chloroform along with a trace amount (< 0.2 mole%) of a fluorescently labeled phospholipid (TR-DHPE) were evaporated to dryness under a steady stream of nitrogen gas and stored under vacuum for at least 16 hours. The dried lipid mixtures were hydrated by adding buffer A to the desired final lipid concentration and agitated on a vortexer for 2 hours at room temperature. The resulting lipid dispersions were placed in a water bath at 37°C and subjected to sonication for 15 min followed by a 15 min pause for cooling (3 cycles). The resulting liposomes were stored at room temperature and used within a week.

Assays for binding of proteins to model liposome membranes: Binding of Lys-His_6, His_6-Eqt, and OlyA-His_6 (unlabeled and fluorescently labeled versions) to liposomes was measured

using a pelleting assay. In these assays, reaction mixtures (200 µL of buffer A) containing 1560 µM liposomes (total lipid) and the indicated proteins (0.1 µg (6 pmol) of fluorescently labeled OlyA-His_6 or 1 µg of Lys-His_6 (29 pmol), His_6-Eqt (47 pmol), or unlabeled OlyA-His_6 (57 pmol)) were set up in 1.7 mL low-retention microcentrifuge tubes (Fisher Scientific). After incubation for 4h at room temperature, the reaction mixtures were subjected to centrifugation at 21,000 x *g* for 1h at room temperature. The resulting supernatants (200 µL) were collected and the pellets were resuspended in 200 µL buffer A. For assays with labeled proteins, equal fractions (100 µL each) of supernatants and pellets were transferred to a 96-well plate (Greiner Bio-One; black, flat-bottom, non-binding). 100 µL of buffer B was added to each well and the plate was placed on a shaker for 1h at room temperature, following which fluorescence from liposomes and labeled protein was measured using a microplate reader (Tecan M1000 Pro) using the following parameters – Texas Red (excitation wavelength, 595 nm; emission wavelength, 617 nm; band pass, 5 nm for each); Alexa Fluor 488 (excitation wavelength, 495 nm; emission wavelength, 516 nm; band pass, 5 nm for each). For assays with unlabeled proteins, aliquots (20 µL) of supernatants and resuspended pellets were subjected to immunoblot analysis. In some cases, the immunoblot LICOR intensities from the supernatants (unbound OlyA) and pellets (bound OlyA) were used to calculate the percentage of OlyA bound to liposomes.

In some studies, binding of OlyA-His_6 to lipid membranes were measured using a dot blot assay. In these assays, 4 nmol of the indicated liposomes (5 µL of stocks prepared at 800 µM total lipid concentration in buffer A) were deposited on nitrocellulose membranes and allowed to dry for 5-10 min. The membranes were then incubated at room temperature in blocking buffer for 30 min, and then switched to blocking buffer containing 1 µg/ml OlyA-His_6 for 1 h. Membranes were then switched to washing buffer for 5 min, incubated with anti-His antibody in blocking buffer (1 µg/ml) for 1 h, and processed for immunoblot analysis.

For measurement of association rates, we used liposomes containing 1 mole% 18:1 Biotinyl CAP PE for quick separation of bound and unbound OlyA using magnetic streptavidin beads (NanoLink™ Streptavidin Magnetic Beads 1.0 μm). Aliquots containing 780 nmoles of indicated liposomes were incubated with 300 μg washed magnetic streptavidin beads for 30 min at room temperature. Preliminary experiments indicated that this amount of streptavidin beads was sufficient to capture all the added liposomes. Reaction mixtures (100 μL of buffer A) containing 1560 μM liposomes bound to streptavidin beads from above and 0.1 μg (6 pmol) of fluorescently labeled OlyA-His_6 (fOlyA) were set up in 1.7 mL low-retention microcentrifuge tubes. After incubation for indicated times at room temperature, the reaction mixtures were subjected to magnetic pull-down (DynaMag™-2 magnet). The resulting supernatants (100 μL), containing unbound proteins were collected and the beads were washed once with 100 μL buffer A. The washed beads containing bound liposomes and proteins were resuspended in 100 μL buffer A. The supernatants and resuspended beads (100 μL each) were transferred to a 96-well plate (Greiner Bio-One; black, flat-bottom, non-binding). 100 μL of buffer B was added to each well and the plate was placed on a shaker for 1h at room temperature, following which fluorescence from liposomes (Texas Red) and labeled protein (Alexa Fluor 488) was measured using a microplate reader as described above for the pelleting assay.

Preparation of supported lipid bilayers in 96-well plates: The glass surface of each well of a 96-well glass-bottom plate (Greiner Bio-One) was cleaned and processed by the following steps: i) wells were washed three times with water (350 μL each); ii) wells were treated with isopropanol (300 μL) for 30 min, followed by three washes with water (350 μL each); iii) wells were treated with 1 M NaOH (250 μL) for 1 hour, followed by five washes with water (350 μL each); iv) wells were dried under a stream of compressed air. Plates were then covered with lids, wrapped in aluminum foil, and used within two days. Supported lipid bilayers were generated on

the processed glass surfaces of these wells by the following steps: i) wells were filled with water (80 μL) followed by addition of liposomes (30 μL of 1.6 mM stock); ii) after incubation for 1 hour, undeposited liposomes were removed by three successive washing steps, each of which consisted of adding buffer A (200 μL) to each well followed by removing a fraction of the well contents (110 μL of 310 μL total); iii) wells were then treated with a blocking agent (150 μL of 0.5 mg/mL BSA in buffer A) to prevent nonspecific binding; iv) after incubation for 1 hour, 200 μl of buffer A was added and unbound BSA was removed by three successive washing steps, each of which consisted of removing a fraction of the well contents (150 μL out of 350 μL total) followed by adding more buffer A (150 μL); v) after the last wash, 300 μL of the well contents was removed, leaving behind a supported lipid bilayer in a total volume of 50 μL of buffer A. All of the preceding steps were carried out at room temperature. Once liposomes were added to wells, caution was exercised to ensure that the glass surface and supported bilayer was not disturbed or exposed to air. For fixation studies, we added 200 μl of a 1:1 mixture of osmium tetroxide (4% stock in water) and PBS to each well. After incubation for 30 min in a chemical hood, 100 μl of buffer A was added to the well, after which the osmium tetroxide fixative was removed by serial dilution with ten successive washing steps, each of which consisted of removing a fraction of the well contents (200 μl of 350 μl total) followed by adding more buffer A (200 μl). Unfixed wells received the same treatment, except that 200 μl of a 1:1 mixture of water and PBS were added to the well during the 30 min fixation step. Membrane fluidity was measured by fluorescence recovery after photobleaching (FRAP). Epifluorescence microscopy (Nikon Ti-E microscope, 60x objective) was used to monitor TR-DHPE from a circular region (~10 μm in diameter) for 30 s, after which a focused beam from a 561 nm laser source was used to photobleach TR-DHPE molecules in that region. After 30 s, the laser was turned off and TR-DHPE fluorescence of the bleached region was

monitored. The fluorescence before bleaching was set to 1 and the fluorescence after the 30 s bleaching step (~40-50% reduction) was normalized to 0.

Assay for binding of fluorescently labeled OlyA (fOlyA) to supported lipid bilayers: Binding reactions were carried out in 96-well plates, the well surfaces of which were covered with supported lipid bilayers and processed as described above. To each well containing 150 µl of buffer A, we added 5 µg of fOlyA proteins (90 pmoles) in a total volume of 10 µl of buffer A. After incubation for 30 min, buffer A (190 µL) was added to increase the total reaction volume to 350 µL. Unbound fOlyA was then removed by serial dilution with ten successive washing steps, each of which consisted of removing a fraction of the well contents (200 µL of 350 µL total) followed by adding more buffer A (200 µL). Membrane-bound fOlyA and fluorescence from supported bilayers was measured using a microplate reader (Tecan M1000 Pro) using the following parameters – Texas Red (excitation wavelength, 595 nm; emission wavelength, 617 nm; band pass, 5 nm for each); Alexa Fluor 488 (excitation wavelength, 495 nm; emission wavelength, 516 nm; band pass, 5 nm for each).

Chemical modification of OlyA: OlyA-liposome binding reactions were carried out as described earlier with the following modifications. Reaction mixtures (400 µL of buffer A) containing 640 nmol of liposomes and 2 µg (120 pmol) of OlyA(WT)-His_6 or OlyA(E69A)-His_6 were set up in 1.7 ml low-retention micro centrifuge tubes. After incubation for 3h at room temperature, the reaction mixtures were subjected to centrifugation at 21,000 x *g* for 30 min at room temperature. The resulting pellets were resuspended in 240 µL buffer A. Chemical modification reaction mixtures, in a final volume of 100 µL of buffer A, containing either resuspended pellets from the above step (60 µL) or 500 µg of soluble OlyA(WT)-His_6 or OlyA(E69A)-His_6 (in a final volume of 60 µL of buffer A), and the indicated amounts of mPEG-

MAL-5000 (in a final volume of 40 µL of buffer A) were incubated in 1.7 ml low-retention microcentrifuge tubes at room temperature. After 2 hours, reactions were quenched by addition of 10mM DTT (1 M stock). Aliquots of the reaction mixtures (20 µL) were subjected to immunoblot analysis.

Hemolysis assays: Fresh rabbit blood was obtained from the Animal Resource Center at UT Southwestern Medical Center and hemolysis assays were carried out as described previously [48]. For a typical assay, 1 mL of rabbit blood was centrifuged at 120xg for 8 min and the erythrocyte pellet was resuspended in 1 mL of ice-cold buffer H. After gentle mixing by hand, the mixture was centrifuged at 500xg for 8 min and the resulting pellet was again resuspended in 1 mL of ice-cold buffer H. After gentle mixing by hand, the mixture was centrifuged at 1000xg for 8 min and the resulting pellet was resuspended in 8 mL of ice-cold buffer H. Standard hemolysis reaction mixtures (250 µL) containing 225 µL of washed and diluted erythrocytes and 25 µL of buffer A containing protein at the indicated concentrations were set up in 1.5 mL tubes. After incubation for 15 min at room temperature, the mixtures were centrifuged at 380xg for 5 min and a portion of the supernatant (100 µL) was transferred to a 96-well plate (clear, flat-bottom; Evergreen Scientific, Los Angeles, CA). The extent of hemolysis was quantified using a microplate reader by measuring the absorbance of released hemoglobin at 540 nm.

Immunoblot analysis: After indicated incubations, samples from liposome pelleting assays were mixed with 5x loading buffer, heated at 95°C for 10 min, and subjected to 10% SDS-PAGE (lysenin) or 15% SDS-PAGE (Eqt, OlyA). Samples containing lysenin were additionally incubated with 4M urea to break down membrane-bound oligomers. The electrophoresed proteins were transferred to nitrocellulose membranes using the Bio-Rad Trans Blot Turbo system. These membranes and nitrocellulose membranes from dot blot assays were subjected to immunoblot

staining with anti-His antibody (1:1000 dilution). Bound antibodies were visualized by chemiluminescence (Super Signal Substrate; Thermo Fisher) by using a 1:5000 dilution of donkey anti-mouse IgG conjugated to horseradish peroxidase (Jackson ImmunoResearch, West Grove, PA). Filters were exposed to Phoenix Blue X-Ray Film (F-BX810; Phoenix Research Products, Pleasanton, CA) at room temperature for 1-30 s or scanned using an Odyssey FC Imager (Dual-Mode Imaging System; 2 min integration time) and analyzed using Image Studio ver. 5.0 (LI-COR, Lincoln, NE).

Crystallization, data collection, structure determination and refinement: Crystals of OlyA(WT) were grown using the sitting-drop vapor-diffusion method from drops composed of 0.75 µl of buffer A containing 30 mg/ml OlyA(WT) and 1 µl of reservoir solution (100 mM ammonium chloride and 16% (w/v) PEG 3350) and equilibrated over reservoir solution at 20˚C. Cryoprotection was performed by transferring the crystals to a final solution of 100 mM ammonium chloride, 50 mM Tris pH 7.5, 150 mM NaCl, 19% (w/v) PEG 3350 and 30% (v/v) ethylene glycol and were flash-cooled in liquid nitrogen. OlyA(WT) crystals diffracted to a minimum Bragg spacing (d_{min}) of 1.1 – 1.3 Å and exhibited the symmetry of space group P21 with cell dimensions of a = 46.4 Å, b = 100.3Å, c = 79.7 Å, b = 106.4˚ and contained four OlyA(WT) molecules per asymmetric unit.

To generate crystals of ligand-bound OlyA(WT), we first dried down 80 µmol of an equimolar mixture of SM and cholesterol on the sides of a 1.7 ml tube. We then added 200 µl buffer A containing 30 mg/ml OlyA(WT) and incubated the mixture overnight at room temperature on a rotator. We also dried down 50 µg each of SM and cholesterol on a sitting-drop vapor-diffusion tray and set up crystals using the SM/cholesterol-saturated OlyA(WT) generated above.

Crystals of OlyA(E69A) were grown by the same method described above for ligand-bound OlyA(WT), but the reservoir solution was 0.1 M Bis-Tris (pH 5.5), 125 mM lithium sulfate and 20-23% (w/v) PEG 3350, and the final cryoprotectant solution was 0.1 M Bis-Tris (pH 5.5), 125 mM lithium sulfate, 25% (w/v) PEG 3350 and 25% (v/v) ethylene glycol. OlyA(E69A) crystals diffracted to a minimum Bragg spacing (d_{min}) of 1.8 Å and exhibited the symmetry of space group C2 with cell dimensions of a = 69.9 Å, b = 86.7Å, c = 92.9 Å, b = 99.1˚ and contained four OlyA(E69A) molecules per asymmetric unit.

All diffraction data were collected at beamline 19-ID (SBC-CAT) at the Advanced Photon Source (Argonne National Laboratory, Argonne, Illinois, USA) and processed in the program HKL-3000 [87] with applied corrections for effects resulting from absorption in a crystal and for radiation damage [15, 92], the calculation of an optimal error model, and corrections to compensate the phasing signal for a radiation-induced increase of non-isomorphism within the crystal [13, 14]. Crystals of OlyA(E69A) displayed anisotropic diffraction and while 99% complete to 2.2 Å resolution, fell off in intensity to the high-resolution limit of 1.8 Å resolution. Phases for OlyA(WT) were obtained by molecular replacement in the program Phaser [83]. The crystal structure of Pleurotus ostreatus PleurotolysinA (PDB ID 4OEB) [78] was modified for use as a search model by truncating non-identical residues to the last common atom. Completion of the protein model was performed by manual rebuilding in the program Coot [38], and model refinement was performed in the program Phenix[1]. For the OlyA(WT) data to 1.1 Å resolution, fully anisotropic atomic displacement parameters for all non-hydrogen protein atoms were refined. Data collection and structure refinement statistics are summarized in Table 1.

Docking Simulations: The binding of the SM ligand to OlyA receptors was studied using molecular docking simulations. The hydrophilic part of SM was chosen for the ligand, and both

OlyA(WT) and OlyA(E69A) crystal structures were used as the protein receptors. The Maestro platform (version 10.3) was used to access modules of the Schrodinger software package (version 3.1, Schrodinger) for structure preparation and docking. Structures of OlyA(WT) and OlyA(E69A) were prepared using Protein Preparation Wizard (version 11.2, Schrodinger) and the PROPKA module to set the protonation state of the protein at pH 7.0. The center of the binding pocket in both proteins was defined by residues that lie within a 5Å radius of the putative SM density in the structure of OlyA (WT). 3D coordinates of the hydrophilic part of SM (ligand) were generated with LigPrep (version 3.5) using the EPIK module (version 3.3) to set the pH to 7.0 and the OPLS_2005 force field option, and the resulting SM structure was then docked to the structural models of OlyA(WT) and OlyA(E69A) using Glide standard precision (SP) scoring function (version 6.8, Schrodinger). The docking procedure yielded a single cluster of poses for each protein. The poses with the highest docking scores were chosen as representatives of the binding model.

RESULTS

OlyA senses SM/cholesterol complexes in membranes: Our strategy for probing the SM/cholesterol interaction was based on previous success in identifying PFO and ALO as sensors for accessible, but not SM-sequestered, cholesterol [32]. We speculated that there may be other toxins that have the opposite ability, to bind SM-sequestered but not accessible cholesterol. A literature search identified several candidate SM-binding toxins, some of which had been reported to also require cholesterol to bind membranes [2, 8, 9, 79, 124, 135, 145]. We overexpressed and purified three toxins from this group, namely lysenin (Lys), equinatoxin II (Eqt), and Ostreolysin A (OlyA), for analysis of their respective membrane-binding specificities (Fig 2-1 a). For these initial experiments, we used a version of SM containing a C16 ceramide base and an amide-linked

oleoyl (18:1) acyl chain (see Fig 2-1 c for lipid structures). Protein-liposome binding was measured using a pelleting assay where centrifugation was used to separate liposome-bound proteins from unbound proteins. Lys and Eqt bound to liposomes containing SM, and their binding did not change in the presence of either cholesterol or epicholesterol, a diastereomer of cholesterol (Fig. 2-1 b, lanes 1-3). Binding was eliminated when SM was replaced with dioleoyl-phosphatidylcholine (DOPC), another choline-containing phospholipid (Fig. 2-1 b, lanes 4, 5). In contrast, OlyA bound to membranes only when they contained both SM and cholesterol (Fig. 2-1 b, lanes 1-5). Thus, we focused on OlyA to gain insight into the SM/cholesterol interaction.

We considered two models to explain the dual specificity of OlyA for SM and cholesterol in membranes. In one model, OlyA contains distinct binding sites for SM and cholesterol, respectively, and these two sites may or may not be allosterically linked. In another model, OlyA contains a single binding site for a pre-existing complex of SM and cholesterol in membranes. We used two approaches to try to distinguish between these models. In one approach, we used a competition assay to test whether pre-incubation with SM alone, cholesterol alone, or mixtures of the two lipids, would prevent the binding of OlyA to red blood cells (RBCs), whose membranes contain high concentrations of SM and cholesterol [35]. While OlyA binding does not disrupt RBC membranes, membrane-bound OlyA can recruit a cofactor, pleurotolysin B (PlyB), to form a transmembrane pore and cause hemolysis (Fig 2-2 a, b). Using PlyB-mediated hemolysis as a convenient readout for OlyA binding, we observed that pre-incubation with either SM or cholesterol did not block OlyA binding to RBCs (Fig 2-2 c). In contrast, pre-incubation with a 1:1 mixture of SM and cholesterol resulted in a complete block of OlyA binding to RBCs (Fig 2-2 c). Sequential pre-incubation, first with SM and then with cholesterol, or vice versa, did not block OlyA binding. A different result was obtained with cholesterol-binding and pore-forming full-length ALO (ALOFL), hemolysis by which was inhibited by pre-incubation with any of the

conditions that included cholesterol irrespective of the order of addition (Fig. 2-2 c). In a second approach, we tested the effect of immobilization of membrane lipids on OlyA binding. If OlyA was sequentially binding SM and cholesterol at two distinct binding sites or was inducing SM/cholesterol complex formation, one might expect that restricting lipid motion would disrupt the membrane binding of OlyA. For this experiment, we generated a fluorescently labeled version of OlyA (Fig 2-2 d) and also prepared supported bilayers containing trace amounts (0.2 mole%) of a fluorescently-labeled phospholipid (TR-DHPE) on the glass surfaces of 96-well glass-bottom plates. The lipid molecules in both SM and SM/sterol membranes were fluid, as judged by fluorescence recovery after photobleaching (FRAP) measurements (Fig 2-2 e). Recovery was slower in sterol-containing membranes compared to SM membranes without sterols. Fixation with osmium tetroxide completely blocked the fluidity of all membranes (Fig 2-2 e), a result that is consistent with previous studies [67]. We then measured fOlyA binding to the unfixed and fixed supported bilayers and found that fOlyA only bound to membranes containing both SM and cholesterol and this binding was unaffected by osmium tetroxide fixation (Fig 2-2 f).

While not conclusive, both of the above experiments favor a model where OlyA contains a single binding site for a pre-formed SM/cholesterol complex in the membrane. We then used the liposome pelleting assay to further define the putative SM/cholesterol complex recognized by OlyA. Binding of OlyA increased in a sigmoidal fashion as cholesterol content of liposomes increased up to 60 mole% (Fig 2-2 g), which is close to the solubility limit of cholesterol in bilayers containing choline-phospholipids [62]. No binding was observed when cholesterol was absent or replaced with epicholesterol. To investigate higher concentrations of cholesterol, we deposited ethanolic mixtures of SM and cholesterol as lipid films on nitrocellulose membranes. This approach allowed us to assay the entire range of SM/cholesterol ratios, and we found that OlyA binding showed a sharp maximum at 65 mole% cholesterol (Fig 2-2 h).

Crystal structure reveals lipid binding site in OlyA: To gain further insight into the nature of OlyA's interaction with SM and cholesterol, we performed structural analysis. We modified the OlyA construct used for the above biochemical studies by inserting a Tobacco Etch virus (TEV) cleavage site to allow for removal of the NH_2-terminal His_6 tag (Fig 2-3 a). This version of OlyA, designated as OlyA(WT), was purified (Fig 2-3 b, c), and crystallized in the absence of lipid ligands, or in the presence of saturating amounts of an equimolar mixture of SM and cholesterol, the same incubation that resulted in complete inhibition of PlyB-mediated hemolysis due to solution binding of the two lipids to OlyA (Fig 2-2 c). Crystals obtained from both conditions were used to determine the structure of OlyA(WT) at resolutions of 1.15 Å (no ligand) and 1.33 Å (with ligand) (Table 2-1). Both OlyA(WT) structures showed a β-sandwich fold, similar to that observed for a related toxin, Pleurotolysin A [78]. The β-sandwich is comprised of nine β-sheets and 1 short α-helix which are connected by 4 flexible loops on the COOH-terminal end and 3 flexible loops on the NH_2-terminal end (Fig 2-3 d and Fig 2-4 a). When we compared the two structures, we observed that crystals obtained with lipid ligands contained additional electron density in a shallow channel bounded by the sidechains of W28 and K99, residues that lie on two separate loops on the NH2-terminal end (Fig 2-4 a, b). This density was strong enough to be modeled in only one of the four monomers in the crystallographic asymmetric unit. Part of the SM ceramide base (Fig 2-4 c, red) was tentatively assigned to this observed density, and a possible orientation of the rest of SM is shown for reference (Fig 2-4 a). No other parts of SM, cholesterol, or crystallization buffer components could adequately account for the observed density. This assignment of a portion of SM is still not definitive as the elongated electron density could be another hydrophobic molecule that co-purified with OlyA(WT). Even with these caveats, it is noteworthy that the only clear bound density may correspond to the ceramide portion of SM, which

is the main structural difference between SM and PC (Fig 2-1 c), lipids for which OlyA(WT) shows all-or-none specificity.

To test the relevance of this structural model, we generated mutant versions of OlyA(WT) where all residues within 5Å of the putative ligand density (13 in total) were individually mutated to alanines (Fig 2-4 d). To rapidly evaluate the membrane-binding properties of these mutant OlyA proteins, we developed a dot blot assay where liposomes deposited on nitrocellulose membranes were incubated with OlyA and bound OlyA was then measured by immunoblot analysis after washing away unbound OlyA. The dot blot assay showed that OlyA bound membranes only when they contained both SM and cholesterol (Fig 2-3 e, f), identical to what was observed in the pelleting assay (Fig 2-1 b). Using this dot blot assay, we found that replacement of Q5, W6, W28, P95, or W96 with alanines completely abolished binding of OlyA to liposomes, while replacement of D93, S94, T100, G70, T71, or T72 with alanines retained specific binding of OlyA to membrane containing SM and cholesterol (Fig 2-4 e). Mutation of K99 to alanine resulted in partial reduction of OlyA binding, while mutation to oppositely-charged glutamate completely abolished binding. We also tested these OlyA mutants for their ability to lyse RBCs in a PlyB-dependent manner and found that mutations that disrupted OlyA binding to membranes in the dot blot assay also disrupted their PlyB-mediated hemolytic capacity, whereas mutations that did not disrupt OlyA binding to membranes did not affect hemolysis (Fig. 2-5). It is worth emphasizing that OlyA binding is abolished by mutation of either W28 or K99, residues that form the boundaries of the shallow channel housing the putative SM density (Fig 2-4 b).

Unexpectedly, mutation of E69 to alanine abolished the cholesterol specificity of OlyA(WT). This mutant protein, designated as OlyA(E69A), bound to membranes containing SM whether or not they also contained cholesterol or epicholesterol (Fig 2-4 e). The specificity for

SM was still intact, since no binding was observed to membranes containing DOPC. To further understand the role of E69, we mutated this residue to every other amino acid, purified each mutant protein, and tested for their lipid specificity. The cholesterol dependence for OlyA(WT) binding was abolished only when E69 was replaced by alanine or serine, both of which have similar small side-chains (Fig 2-6 a). However, replacement with even smaller glycine did not affect OlyA's cholesterol specificity, while replacement with oppositely charged arginine or similarly charged but smaller aspartate completely eliminated OlyA binding. To understand how both the size and charge of E69 combine to confer cholesterol specificity on OlyA(WT)'s binding pocket, we performed structural analysis of OlyA(E69A), one of the two mutations that abolished cholesterol specificity. OlyA(E69A) was purified (Fig 2-6 b-d) and crystallized in the presence of lipids, using procedures described above for OlyA(WT). In contrast to OlyA(WT), which only formed crystals in the presence of ammonium chloride, OlyA(E69A) only formed crystals in bis-tris buffers (pH 5.5) containing lithium sulfate. These crystals were used to determine the structure of OlyA(E69A) at a resolution of 1.80 Å (Table 2-1).

A single amino acid (E69) determines SM/cholesterol specificity of OlyA: The structures of OlyA(E69A) (Fig 2-7 a) and OlyA(WT) (Fig 2-4 a) were virtually super-imposable (root-mean-squared deviation of just 0.26 Å for 137 aligned C-α atoms). We once again observed extra electron density in one of the four OlyA(E69A) monomers in the crystallographic asymmetric unit. The density was located in the same shallow channel bordered by W28 and K99 where we had previously observed density in the structure of OlyA(WT) (Fig 2-7 b). In the case of OlyA(WT), the density was assigned to a portion of SM containing the ceramide base (Fig 2-4 c). However, in the case of OlyA(E69A), the observed density was fit best by a molecule of bis-tris (Fig 2-7 c), which was present at high concentrations (100 mM) in the crystallization buffers for OlyA(E69A). Bis-tris was not used in the purification or crystallization buffers for OlyA(WT) crystals.

Inasmuch as the structure of bis-tris (Fig 2-7 c) shares some common features with the structure of the ceramide base portion of SM (Fig 2-4 b), we speculate that the shallow channels in both OlyA(WT) and OlyA(E69A) constitute a binding "hot spot" that accommodates SM. When we compared the location and orientation of amino acids within 5Å of the center of the shallow channel, we observed that the E69A mutation resulted in three significant differences between the two structures (overlay in Fig 2-7 d). Two of the differences were in the orientation of the side chains of channel-bordering K99 and W28. The third difference was in the orientation of the side chain of Q5, which lies on the protein surface on the side opposite to the shallow channel and was previously shown to be required for specific binding of OlyA(WT) (Fig 2-4 e).

To better understand the altered lipid binding surface of OlyA(E69A), we carried out a detailed comparison of the binding affinities of OlyA(WT) and OlyA(E69A). A dose curve analysis showed that OlyA(E69A) had an ~100-fold greater concentration sensitivity than OlyA(WT) for binding to SM-containing membranes (Fig 2-8 a). When compared to OlyA(WT), the association rate of OlyA(E69A) for SM/cholesterol membranes was only ~3-fold higher (Fig 2-8 b), suggesting that a much slower dissociation rate from the membrane likely determines the increased binding affinity of OlyA(E69A). We then carried out a detailed analysis of the varying ligand specificities of OlyA(WT) and OlyA(E69A). First, we tested the specificity of both proteins for various structural features of SM. We measured binding to a panel of liposomes, each of which contained equimolar amounts of cholesterol and phospholipids with identical oleic acid acyl chains but varying headgroups (Fig 2-8 c, left). Both OlyA(WT) and OlyA(E69A) only bound to membranes containing cholesterol and C16 ceramide-based SM and showed no binding to membranes containing glycerol-based phospholipids with choline, ethanolamine, serine, inositol, glycerol, or phosphatidic acid headgroups. We then examined the effect of varying the length of the amide-linked acyl chain of SM in liposomes composed of 50 mole% cholesterol and 50 mole%

SM (Fig 2-8 c, right). Both OlyA(WT) and OlyA(E69A) bound strongly to membranes containing SM with 18:1, 24:0, or 24:1 amide-linked chains. Binding of OlyA(WT), but not of OlyA(E69A), was reduced by >75% when the membranes contained SM with 16:0 or 18:0 amide-linked chains, and binding of both proteins was reduced by > 80% when membranes contained SM with short 2:0 or 6:0 chains. Binding was also eliminated when SM was replaced by lyso-sphingomyelin, erythro-sphingosine, or naturally-derived mixtures of ceramides, gangliosides, or cerebrosides (Fig 2-8 d).

The all-or-none difference observed in Fig 2-8 c for OlyA binding to membranes with SM compared to those with DOPC was striking considering both phospholipids have identical choline headgroups that extend out of the lipid bilayer (see Fig 2-1 c). We also tested whether the acyl chain composition of PC would affect binding, but did not observe any binding of OlyA(WT) or OlyA(E69A) to membranes composed of PCs with various acyl chain combinations (16:0 – 16:0, 16:0 – 18:1, 18:0 – 18:1, or 18:1 – 18:1) without and with cholesterol (Fig 2-9 a). To study the effects of phosphatidylcholines on SM/cholesterol interactions in membranes, we measured OlyA binding to three-component liposomes comprised of cholesterol, SM with a C16 ceramide chain and an 18:1 amide-linked chain, and phosphatidylcholine with 16:0 – 18:1 acyl chains (POPC). When cholesterol was absent or present at a low concentration of 20 mole%, OlyA(WT) showed no binding to POPC/SM membranes whereas binding of OlyA(E69A) increased in a linear fashion as the fraction of SM increased (Fig 2-9 b). When the cholesterol content was raised to 40 mole% or 60 mole%, we observed increased binding of OlyA(WT) as the fraction of SM increased and this binding reached a plateau value when the ratio of cholesterol to SM was between 1:1 and 2:1 (Fig 2-9 b). At these higher cholesterol concentrations, the binding of OlyA(E69A) retained its linear dependence on the fraction of SM and did not show sharp plateaus as observed for OlyA(WT). These results suggest the presence of SM/cholesterol complexes in membranes

containing high amounts of competing phospholipids such as POPC, consistent with earlier studies showing that cholesterol interacts better with SM than other phospholipids [81, 96].

We then tested the specificity of OlyA(WT) and OlyA(E69A) for various structural features of cholesterol by measuring binding to a panel of liposomes, each of which contained equimolar amounts of SM with an 18:1 amide-linked chain and various sterols (structures shown in Fig 2-1 c). As expected, OlyA(E69A) showed no sterol specificity and bound equally well to SM-containing membranes without or with any of the panel of sterols tested here (Fig 2-9 c). In contrast, OlyA(WT) did not bind to membranes without any sterols and showed sharp specificity for distinct structural features of cholesterol. OlyA(WT) bound to membranes containing cholesterol, but not epicholesterol where the 3-hydroxyl is in the opposite α-orientation. Binding was reduced by > 80% when the structure of the steroid nucleus was altered (dihydrocholesterol, lanosterol, ergosterol). Modification of the iso-octyl side chain with a polar group (25-hydroxycholesterol) eliminated OlyA(WT) binding, whereas modification with a double bond (desmosterol) did not affect binding. Adding an ethyl group (sitosterol) increased binding by ~2-fold. The structural specificity is consistent with previously proposed requirements for optimal interactions of SM with cholesterol: i) 3-hydroxyl group in the α-orientation which allows for hydrogen bond formation with the amide nitrogen on SM [126], ii) a "smooth" steroid nucleus that can pack optimally with the SM acyl chains [12, 86], and iii) a non-polar iso-octyl side chain that anchors cholesterol in membranes and interacts with the acyl chain of SM [10, 12].

We then probed the temperature dependence for binding to SM/cholesterol membranes and observed that binding of OlyA(WT), but not that of OlyA(E69A), was reduced by ~70% when the temperature was raised from 23°C to 37°C (Fig 2-9 d). When binding to SM/epicholesterol membranes was measured, we obtained results consistent with the specificity previously observed

for the two proteins (Fig 2-9 c). OlyA(WT) showed no binding at any temperatures, whereas OlyA(E69A) showed strong binding that was not affected by temperature. The circular dichroism spectra for OlyA(WT) and the cholesterol concentration dependence for OlyA(WT) binding were similar at 23°C and 37°C (Fig 2-9 e, f). This suggests that OlyA(WT)'s lowered binding to SM/cholesterol membranes at higher temperatures is not simply due to denaturation of the protein or changes in SM/cholesterol complex stoichiometries, but rather due to dissociation of SM/cholesterol complexes in the membrane. OlyA(E69A) does not show significant temperature dependence because it has lost specificity for SM/cholesterol complexes and can also bind to SM that is free from association with cholesterol. The strong temperature dependence of OlyA(WT) binding is consistent with previous scanning calorimetry analysis of model cholesterol/phospholipid membranes [3, 60, 84] and measurements of membrane cholesterol accessibility to cyclodextrins at various temperatures [102], the results from which were accounted for in terms of formation of complexes with exothermic heats of formation of 6-9 kcal/mol of phospholipid.

Binding pockets in OlyA(WT) and OlyA(E69A) accommodate distinct conformations of SM: Our results so far suggest that OlyA(WT) binds SM/cholesterol complexes, but not uncomplexed SM, and that mutation of E69 to alanine abolishes this specificity. However, we have not observed any electron density in the OlyA(WT) structure that could be attributed to any part of cholesterol. This raises the possibility that OlyA(WT) directly binds only to SM and that cholesterol specificity arises indirectly because OlyA(WT) distinguishes SM's conformation when bound to cholesterol from SM's conformation when free from cholesterol. To address this possibility, we performed comparative docking simulations of OlyA(WT) and OlyA(E69A). For the docking ligand, we used a portion of SM containing the phosophocholine headgroup and part of the ceramide base and N-linked acyl chain (Fig 2-10 a, red). We did not include the rest of the

ceramide or N-linked acyl chains to minimize non-specific associations of these hydrophobic, membrane-embedded flexible chains with soluble, membrane surface-scanning OlyA proteins. For the docking surface, we used portions of OlyA(WT) and OlyA(E69A) centered on the shallow lipid-binding channel (Fig 2-4 b, 2-7 b) and extended out by 5 Å in all directions.

The docking simulations generated distinct models for binding of the SM fragment to OlyA(WT) and OlyA(E69A). For OlyA(WT), the top 100 binding poses clustered to yield a binding model where the positively-charged choline of SM forms an ionic interaction with E69 and the rest of the SM fragment is stably nestled in the shallow channel bordered by W28 and K99 (top 10 poses in Fig 2-11, topmost pose in Fig 2-10 b). Binding is further stabilized by an interaction between the nitrogen of the K99 sidechain and the carbonyl oxygen on SM's amide-linked acyl chain. Using this model for binding of SM to OlyA(WT) at the membrane surface, we extrapolated the rest of SM's acyl chains into the core of a hypothetical lipid bilayer. The result is schematically shown in Fig 2-10 c where OlyA(WT) is oriented such that its N-to-C axis forms an angle of 26° with the bilayer surface. In this orientation, the choline group of OlyA(WT)-bound SM is parallel to the bilayer surface, possibly interacting with the cholesterol headgroup and steroid nucleus.

For OlyA(E69A), the top 100 binding poses of the SM fragment once again clustered in the same shallow channel, but in an orientation opposite to that observed for OlyA(WT) (top 10 poses in Fig 2-11, topmost pose in Fig 2-10 d). This difference arises due to elimination of E69 and alterations in the lipid-binding channel of OlyA(E69A) caused by the different configurations of W28 and K99 (Fig. 2-7 b, d). The carbonyl oxygen on the amide-linked acyl chain of SM can still interact with the nitrogen of the K99 sidechain, however the choline of SM is no longer stabilized by E69 and flips to the opposite end of the channel. Using this different model for

binding of SM to OlyA(E69A) at the membrane surface, we extrapolated the rest of SM's acyl chains into a hypothetical bilayer as shown in Fig 2-10 e. In this model, OlyA(E69A) is oriented such that its N-to-C axis is almost perpendicular to the bilayer surface, and the choline group of OlyA(E69A)-bound SM is also perpendicular to the bilayer in a conformation that may be adopted by SM when free from cholesterol. Steric clashes prevent fitting of the OlyA(E69A)-bound SM conformation into the binding channel of OlyA(WT). In contrast, there is no steric hindrance to fitting the OlyA(WT)-bound SM conformation into the binding channel of OlyA(E69A). We speculate that OlyA(E69A) can recognize both the cholesterol-free and cholesterol-bound conformations of SM whereas OlyA(WT) only detects cholesterol-bound SM.

To detect the distinct membrane-bound orientations of OlyA(WT) and OlyA(E69A) predicted by the docking simulations, we assayed for the membrane proximity of the sole cysteine residue at the COOH-terminus of each of these proteins when bound to 1:1 SM:cholesterol or SM membranes. We probed for accessibility of OlyA's cysteine using mPEG-MAL-5000, a high molecular weight membrane-impermeable reagent that forms a covalent bond with exposed cysteines and causes proteins to migrate with higher molecular weight on SDS/PAGE [75]. After incubation with liposomes, liposome-bound OlyA(WT) and OlyA(E69A) were isolated by centrifugation and treated with mPEG-MAL-5000. As controls, both proteins were incubated in solutions without liposomes and then treated with mPEG-MAL-5000. When in solution, we observed mPEG-MAL-5000 modification of both OlyA(WT) and OlyA(E69A) (Fig 2-10 f, g, lanes 1-4). However, when bound to SM/cholesterol liposomes, mPEG-MAL-5000 did not react with either OlyA(WT) or OlyA(E69A) (Fig 2-10 f, g, lanes 5-8). In contrast, when bound to 100% SM liposomes, OlyA(E69A) was modified by mPEG-MAL-5000 to a degree similar to that observed for OlyA(E69A) in solution (Fig 2-10 g, lanes 1-4, 9-12). Our interpretation of these results are summarized in the schematic of Fig 2-10 h and support a model where OlyA(E69A)

can adopt two different orientations on membranes to recognize both cholesterol-free and cholesterol-bound SM conformations whereas OlyA(WT) only detects the cholesterol-bound conformation of SM. We did not observe any modification of OlyA(E69A) when it was bound to 1:1 SM:cholesterol liposomes because most of the SM in these bilayers was likely complexed to cholesterol and not in a free form.

Further insight into OlyA's SM-binding pocket was gained by comparison to structures of Sticholysin II (Stn), an ~20 kDa soluble protein that belongs to the equinatoxin family, members of which bind SM in membranes but show no requirement for cholesterol (Fig 2-1 b and ref. [138]). Structures of Stn have been determined in its ligand-free state (PDB 1O71) and in a state bound to phosphocholine (POC), the headgroup of SM (PDB 1O72) [80]. The primary sequences of Stn and OlyA are only 11% identical, but when we compared the structure of Stn to cholesterol-insensitive OlyA(E69A), we found that they superimposed well with a root-mean-squared deviation of just 2.2 Å for 115 aligned C-α atoms. Moreover, the POC binding pocket in Stn is also bounded by two loops connecting β-strands, in a structurally equivalent location as the SM binding pockets in OlyA(WT) and OlyA(E69A). Despite these similarities, several key differences provided clues into the differential lipid specificity of these pockets (Fig 2-12). The binding pocket in Stn is larger than in OlyA(WT) or OlyA(E69A), and is more electropositive, primarily due to an arginine residue (R51). Removal of the negatively-charged sidechain in the OlyA(E69A) mutant does not drastically change the electrostatic properties of the interior of the pocket, but it does enlarge the pocket in this mutant. It is possible that the pocket in OlyA, which is exquisitely formed to bind to the very specific conformation of SM found in SM/cholesterol complexes, loses this specificity when enlarged in the E69A mutant, and can accommodate a wider range of SM conformations, both bound to and free from cholesterol. Mutations of residues in or

near the binding pocket of OlyA (Q5, W6, W28, P95 and W96) likely deform the pocket enough to entirely abolish binding of SM (Fig 2-4 e).

Cholesterol specificity of OlyA(E69A) can be restored by additional mutations: When we compared the structures of OlyA(WT) and OlyA(E69A), we observed significant differences in the orientations of three amino acid side chains : Q5, W28 and K99 (Fig 2-7 d). To further understand the SM binding pocket and the role of individual residues in determining SM and cholesterol specificity, we generated mutant versions of OlyA(WT) and OlyA(E69A) where each of the above three residues were individually mutated. We tested the binding of these mutants to SM-containing membranes using dot blot assays. Mutation of W28 to alanine in either OlyA(WT) or OlyA(E69A) completely abolished binding (Fig 2-13 a, top). Surprisingly, mutation of K99 to glutamate or Q5 to alanine, both of which abolished binding of OlyA(WT) to liposomes, resulted in restoration of cholesterol specificity of OlyA(E69A) (Fig 2-13 a). This observation is not a result of a dilution effect, since we observe cholesterol specificity was retained on the E69A double mutants at 10 times the concentration used in the above experiment (Fig 2-13 b). When we tested these mutants for their PlyB-dependent hemolytic ability, we observed results consistent with the dot blot assay (Fig 2-13 c). While Q5A and K99E mutations resulted in no hemolysis in OlyA(WT) as seen before, the hemolytic ability was comparable to OlyA(WT) when the mutations were made in OlyA(E69A). The orientation of W28 is critical in the formation of SM-binding channel in both Oly(WT) and OlyA(E69A) (Fig 2-4 b, 2-7 b). Mutation to alanine possibly collapses the entire channel and renders the protein inactive in both cases. On the other hand, it is interesting that the mutations Q5A and K99E possibly change the SM-binding channel on OlyA(E69A) in a way that it can no longer accommodate the cholesterol-free conformation of SM while retaining the ability to bind to the cholesterol-bound conformation of SM (Fig 2-10).

TABLE 2-1

Data collection			
Crystal	OlyA(WT)	OlyA(WT) + lipids	OlyA(E69A) + lipids
PDB accession code	6MQI	6MQJ	6MQK
Space group	$P2_1$	$P2_1$	C2
Cell constants	46.43 Å, 100.33 Å, 59.02 Å, 106.43°	46.43 Å, 100.56 Å, 58.81 Å, 106.29°	69.86 Å, 86.68 Å, 92.88 Å, 99.13°
Wavelength (Å)	0.97926	0.97926	0.97903
Resolution range (Å)	33.30 – 1.15 (1.17 – 1.15)	44.56 – 1.33 (1.36 – 1.33)	49.27 – 1.80 (1.83 – 1.80)
Unique reflections	181,403 (8,891)	117,866 (5,878)	47,399 (1,701)
Multiplicity	6.4 (6.0)	7.5 (7.2)	5.2 (3.9)
Data completeness (%)	98.6 (96.8)	99.4 (99.7)	93.4 (68.4)
R_{merge} (%)[a]	4.4 (43.0)	4.9 (46.2)	3.9 (43.8)
R_{pim} (%)[b]	1.8 (31.3)	1.8 (17.0)	1.8 (23.3)
$CC_{1/2}$ (last resolution shell)	0.78	0.91	0.89
I/σ(I)	37.7 (2.4)	41.6 (4.0)	38.2 (2.2)
Wilson *B*-value (Å^2)	15.1	13.5	18.1
Refinement statistics			
Resolution range (Å)	33.30 – 1.15 (1.19 – 1.15)	44.56 – 1.33 (1.36 – 1.33)	49.27 – 1.800 (1.86 – 1.80)
No. of reflections R_{work}/R_{free}	166,128/1,451 (7,433/66)	117,716/2,000 (8,086/140)	41,217/1,401 (2,181/77)
Data completeness (%)	90.7 (41.0)	99.3 (97.0)	81.4 (44.0)
Atoms (non-H protein/metal ions/ligand/solvent/waters)	4,272/4/NA/44/626	4,253/4/10/80/554	4,204/4/NA/66/503
R_{work} (%)	14.2 (20.5)	15.5 (20.8)	19.4 (25.4)
R_{free} (%)	16.1 (26.9)	16.8 (22.8)	21.9 (31.3)
R.m.s.d. bond length (Å)	0.018	0.016	0.004
R.m.s.d. bond angle (°)	1.15	0.95	0.62
Mean B-value (Å^2) (chains A/B/C/D/metal ions/ligand/solvent/waters)	17.3/20.6/20.9/20.0/28.4 NA/28.7/29.8	19.7/19.9/19.9/17.1/32.5 /63.7/29.8/27.0	15.7/27.1/25.3/27.9/31.7 40.4/36.1/29.1

Ramachandran plot (%) (favored/additional/disallowed)[c]	97.8/2.3/0.0	97.6/2.4/0.0	96.6/3.2/0.2
Clashscore/Overall score[c]	2.44/1.06	1.62/0.91	1.66/1.13
Maximum likelihood coordinate error	0.09	0.11	0.21
Missing residues	A:1. B:1-3. C:1-2, 66. D:137-138.	A:1-2, 138. B:1-2, 138. C:1-3. D:1.	A:1, 137-138. B:1. C:1, 137-138. D:1, 137-138.

Table 1. Data collection and refinement statistics for OlyA

Data for the outermost shell are given in parentheses.

[a]$R_{merge} = 100\ \Sigma_h\Sigma_i|I_{h,i} - \langle I_h\rangle|/\Sigma_h\Sigma_i\ \langle I_{h,i}\rangle$, where the outer sum (h) is over the unique reflections and the inner sum (i) is over the set of independent observations of each unique reflection.

[b]$R_{pim} = 100\ \Sigma_h\Sigma_i\ [1/(n_h - 1)]^{1/2}|I_{h,i} - \langle I_h\rangle|/\Sigma_h\Sigma_i\ \langle I_{h,i}\rangle$, where n_h is the number of observations of reflections **h**.

[c]As defined by the validation suite MolProbity [27].

FIGURE 2-1

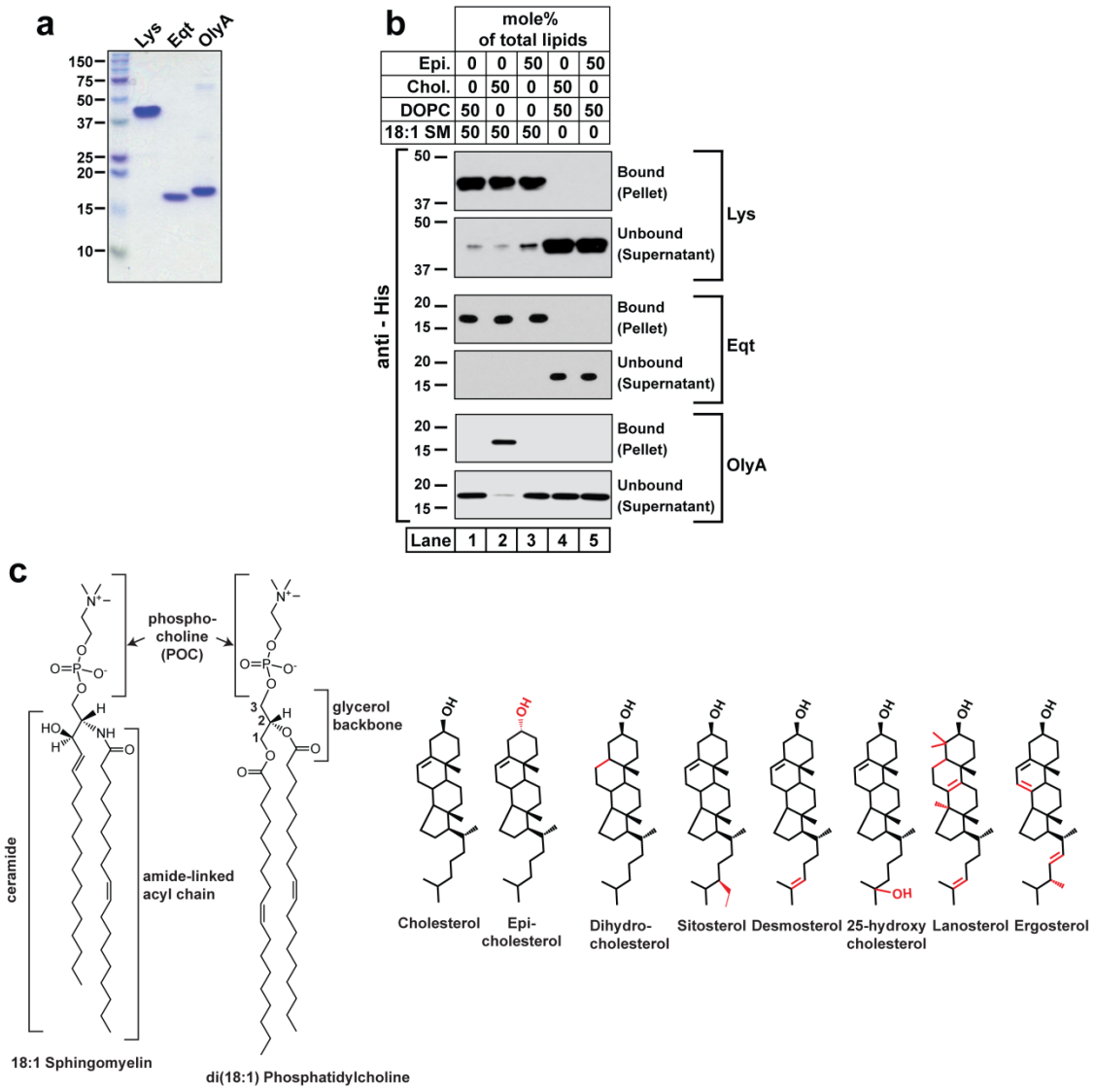

FIGURE 2-1: Identification of a sensor for sphingomyelin-cholesterol complexes. a, Purified SM sensors. Recombinant Lys-His6, His6-Eqt II, and OlyA-His6 were overexpressed and purified as described in Methods. Aliquots (2 µg each) were subjected to 15% SDS-PAGE and proteins were visualized with Coomassie stain. **b,** Lipid specificity. Each liposome binding reaction, in a final volume of 200 µl of buffer A, contained 1 µg of Lys-His6, His6-Eqt II, or OlyA-His6 and 1560 µM liposomes with the indicated compositions. After incubation for 1h at room temperature,

liposome-bound proteins were measured using a pelleting assay. **c,** Chemical structures of phospholipids and sterols used in this study. Various structural features of sphingophospholipids (18:1 sphingomyelin) and glycerophospholipids (di(18:1) phosphatidylcholine) are labeled. The three carbons of the glycerol backbone are also indicated. Chol., cholesterol; Epi., epicholesterol.

FIGURE 2-2

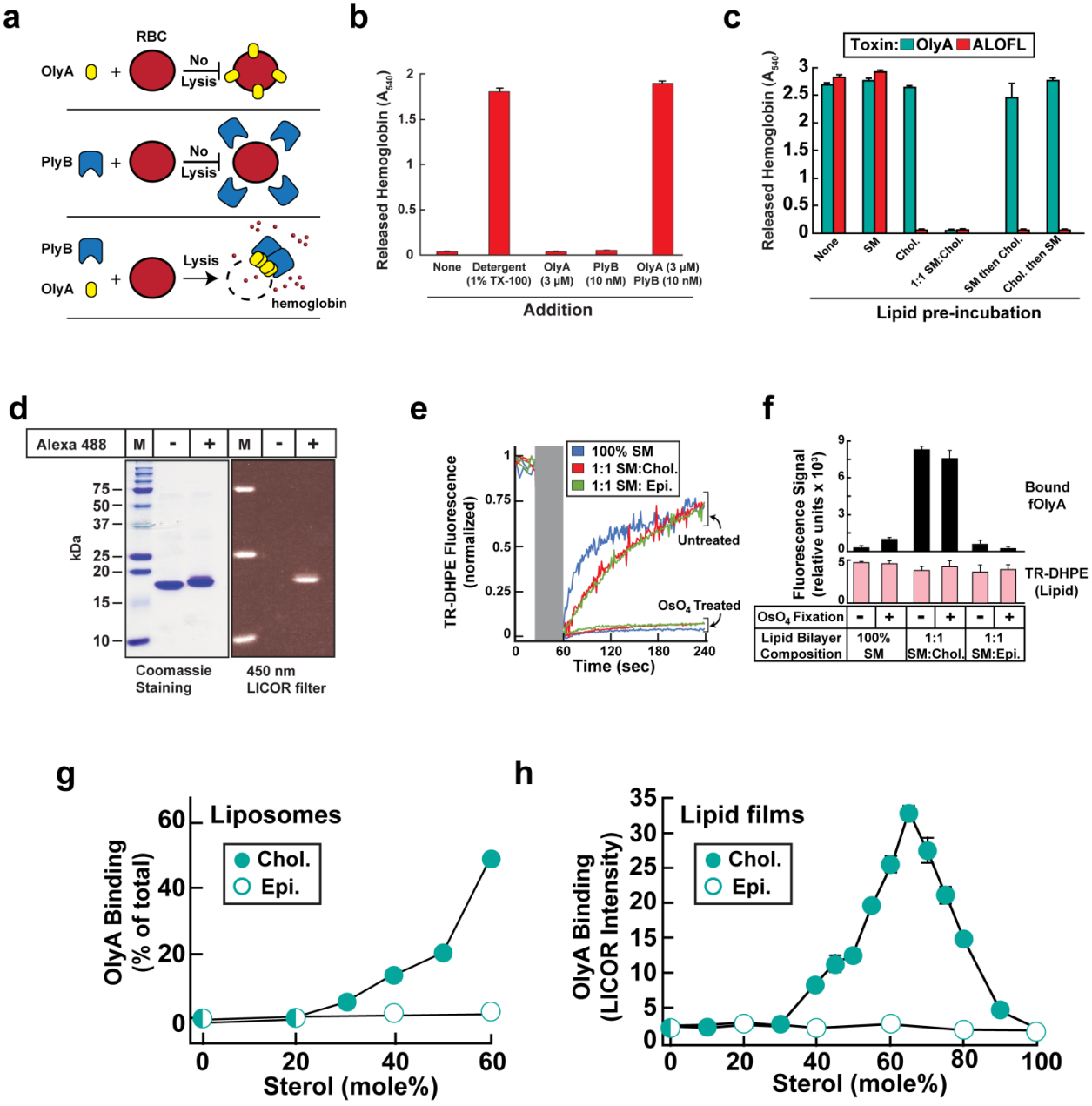

FIGURE 2-2: OlyA senses sphingomyelin-cholesterol complexes in membranes. a, Schematic of dual requirement of OlyA and PlyB for pore formation in RBC membranes. **b,** Hemolysis assays. Recombinant OlyA-His6 and His8-PlyB were overexpressed and purified as described in Methods. Each reaction, in a total volume of 500 µl of buffer C, contained 450 µl of rabbit RBCs

washed and diluted as described in Methods and the indicated concentrations of OlyA, PlyB, or Triton X-100 detergent. After incubation on a rotator for 30 min at room temperature, each reaction was subjected to 2000 x g centrifugation for 15 min at room temperature, following which an aliquot of the supernatant (100 µl) was assayed for released hemoglobin (absorbance at 540 nm). **c,** Hemolysis inhibition assay to measure solution binding of SM and cholesterol to OlyA and ALOFL. In each reaction, 0.6 µmol of either 18:1 SM or cholesterol, or 1.2 µmol of an equimolar mixture of 18:1 SM and cholesterol, were dried on the sides of a tube, after which 50 µl of buffer A containing either OlyA (3 µM) or ALOFL (30 nM) was added. Following overnight incubation, tubes containing OlyA were supplemented with PlyB (10 nM) and then all tubes received 450 µl of buffer C containing ~3 x 108 RBCs. After incubation for 30 min, each reaction was subjected to 2000 x g centrifugation for 15 min and an aliquot of the supernatant (100 µl) was assayed for released hemoglobin (absorbance at 540 nm). For testing sequential addition, after overnight incubation of proteins with either 18:1 SM or cholesterol, the contents of the assay tubes were transferred to another tube containing dried cholesterol or 18:1 SM, respectively, and the remainder of the assay was carried out as above. **d,** Recombinant OlyA(WT) was purified and labeled with Alexa Fluor 488 maleimide as described in Methods. Aliquots (2 µg each) were collected before and after the labeling reaction, subjected to 15% SDS-PAGE, and proteins were visualized with Coomassie stain (left) or by fluorescence scanning (450 nm channel) (right). **e-f,** Dependence of OlyA binding on membrane lipid mobility. **e,** Supported bilayers of the indicated lipid compositions containing 0.2 mole% TR-DHPE (fluorescent lipid) were generated in glass-bottom 96-well plates and lateral fluidity of lipid molecules was measured by fluorescence recovery after photobleaching (FRAP) before and after fixation with osmium tetroxide. Gray bar denotes the 30s photobleaching step. Shown are averages of fluorescence values from three different regions in a well. **f,** Unfixed and osmium tetroxide-fixed supported bilayers of the

indicated lipid composition were incubated with 5 μg of fOlyA for 30 min, after which fluorescence of membrane-bound fOlyA and TR-DHPE was measured as described in Methods. Values shown are averages of binding to four different wells. **g-h,** Dependence of OlyA binding on SM:cholesterol ratio. **g,** Binding to liposomes containing SM and varying molar concentrations of the indicated sterol was measured as in b, except that the incubation time was 4 h. **h,** Binding to lipid films. Ethanolic solutions of varying molar ratios of SM and the indicated sterol were prepared and 80 nmol of each mixture was deposited on nitrocellulose membranes and allowed to dry for 5-10 min. Each membrane strip was then subjected to dot blot analysis as described in Methods to measure bound OlyA. Values shown are averages of triplicate assays. Chol., cholesterol; Epi., epicholesterol.

FIGURE 2-3

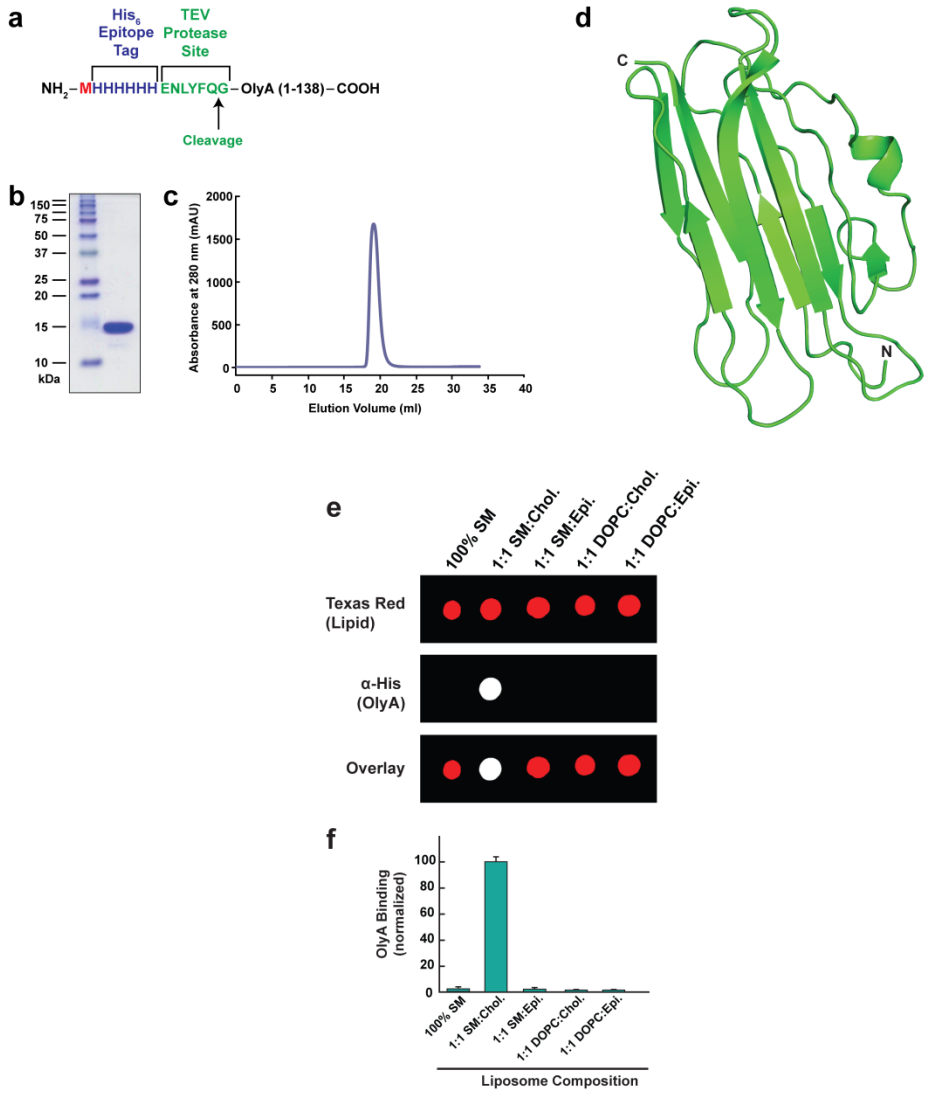

FIGURE 2-3: Purification of OlyA(WT) for crystallography, structure of OlyA(WT) and dot blot assay with OlyA(WT). a, Schematic of recombinant wild-type OlyA plasmid overexpressed in E. Coli. Starting at the NH_2-terminus, pHis_6-TEV-OlyA(WT) contains a His6 epitope tag, a TEV protease cleavage site, and OlyA (aa 1-138). **b,** His_6-TEV-OlyA was purified and cleaved with TEV protease as described in Methods to generate tag-free OlyA, an aliquot (5 µg) of which was subjected to 15% SDS-PAGE, after which the protein was visualized with Coomassie stain.

c, gel filtration chromatography of tag-free OlyA on a Superdex 200 column. **d,** Overall structure of wild-type OlyA (green) in the absence of lipid ligands. **e-f,** Dot blot assay for OlyA binding to liposomes. Liposomes of the indicated compositions, each containing 0.02 mole% of Texas Red DHPE, were deposited on nitrocellulose membranes and allowed to dry for 5-10 min. Each membrane strip was then incubated for 1h at room temperature with OlyA-His6 (1 μg/ml) and subjected to anti-His immunoblot analysis as described in Methods. LICOR imaging was used to visualize deposited liposomes (Texas Red, 600 nm channel) (**e, top**) and liposome-bound OlyA-His6 (chemiluminescence channel) (**e, middle**). An overlay of both signals is shown in the bottom panel of **e**. **f,** Quantification of LICOR signal for bound OlyA. The signal intensity from OlyA-His6 bound to liposomes composed of an equimolar mixture of SM and cholesterol (1:1 SM:Chol) was set to 100% and all other binding signal intensities were normalized to this set-point. Values shown are averages of triplicate assays. SM, 18:1 sphingomyelin; Chol., cholesterol; Epi., epicholesterol; DOPC, di(18:1) phosphatidylcholine; N, NH_2-terminus; C, COOH-terminus.

FIGURE 2-4

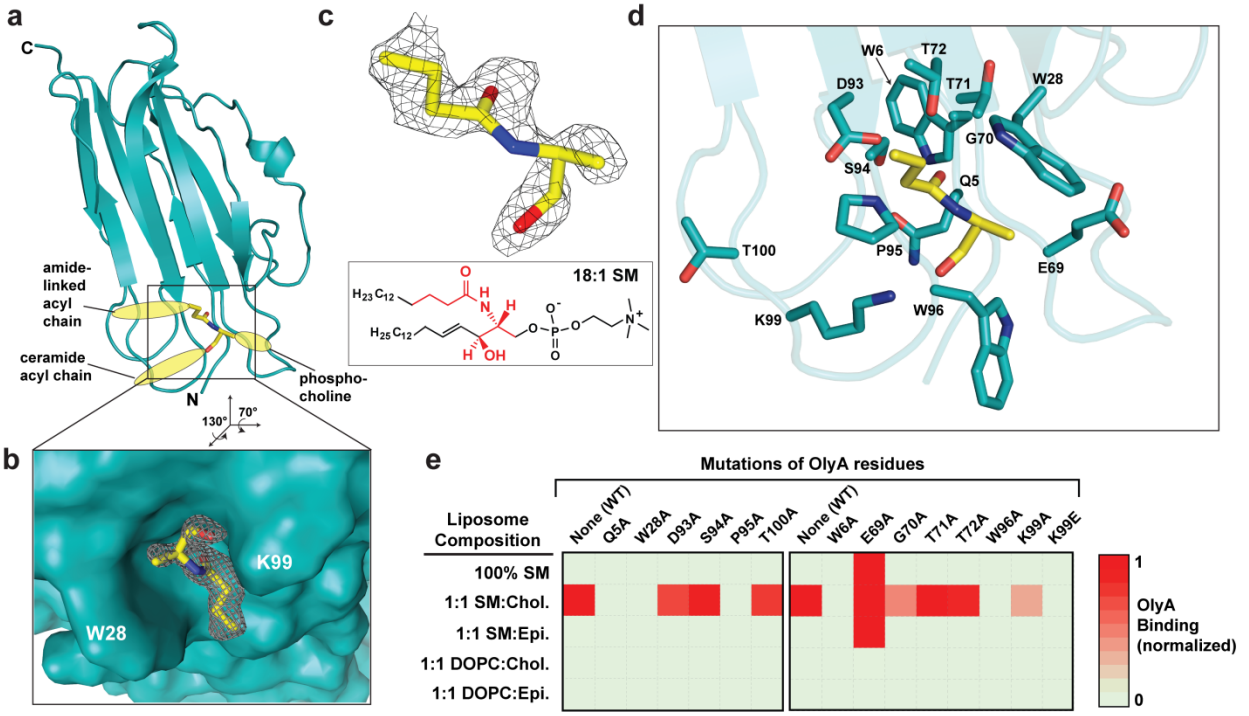

FIGURE 2-4: Structural analysis of SM binding by wild-type OlyA. a, (Top) Overall structure of OlyA (teal) bound to a portion of SM (yellow sticks, see **c**). Possible orientations for the rest of OlyA-bound SM are shown as yellow ovals. **b,** Close-up view of a surface representation of the shallow channel formed by K99 and W28 (boxed region in **a**) which houses the observed electron density (gray mesh, see **c**). **c,** Shown in gray mesh is the |mFo – DFc| electron density calculated after omitting the ligand from the model and contoured at 2.5σ. A portion of 18:1 SM (highlighted in **red**) was superimposed on this electron density. Superimposed on the density is the modeled portion of SM (yellow sticks, see b). **d,** Close-up view of the region of OlyA with bound SM. Side-chains of amino acids that lie within 5 Å of the modeled portion of SM (yellow) are shown as sticks (teal) against a semi-transparent main chain backbone (light teal). **e,** Binding properties of OlyA mutants. Indicated His_6-tagged point mutant versions of OlyA were overexpressed, purified, and their lipid specificities were measured using liposome dot blot assays as described in

Methods. Liposomes of the indicated compositions were deposited on nitrocellulose membranes, the membrane strips were incubated for 1h at room temperature with the indicated versions of OlyA-His_6 (0.5 μg/ml of E69A, 1 μg/ml of all other versions), and then subjected to immunoblot analysis followed by LICOR imaging to measure liposome-bound proteins. The mean value (n = 3) for binding of wild-type (WT) OlyA to liposomes composed of an equimolar mixture of SM and cholesterol was set to 1. All other mean binding values (n = 3) were normalized relative to this set-point and converted to a green-to-red color scale. Standard errors for all measurements were less than 10%. Chol., cholesterol; Epi., epicholesterol; N, NH_2-terminus; C, COOH-terminus.

FIGURE 2-5

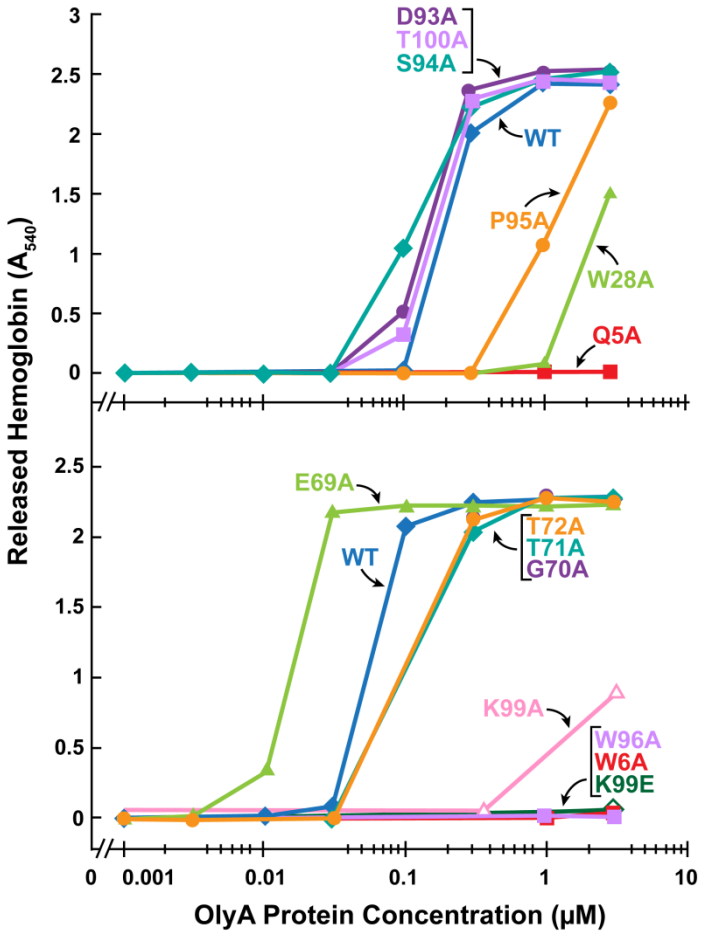

FIGURE 2-5: Effect of mutations on OlyA's PlyB-mediated hemolytic activity. (**top** and **bottom**) Recombinant OlyA-His_6, the indicated mutant versions of OlyA-His_6, and His8-PlyB were overexpressed and purified as described in Methods. Each reaction, in a total volume of 500 µl of buffer C, contained 450 µl of rabbit RBCs washed and diluted as described in Methods, 10 nM of PlyB, and various concentrations of the indicated mutant version of OlyA. After incubation on a rotator for 30 min at room temperature, each reaction was subjected to 2000 x g centrifugation for 15 min at room temperature and an aliquot of the supernatant (100 µl) was assayed for released hemoglobin (absorbance at 540 nm). Values shown are averages of triplicate assays.

FIGURE 2-6

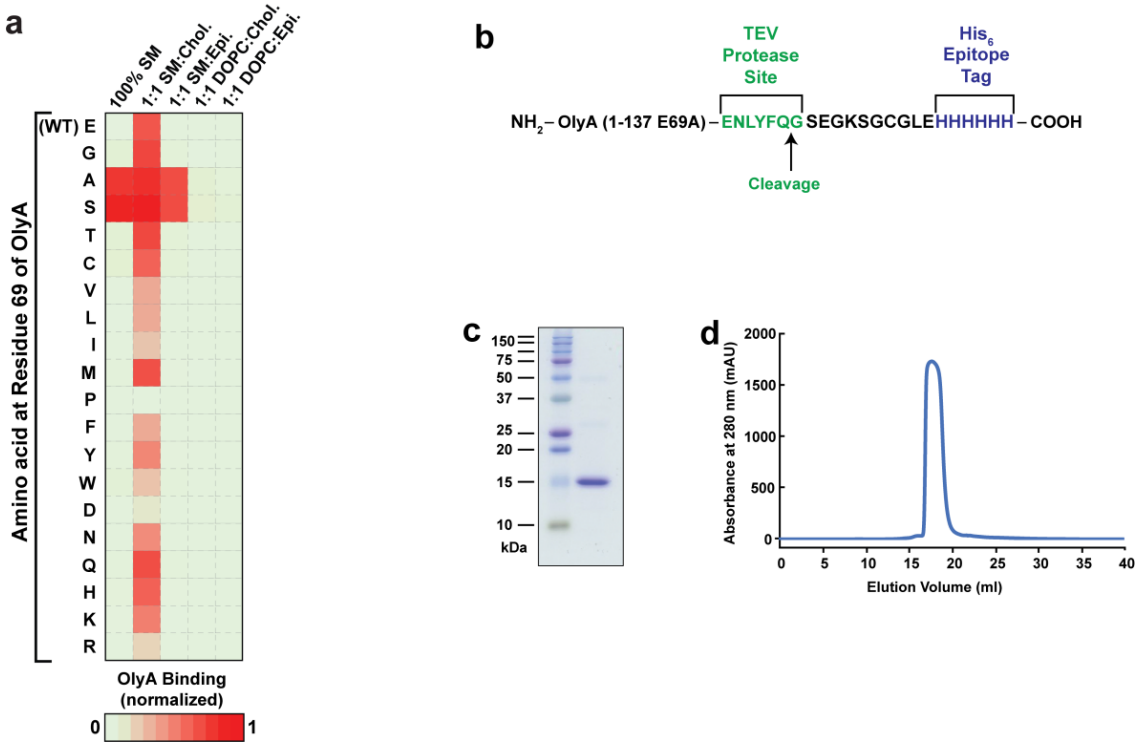

FIGURE 2-6: Effect of mutation of E69 on OlyA's lipid specificity and purification of OlyA(E69A) for crystallization. a, Indicated His_6-tagged point mutant versions of OlyA were overexpressed, purified, and their lipid specificities were measured using liposome dot blot assays as described in Methods. Liposomes of the indicated compositions were deposited on nitrocellulose membranes, the membrane strips were incubated for 1h at room temperature with the indicated versions of OlyA-His6 (0.5 µg/ml of E69A, 1 µg/ml of all other versions), and then subjected to immunoblot analysis followed by LICOR imaging to measure liposome-bound proteins. The mean value (n = 3) for binding of wild-type (WT) OlyA to liposomes composed of an equimolar mixture of SM and cholesterol was set to 1. All other mean binding values (n = 3) were normalized relative to this set-point and converted to a green-to-red color scale. Standard errors for all measurements were less than 10%. **b,** Schematic of recombinant OlyA(E69A) plasmid overexpressed in E. Coli. Starting at the NH2-terminus, pOlyA(E69A)-TEV-His_6

contains OlyA (aa 1-137 with the E69A point mutation), a TEV protease cleavage site, a 10-aa linker, and a His_6 epitope tag. **c,** OlyA(E69A)-TEV-His_6 was purified and cleaved with TEV protease as described in Methods to generate tag-free OlyA(E69A), an aliquot (2 μg) of which was subjected to 15% SDS-PAGE, after which the protein was visualized with Coomassie stain. **d,** gel filtration chromatography of tag-free OlyA(E69A) on a Superdex 200 column.

FIGURE 2-7

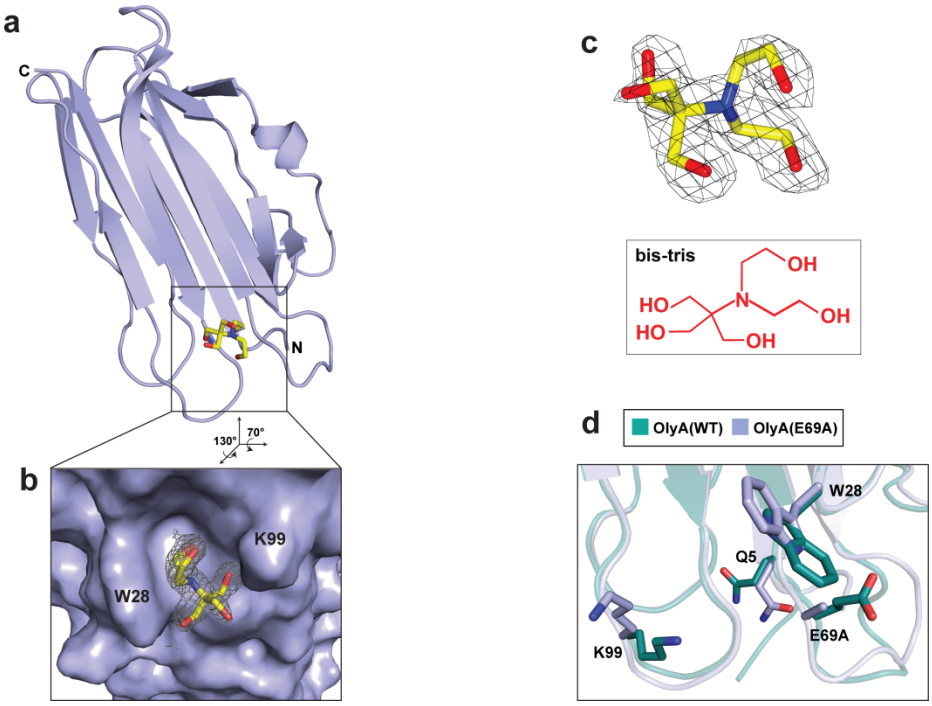

FIGURE 2-7. Structural analysis of SM binding by OlyA(E69A). a, Overall structure of OlyA(E69A) (purple) bound to bis-tris (yellow sticks, see c). **b,** Close-up view of a surface representation of the shallow channel formed by K99 and W28 (boxed region in **a**) which houses the observed electron density (gray mesh, see **c**). Superimposed on the density is the modeled bis-tris structure (yellow sticks, see **c**) **c,** Shown in gray mesh is the |mFo – DFc| electron density calculated after omitting the ligand from the model and contoured at 2.5σ. The structure of bis-tris (highlighted in red) was superimposed on this electron density. **d,** Overlay of the regions containing bound ligands in OlyA(WT) (teal) and OlyA(E69A) (purple). Side-chains of amino acids that have different orientations in the two structures are shown as sticks against a semi-transparent main chain backbone. Chol., cholesterol; Epi., epicholesterol; N, NH_2-terminus; C, COOH-terminus.

FIGURE 2-8

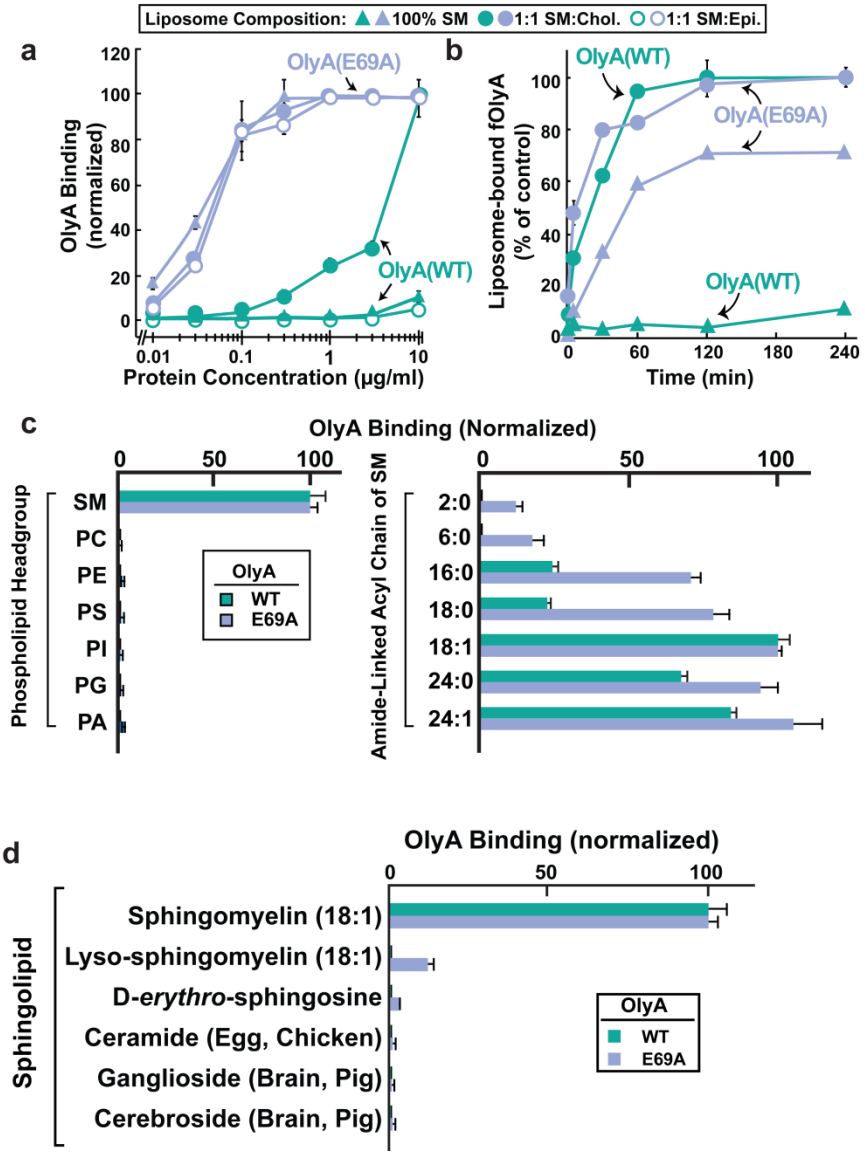

FIGURE 2-8: Comparison of affinities and phospholipid specificities of OlyA(WT) and OlyA(E69A). a, Concentration dependence. Liposomes of the indicated compositions were deposited on nitrocellulose membranes and allowed to dry for 5-10 min. Each membrane strip was then incubated for 1h at room temperature with the indicated concentrations of either OlyA(WT)-His_6 or OlyA(E69A)-His_6 and subjected to anti-His immunoblot analysis followed by LICOR imaging to quantify liposome-bound OlyA (1 µg/ml of OlyA = 57.6 nM). The mean value (n = 3)

for binding of each protein to liposomes composed of 1:1 SM:Chol. at the highest protein concentration was set to 100% and all other mean binding values (n = 3) were normalized relative to these set-points. **b,** Association rates. Liposomes of the indicated compositions, each containing 1 mole% of 18:1 Biotin-PE, were captured on magnetic streptavidin beads and incubated with 0.1 μg of either fOlyA(WT) or fOlyA(E69A). After the indicated times, liposomes were isolated by magnetic pull-down and liposome-bound fOlyA was measured. 100% of control values for fraction of bound proteins were 0.33 for OlyA(WT) and 0.604 for OlyA(E69A). Values shown are averages of triplicate assays. **c-d,** Phospholipid specificity. Liposomes composed of equimolar mixtures of cholesterol and phospholipids with 18:1 acyl chains and the indicated headgroup (**c, left**), cholesterol and SM with the indicated amide-linked acyl chain length (**c, right**), or 50 mole% cholesterol, 25 mole% DOPC, and 25 mole% of the indicated sphingolipid (**d**) were deposited on nitrocellulose membranes. The membrane strips were incubated for 1h at room temperature with either OlyA(WT)-His_6 (1 μg/ml) or OlyA(E69A)-His_6 (0.5 μg/ml), and then subjected to immunoblot analysis followed by LICOR imaging to measure liposome-bound proteins. The mean value (n = 3) for binding of each protein to liposomes composed of cholesterol and 18:1 SM (c) and liposomes composed of 18:1 SM and cholesterol (**d**) were set to 100%. All other mean binding values (n = 3) were normalized relative to these set-points. (a fixed amount of DOPC (25 mole%) was included in all cases to ensure liposome stability). Epi., epicholesterol; Dchol., dihydrocholesterol; Chol., cholesterol.

FIGURE 2-9

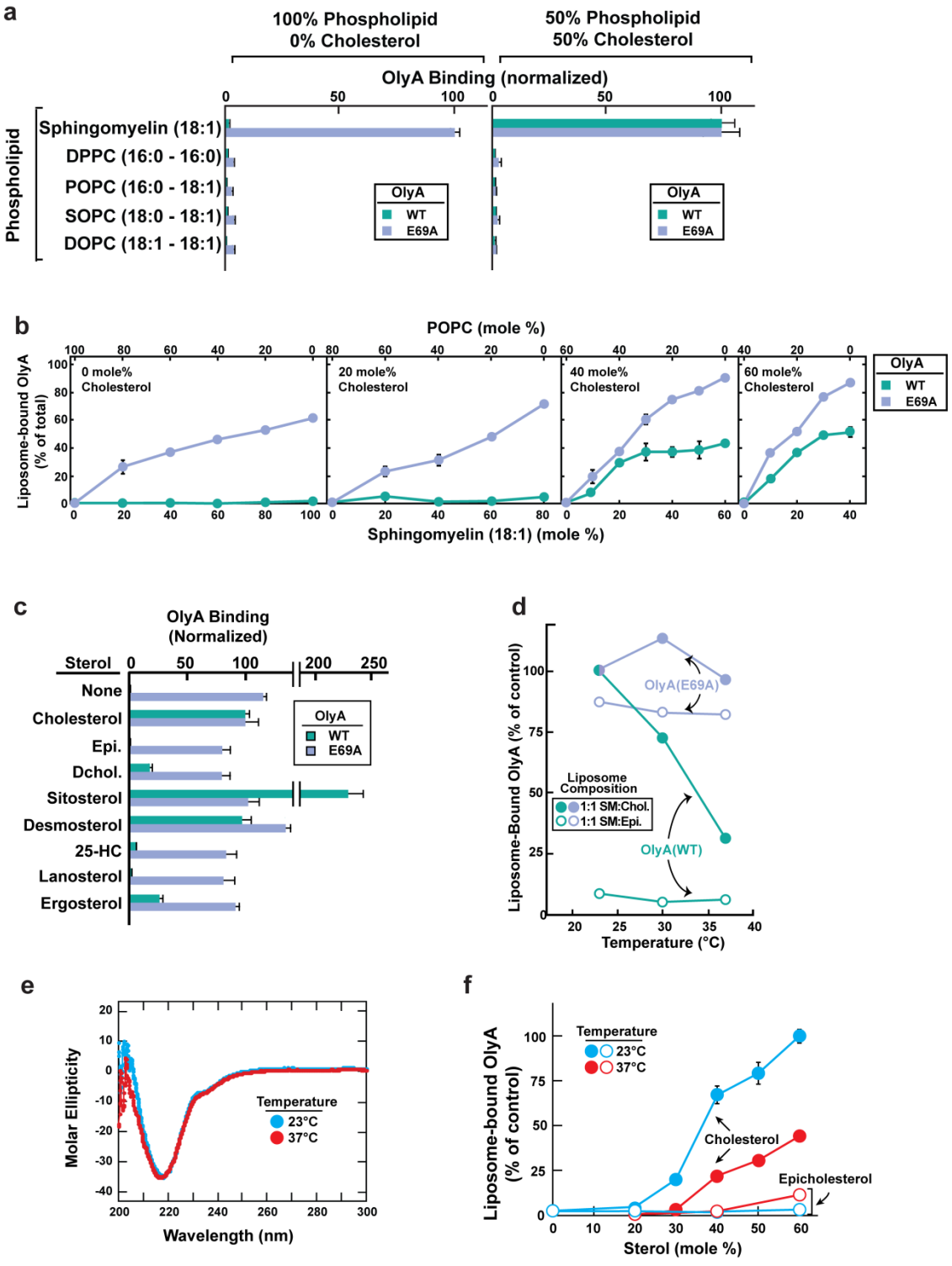
a
100% Phospholipid
0% Cholesterol
50% Phospholipid
50% Cholesterol
OlyA Binding (normalized)
Phospholipid
Sphingomyelin (18:1)
DPPC (16:0 - 16:0)
POPC (16:0 - 18:1)
SOPC (18:0 - 18:1)
DOPC (18:1 - 18:1)
OlyA
WT
E69A
b
POPC (mole %)
0 mole% Cholesterol
20 mole% Cholesterol
40 mole% Cholesterol
60 mole% Cholesterol
Liposome-bound OlyA (% of total)
Sphingomyelin (18:1) (mole %)
c
OlyA Binding (Normalized)
Sterol
None
Cholesterol
Epi.
Dchol.
Sitosterol
Desmosterol
25-HC
Lanosterol
Ergosterol
d
Liposome-Bound OlyA (% of control)
OlyA(E69A)
OlyA(WT)
Liposome Composition
1:1 SM:Chol.
1:1 SM:Epi.
Temperature (°C)
e
Molar Ellipticity
Temperature
23°C
37°C
Wavelength (nm)
f
Liposome-bound OlyA (% of control)
Temperature
23°C
37°C
Cholesterol
Epicholesterol
Sterol (mole %)

FIGURE 2-9: Phospholipid and sterol specificity, and temperature dependence of OlyA. a, Phospholipid headgroup and acyl chain specificity. Liposomes composed of either 100 mole% of the indicated phospholipid without cholesterol or 50 mole% of the indicated phospholipid and 50 mole% cholesterol were deposited on nitrocellulose membranes and allowed to dry for 5-10 min. Each membrane strip was then incubated for 1h at room temperature with the indicated concentrations of either OlyA(WT)-His_6 or OlyA(E69A)-His_6 and subjected to anti-His immunoblot analysis followed by LICOR imaging to quantify liposome-bound OlyA. (**left panel**) Signal intensities from OlyA (E69A) bound to liposomes containing sphingomyelin (18:1) were set to 100% and all other binding signal intensities were normalized to this set-point. (**right panel**) Signal intensities from OlyA proteins bound to liposomes containing 50 mole% sphingomyelin (18:1) and 50 mole% cholesterol were set to 100% and all other binding signal intensities were normalized to this set-point. **b,** OlyA binding to three component liposomes. Each reaction, in a final volume of 200 µl of buffer A, contained 1 µg of either OlyA(WT)-His_6 or OlyA(E69A)-His_6 and 1560 µM liposomes with the indicated mole fractions of sphingomyelin (18:1), cholesterol, and POPC. After incubation for 4h at room temperature, liposome-bound proteins were measured using a pelleting assay as described in Methods. Values shown are averages of triplicate assays. **c,** Liposomes composed of equimolar mixtures of 18:1 SM and the indicated sterol were deposited on nitrocellulose membranes and binding of 1 µg/ml OlyA(WT)-His_6 or 0.5 µg/ml OlyA(E69A)-His_6 was measured as in **a**. The mean value (n = 3) for binding of each protein to liposomes composed of 18:1 SM and cholesterol (d) were set to 100%. **d-f,** Temperature dependence of OlyA. **d,** Each reaction, in a final volume of 200 µl of buffer A, contained 1 µg of OlyA(WT)-His_6 or OlyA(E69A)-His_6 and 1560 µM of liposomes of the indicated compositions. After incubation for 4h at varying temperatures, liposome-bound OlyA was measured using a pelleting assay as described in Methods (centrifugation was also carried out at varying temperatures). 100% of

control values for fraction of bound proteins were 0.604 for OlyA(WT) and 0.704 for OlyA(E69A). Values shown are averages of triplicate assays. **e,** Circular dichroism spectra. Spectroscopic measurements of 110 μg of OlyA(WT)-His_6 in a final volume of 220 μl of buffer A were carried out in a JASCO J-815 CD spectrometer using a 1-mm path length cuvette. The spectra at each indicated temperature represents the average of ten measurements. **f,** Cholesterol dependence of OlyA binding. Liposomes containing 18:1 SM and indicated mole % of cholesterol or epicholesterol were prepared as described in methods and pelleting assays at indicated temperatures were carried out with 1 μg of OlyA(WT)-His_6 as in **d**. The 100% of control value for fraction of bound OlyA-His_6 was 0.62. Values shown are averages of triplicate assays. Epi., epicholesterol; Dchol., dihydrocholesterol; Chol., cholesterol.

FIGURE 2-10

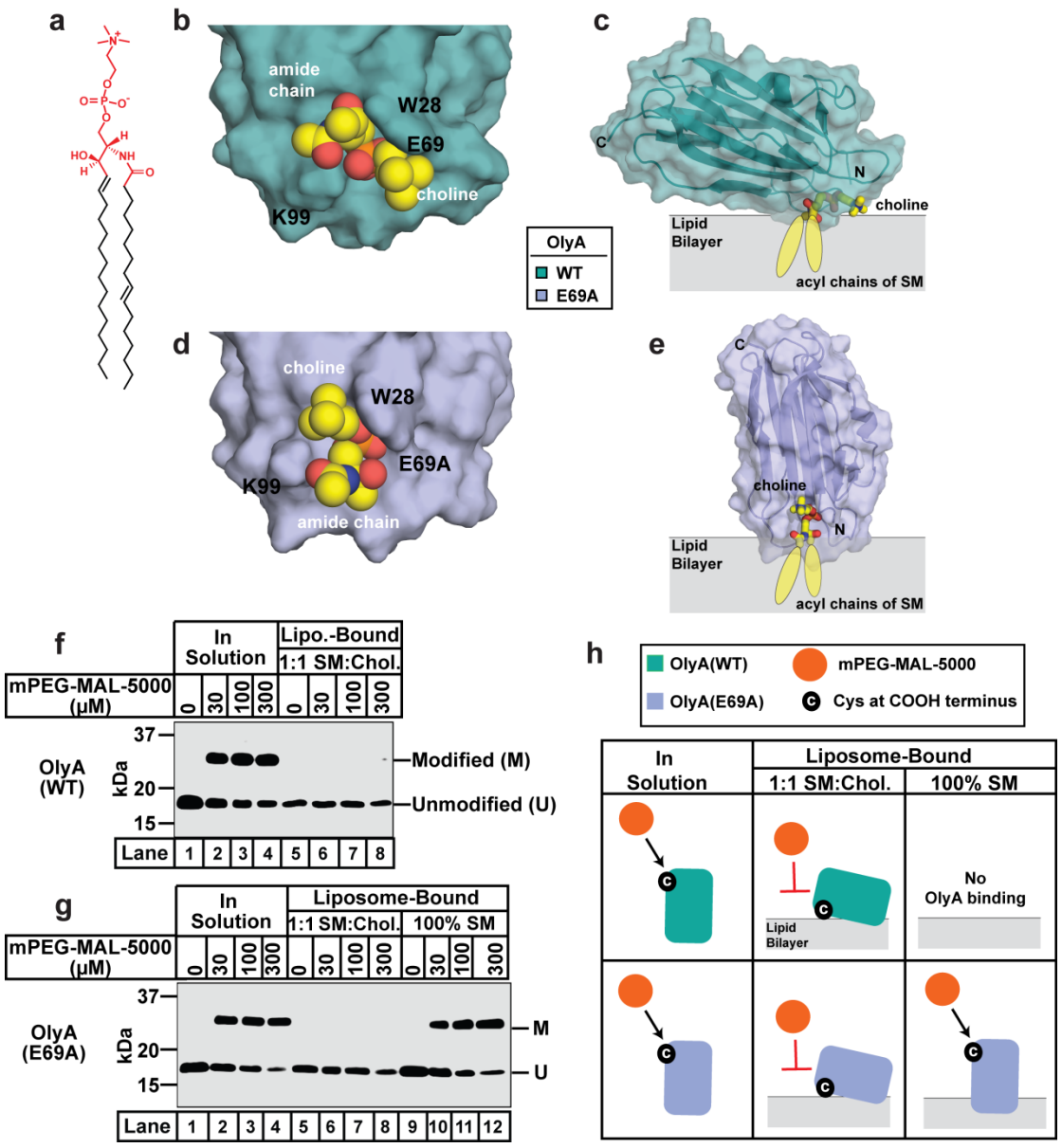

FIGURE 2-10: Docking simulations for binding of SM to OlyA(WT) and OlyA(E69A) and chemical modification assays. a, Chemical structure of 18:1 SM with the fragment used in simulations highlighted (red). **b – e,** Top-scoring models are shown for binding of SM (yellow spheres) to OlyA(WT) (**b**) and OlyA(E69A) (**d**). Plausible schematic models for binding of OlyA(WT) (**c**) and OlyA(E69A) € to SM in membranes are shown with proteins depicted as

cartoons with transparent surfaces and the top scoring docking poses of bound SM (yellow sticks) oriented on the membrane surface with acyl chains extrapolated into membrane bilayer (yellow ovals). **f, g,** Chemical modification of OlyA(WT) and OlyA(E69A). Each reaction, in a final volume of 400 µl of buffer A, contained 640 nmol of the indicated liposomes and 2 µg of either OlyA(WT)-His_6 (**f**) or OlyA(E69A)-His_6 (**g**). After incubation for 3h at room temperature, liposome-bound OlyA proteins were subjected to modification with increasing amounts of mPEG-MAL-5000 followed by immunoblot analysis. As controls, 500 µg of either OlyA(WT)-His_6 or OlyA(E69A)-His_6 in solution were also subjected to modification with mPEG-MAL-5000 followed by immunoblot analysis. M, modified form of OlyA; U, unmodified form of OlyA. **h,** Schematic description of mPEG-MAL-5000 modification results from **f** and **g**.

FIGURE 2-11

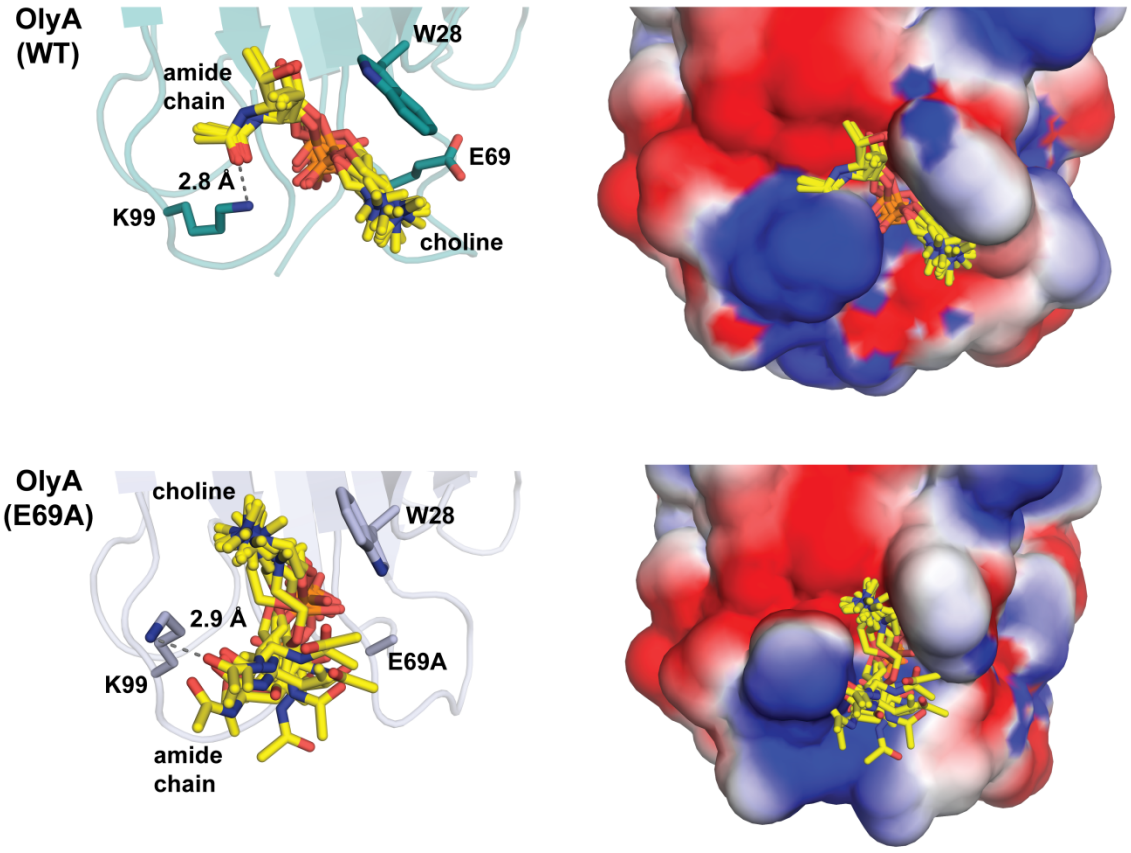

FIGURE 2-11: Top 10 docking poses for binding of SM to OlyA(WT) and OlyA(E69A). Docking simulations of a fragment of SM (Fig 2-10 a) to both OlyA(WT) (**top**) and OlyA(E69A) (**bottom**) were carried out as described in Methods. The top 10 scoring poses of SM (yellow sticks) bound to OlyA(WT) (transparent teal) and OlyA(E69A) (transparent purple) are overlaid with key residues represented as sticks (**left**). On the **right**, the same top 10 scoring poses of SM are shown bound to surface representations of OlyA(WT) and OlyA(E69A) colored according to electrostatic potential, from negative (red) to positive (blue) (scale ranges from -1 kBT/e to +1 kBT/e). Electrostatic potentials were calculated with the APBS module [4] implemented in PyMOL (version 1.8.2.0., Schrodinger, LLC).

FIGURE 2-12

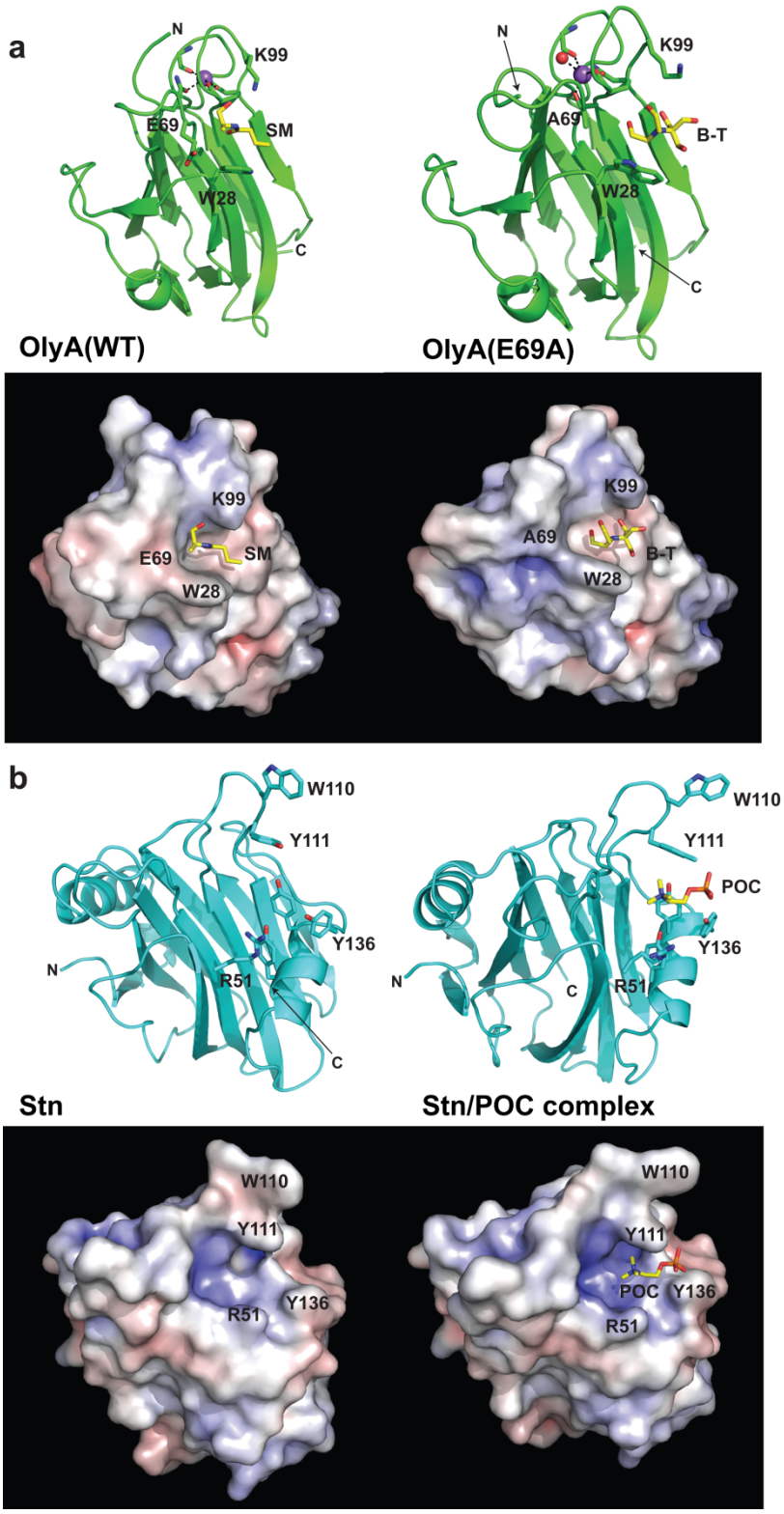
a
N
K99
E69
SM
W28
C
OlyA(WT)
N
K99
A69
B-T
W28
C
OlyA(E69A)
K99
E69
SM
W28
K99
A69
B-T
W28
b
W110
Y111
Y136
N
R51
C
Stn
W110
Y111
POC
Y136
N
C
R51
Stn/POC complex
W110
Y111
R51
Y136
W110
Y111
POC
Y136
R51

FIGURE 2-12: Sphingomyelin binding pockets occur in structurally similar locations in OlyA(WT), OlyA(E69A), and Stn. a, Ribbon diagrams (**top**) and electrostatic surface potentials (**bottom**) of OlyA(WT) (**left**) and OlyA(E69A) (**right**). Models for a portion of sphingomyelin (SM) bound to OlyA(WT) (**left**) and for bis-tris (B-T) bound to OlyA(E69A) (**right**) are represented as yellow sticks. The loops that form the pockets for OlyA(WT) and OlyA(E69A) are held in place by the coordination of a sodium ion (purple spheres) **b,** Ribbon diagrams (**top**) and electrostatic surface potentials (bottom) of Stn (**left**) and Stn-phosphocholine (POC) complex (**right**). The model for POC is represented as yellow sticks. Key sidechains and bound ligands are shown in stick representation, and sodium ions and waters are shown as purple and red spheres, respectively. All electrostatic potentials were calculated with the APBS module [4] implemented in PyMOL (version 1.8.2.0., Schrodinger, LLC), and the gradients shown ranged from -10kBT/e (red) to +10 kBT/e (blue). N, NH_2-terminus; C, COOH-terminus.

FIGURE 2-13

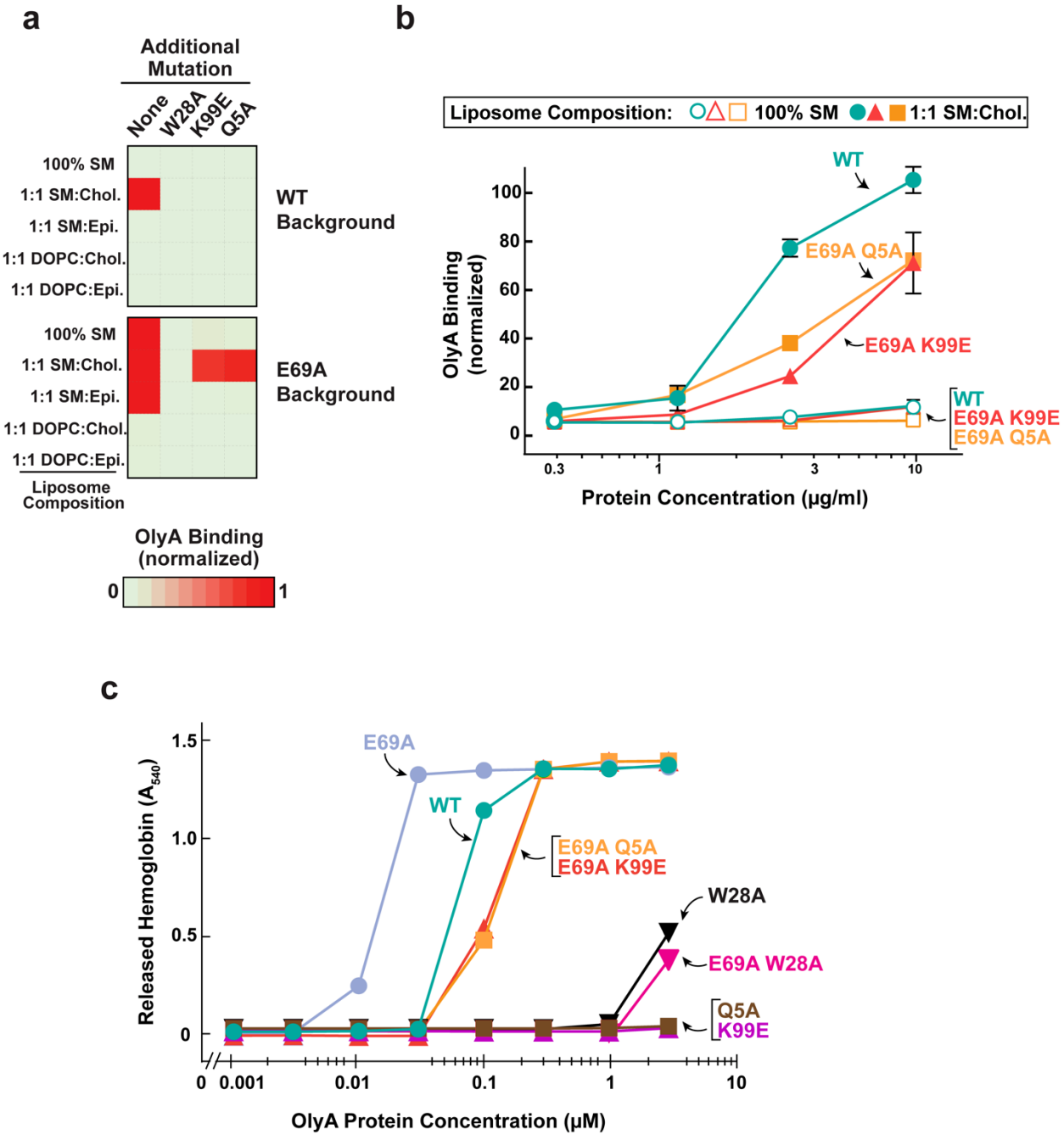

FIGURE 2-13: Recovery of cholesterol specificity on OlyA(E69A). a, Liposomes of the indicated compositions were deposited on nitrocellulose membranes, the membrane strips were incubated for 1h at room temperature with the indicated mutant versions of OlyA-His_6 (0.5 µg/ml

of E69A, 1 μg/ml of all other versions), and then subjected to immunoblot analysis followed by LICOR imaging to measure liposome-bound proteins. The mean value (n = 3) for binding of wild-type (WT) OlyA to liposomes composed of an equimolar mixture of SM and cholesterol was set to 1. All other mean binding values (n = 3) were normalized relative to this set-point and converted to a green-to-red color scale. Standard errors for all measurements were less than 10%. **b,** Liposomes of the indicated compositions were deposited on nitrocellulose membranes and dot blot assay was performed as in **a** using indicated concentrations of OlyA-His_6 mutants. The mean value (n = 3) for binding of OlyA(WT) to liposomes composed of 1:1 SM:Chol. at the highest protein concentration was set to 100% and all other mean binding values (n = 3) were normalized relative to these set-points. **c,** Each reaction, in a total volume of 500 μl of buffer C, contained 450 μl of rabbit RBCs washed and diluted as described in Methods, 10 nM of His_8-PlyB, and various concentrations of the indicated mutant version of OlyA-His_6. After incubation on a rotator for 30 min at room temperature, each reaction was subjected to 2000 x g centrifugation for 15 min at room temperature and an aliquot of the supernatant (100 μl) was assayed for released hemoglobin (absorbance at 540 nm). Values shown are averages of triplicate assays.

DISCUSSION

The current studies highlight how distinct conformations of lipids in membranes can modulate their interactions with sensor proteins in an all-or-none fashion. In particular, we show here that SM adopts two conformations, one of which is induced by complex formation with cholesterol and the second of which is adopted when SM is free from cholesterol. We are able to discriminate between these two conformations of SM in membranes using a soluble lipid-sensing protein, OlyA. Our biochemical and structural analyses reveal that OlyA binds specifically to SM/cholesterol complexes but not to free SM, and that this specificity is controlled by a single glutamic acid residue near the binding pocket.

The idea of SM/cholesterol complexes in membranes is not new [44], [82], [125], however, they have been resistant to direct detection and remain controversial [62], [117]. The difficulty in detecting SM/cholesterol complexes likely stems from their small sizes and short lifetimes in fluid bilayers of cellular PMs. (It is worth noting that many examples of molecular complexes in liquids with relatively well-defined structures but very short lifetimes have been described [42]). Previous structural studies of SM-bound sensor proteins did not reveal cholesterol-induced changes in SM conformation since they focused on lysenin [34] and sticholysin [80], both of which do not require cholesterol for binding SM-containing membranes (Fig. 1b). There have also been elegant structural studies of Nakanori [79] and Pleurotolysin A [78], two proteins that may discriminate between free and cholesterol-bound SM in a manner similar to OlyA. Unfortunately, these earlier studies did not contain bound lipids in their reported structures. There have also been several studies of protein sensors such as PFO and ALO that discriminate between conformations of another lipid, cholesterol, at membrane surfaces [45, 48], however there is no structural information on the interaction of these proteins with cholesterol.

The sigmoidicity of the OlyA binding curves (Fig 2-2 g, 2-9 f) suggests cooperativity in formation of SM/cholesterol complexes in membranes. Studies of phospholipid/cholesterol complexes in model membranes have yielded cooperativity values in the range of 3-12 [82]. Using an average molecular area of ~45 $Å^2$/lipid obtained in these earlier studies, the size of such cooperative complexes would range from ~500 – 1600 $Å^2$, which is below optical resolution. In our studies we possibly overcome this limitation by OlyA stabilizing these complexes. Molecular dynamics simulations of membranes containing SM and cholesterol combined with the information from this study on OlyA binding to different conformations of SM could provide us with a molecular model of the long-hypothesized SM-cholesterol complexes. We have also begun using OlyA as a tool to probe for these complexes on PMs of live cells and this work is summarized in Chapter 3.

CHAPTER 3

MONITORING DIFFFERENT POOLS OF CHOLESTEROL IN PLASMA MEMBRANES

INTRODUCTION

Cholesterol levels are highest in the plasma membrane (PM), which contains ~80% of total cellular cholesterol [73]. To meet the needs of PM, most of the cholesterol synthesized in ER or LDL-derived cholesterol from lysosomes must be ultimately transported to the PM. However, the cholesterol control machinery that regulates this cholesterol synthesis and uptake resides in the ER, which contains only ~1% of the cell's total cholesterol [72]. This raises the question: How does the ER communicate with PM to monitor cholesterol levels in that membrane?

Recent studies that focused on the organization of cholesterol in PM have provided some insights into this problem of organelle communication. These studies showed that cholesterol in PMs, which comprises 40 - 45 mole % of total PM lipids when cells are grown in lipoprotein-rich serum, is organized into three different pools [31]. Two of these pools of cholesterol (~27 mole % of total PM lipids) are sequestered by sphingomyelin and other membrane factors, respectively, and are inaccessible to soluble proteins that bind membrane cholesterol. PM cholesterol in excess of these two pools constitutes a third pool that is accessible to cholesterol-binding proteins and can be transported to ER to block Scap-mediated activation of SREBP, thereby inhibiting cholesterol synthesis and uptake. Thus, controlling the accessibility of PM cholesterol allows regulated communication between PM and ER, ensuring that cholesterol uptake and synthesis is not prematurely shut down before the cell's cholesterol needs are met [64].

Accessibility of cholesterol depends on the distribution of cholesterol between the three pools of cholesterol. Monitoring these pools of cholesterol could provide more insight into cholesterol homeostasis. Here, we use the proteins described in the last two chapters as tools to monitor two different pools of cholesterol in PMs of live mammalian cells. ALOD4 binds to accessible cholesterol and OlyA binds to SM-sequestered cholesterol. Conveniently, neither of these proteins have pore forming abilities and hence can be used on live cells to monitor their respective pools of cholesterol.

MATERIALS AND METHODS

Materials: We obtained all media and fetal calf serum (FCS) from Sigma-Aldrich; penicillin and streptomycin sulfate from Corning; hydroxypropyl beta cyclodextrin (HPCD) from CTD holdings; osmium tetraoxide from Electron Microscopy Sciences.

Buffers and media: Buffer A contains 50 mM Tris-HCl (pH 7.5), 150 mM NaCl and 1 mM TCEP. Buffer B is buffer A supplemented with 1% (w/v) SDS. Buffer C contains 25 mM HEPES-KOH (pH 7.4), 150 mM NaCl and 0.2% (w/v) bovine serum albumin. Medium A is a 1:1 mixture of Ham's F-12 and Dulbecco's modified Eagle's medium (DMEM) supplemented with 100 units/ml penicillin and 100 µg/ml streptomycin sulfate. Medium B is medium A supplemented with 5% (v/v) FCS. Medium C is medium A supplemented with 5% (v/v) LPDS (prepared as described in [51]). Medium D is medium C supplemented with 50 µM compactin and 50 µM sodium mevalonate. Medium E is DMEM-low glucose supplemented with 100 units/ml penicillin and 100 µg/ml streptomycin sulfate. Medium F is medium E supplemented with 5% (v/v) FCS. Medium G is medium E supplemented with 10% (v/v) FCS. Medium H is DMEM-high glucose supplemented with 100 units/ml penicillin and 100 µg/ml streptomycin sulfate. Medium I is

medium H supplemented with 10% (v/v) FCS. Medium J is medium H supplemented with 20% (v/v) FCS.

Overexpression, purification and labeling of recombinant proteins: ALOD4, OlyA(WT) and OlyA(E69A) were overexpressed, purified and fluorescently labeled as described in Chapters 1 and 2.

Cell lines and culture: Hamster CHO-K1 cells (female) were cultured in Medium B and were maintained at 37°C in 8.8% CO_2. Human fibroblast SV-589 cells were cultured in Medium F and were maintained at 37°C in 5% CO_2. Canine kidney epithelial (MDCK) cells (female) and human Schwannoma (ST88-14) cells were cultured in Medium G and were maintained at 37°C in 5% CO_2. Mouse neuroblast (Neuro-2A) cells were cultured in Medium I and were maintained at 37°C in 5% CO_2. Human colon epithelial (Caco-2) cells (male) were cultured in Medium J and were maintained at 37°C in 5% CO_2. If not specified, the sex of the animal from which the cell line was derived is not known.

Fixation of cells and measurement of FRAP and OlyA binding: For fixation studies, CHO-K1 cells were set up on day 0 in medium B in 96-well glass-bottom plates at a density of 5000 cells/well. When cells had reached full confluency (usually day 2), media was removed and replaced with 200 µl medium B containing 1 µg/ml of a fluorescent lipid (TR-DHPE) (1 mg/ml stock in ethanol). After incubation for 4 h for incorporation of TR-DHPE, media was removed, cells were washed five times with PBS, and then incubated with 200 µl of a 1:1 mixture of osmium tetroxide (4% stock in water) and PBS. After incubation for 30 min in a chemical hood, the fixing solution was removed, cells were washed 5 times with buffer C, after which 200 µl of PBS was added to each well. Unfixed wells received the same treatment, except that 200 µl of a 1:1 mixture of water and PBS were added to the well during the 30 min fixation step. Membrane fluidity was

measured by fluorescence recovery after photobleaching (FRAP). Epifluorescence microscopy (Nikon Ti-E microscope, 60x objective) was used to monitor TR-DHPE from a circular region (~5 μm in diameter) for 30 s, after which a focused beam from a 561 nm laser source was used to photobleach TR-DHPE molecules in that region. After 30 s, the laser was turned off and TR-DHPE fluorescence of the bleached region was monitored. The fluorescence before bleaching was set to 1 and the fluorescence after the 30 s bleaching step (~40-50% reduction) was normalized to 0.

To measure binding of OlyA to unfixed and fixed wells, we used fluorescently-labeled OlyA (fOlyA) proteins. After the above fixation or control treatments, cells were subjected to two 10-min washes with buffer C at room temperature. After these washes, each well was incubated with 3 μM of fOlyA proteins in a total volume of 100 μl of buffer C. After incubation for 30 min, cells were washed six times with PBS to remove unbound fOlyA and membrane-bound fOlyA and lipid fluorescence from cell membranes was measured using a microplate reader (Tecan M1000 Pro) using the following parameters – Texas Red (excitation wavelength, 595 nm; emission wavelength, 617 nm; band pass, 5 nm for each); Alexa Fluor 488 (excitation wavelength, 495 nm; emission wavelength, 516 nm; band pass, 5 nm for each).

Quantification of PM cholesterol and bound fluorescently-labeled OlyA and ALOD4 proteins: After indicated treatments, PM membranes were purified and their cholesterol content was quantified as described previously [32]. For measurement of binding of fluorescently-labeled OlyA or ALOD4, cells were first washed after indicated treatments as follows to remove surface-bound lipoproteins or HPCD: three rapid washes with buffer C at room temperature, followed by two 10-min washes with ice-cold buffer C at 4°C (for binding measurements at 4°C) or warm buffer C at 37°C (for binding measurements at 37°C). After these washes, each dish was incubated at 4°C or 37°C with 2 ml of buffer C containing fluorescent sensors as described in the Figure

Legends. After indicated times, cells were washed three times with ice-cold or warm PBS, solubilized in 1 ml of buffer B, and shaken on a rotator at room temperature. Cell-bound fluorescently-labeled proteins were quantified as described previously (Infante and Radhakrishnan, 2017). Total cell protein was quantified using a BCA colorimetric assay.

RESULTS

SM/cholesterol complexes in plasma membranes are maintained at constant levels over a wide range of cholesterol concentrations. We used OlyA(WT) and OlyA(E69A) to probe the conformation of SM in PMs of cultured cells. For this purpose, we used fluorescently-labeled versions of these sensors along with fluorescently-labeled OlyA(W6A), which does not bind any SM-containing membrane (Fig 2-4 e), as a negative control (Fig 3-1 a, lanes 1-6). When we incubated these proteins with CHO-K1 cells, we observed time-dependent binding of OlyA(WT) and OlyA(E69A) that reached a saturating value after 30 min (Fig 3-2 a). Maximal binding for OlyA(WT) was ~3-fold higher at 4°C compared to 37°C, consistent with the temperature dependence observed earlier for binding to liposomes (Fig 2-9 d, f). Maximal binding of OlyA(E69A) was higher than that of OlyA(WT) and did not change with temperature (Fig 3-2 a). No binding was observed for OlyA(W6A) at either temperature (Fig 3-2 a). Dose curve analysis showed saturable binding of both OlyA(WT) and OlyA(E69A) to CHO-K1 cells at 4°C (Fig 3-2 b). OlyA(W6A) showed minimal binding even at the highest tested concentration (Fig 3-2 b). We first analyzed the effects of PM lipid immobilization on OlyA binding by the same approach that we had used previously with liposomes (Fig 2-2 e, f). For this experiment, CHO-K1 cells were set up in 96-well glass-bottom plates, and a fluorescent phospholipid (TR-DHPE) was incorporated into the cellular membranes. The lipid molecules in these cellular membranes were fluid as judged by FRAP analysis and this fluidity was blocked by osmium tetroxide fixation (Fig 3-2 c). We then conducted OlyA binding studies and found that fluorescently-labeled versions of both OlyA(WT)

and OlyA(E69A) bound cells to a similar degree even after osmium tetroxide fixation (Fig 3-2 d), suggesting that SM/cholesterol complexes may be present in the plasma membranes of cultured cells under normal conditions without inducement by OlyA(WT). No binding of fluorescently-labeled OlyA(W6A) was observed in unfixed or fixed cells.

We next tested the effects of modulating the cellular lipid composition on binding of OlyA(WT) and OlyA(E69A) to PMs using the assay conditions established above (OlyA concentration: 3 μM; Incubation time: 1 h; Incubation temperature: 4°C). Measuring binding at 4°C eliminates internalization of OlyA, as has been reported previously [124], allowing for assaying the disposition of SM on just the PM. For comparison, we also measured the binding of fluorescently-labeled ALOD4 (Fig 3-1 b), a domain of ALO, which binds accessible cholesterol in PM but not SM-sequestered cholesterol [25, 64].

We first altered SM levels in PMs of CHO-K1 cells. When cells were grown in lipoprotein-rich serum, we observed robust binding of ALOD4, OlyA(WT), and OlyA(E69A) (Fig 3-3 a). Treatment with SM-degrading SMase abolished binding of both OlyA(WT) and OlyA(E69A) (Fig 3-3 a), consistent with the inability of these proteins to bind membranes containing ceramide, the product of SMase treatment (Fig 2-8 d). In contrast, binding of ALOD4 increased with SMase treatment (Fig 3-3 a), a result in line with previous observations where cholesterol sequestered by SM was liberated upon SMase treatment and made accessible for binding to ALOD4 [25, 31].

We then tested the effects of changing cellular cholesterol levels by growing cells in lipoprotein-rich serum to increase cholesterol levels or lipoprotein-deficient serum without or with compactin (inhibitor of cholesterol synthesis [18]) to decrease cholesterol levels. For each condition, an aliquot of cells was used to purify PMs and measure their cholesterol content and the rest of the cells were used to measure binding of the three lipid-sensing proteins. When grown in lipoprotein-

rich serum, PMs of CHO-K1 cells contained 44.1 mole% cholesterol and showed robust binding of ALOD4, which binds accessible cholesterol (Fig 3-3 b). As expected, when cells were switched to lipoprotein-deficient serum, their PM cholesterol content was lowered to 35.2 mole% and ALOD4 binding decreased. Incubation with compactin further lowered PM cholesterol to 33.7 mole% and ALOD4 binding was diminished even more. In contrast, OlyA(E69A), which binds both SM/cholesterol complexes and free SM, showed no change in binding to PMs containing different amounts of cholesterol (Fig 3-3 b). Surprisingly, OlyA(WT), which only binds SM/cholesterol complexes, showed no reduction in binding even when PM cholesterol content was reduced from 44.1 to 33.7 mole% (Fig 3-3 b). To further test the cholesterol dependence of OlyA(WT), we treated CHO-K1 cells with a cholesterol-extracting cyclodextrin reagent (HPCD), which has been shown to deplete PM cholesterol to a greater extent than the milder treatments of Fig 3-3 b [31]. As shown in Fig 3-3 c, HPCD treatment depleted PM cholesterol from 42.4 mole% down to 22 mole%, resulting in the expected sharp sigmoidal decline of ALOD4 binding. Binding of cholesterol-insensitive OlyA(E69A) was not affected even by the most severe cholesterol reduction. Similar to what was observed in Fig 3-3 b, the binding of OlyA(WT) was stable as PM cholesterol decreased from 42.4 mole% to 32.4 mole%. However, the binding of OlyA(WT) declined sharply as PM cholesterol declined even further to 22 mole%, likely due to dissociation of SM/cholesterol complexes under these conditions of extreme cholesterol depletion.

To test the generality of the OlyA binding results obtained with CHO-K1 cells, we also tested the binding of OlyA(WT), OlyA(E69A), and ALOD4 to five other cell types – human fibroblast cells (SV-589), mouse neuroblast cells (Neuro-2A), human schwannoma cells (ST88-14), canine kidney epithelial cells (MDCK), and human colon epithelial cells (Caco-2). As shown in Fig 3-4, all cell lines showed the same general binding properties as observed with CHO-K1 cells. In all cases, binding of ALOD4 was reduced by more than 80% when cells were switched from

lipoprotein-rich serum to lipoprotein-deficient serum along with compactin, whereas binding of OlyA(WT) and OlyA(E69A) was not reduced. Further depletion of cholesterol using HPCD lowered ALOD4 binding by more than 90% and also lowered OlyA(WT) binding by more than 80%, while leaving binding of cholesterol-insensitive OlyA(E69A) unaffected. Treatment of cells with SMase eliminated binding of both OlyA(WT) and OlyA(E69A) and increased binding of ALOD4. In the case of ST88-14 schwannoma cells, the cholesterol released by SMase treatment was consistently higher (~270% of control) compared to that observed in the other five cell lines tested (150-190% of control). Combined, these results suggest that SM/cholesterol complexes are present and maintained at stable levels in all six of these cell lines.

FIGURE 3-1

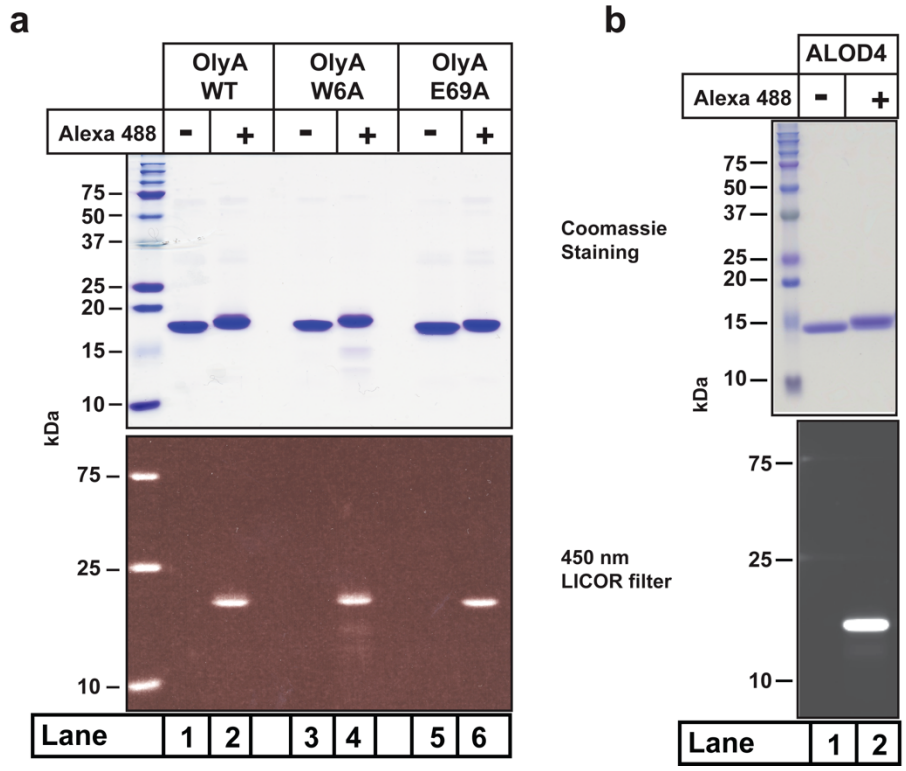

FIGURE 3-1: Fluorescent labeling of OlyA and ALOD4. a, b Recombinant OlyA(WT), OlyA(W6A), OlyA(E69A) (**a**) and ALOD4 (**b**) were purified and labeled with Alexa Fluor 488 maleimide as described in Methods. Aliquots (2 µg each) were collected before and after the labeling reaction, subjected to 15% SDS-PAGE, and proteins were visualized with Coomassie stain (**top**) or by fluorescence scanning (450 nm channel) (**bottom**).

FIGURE 3-2

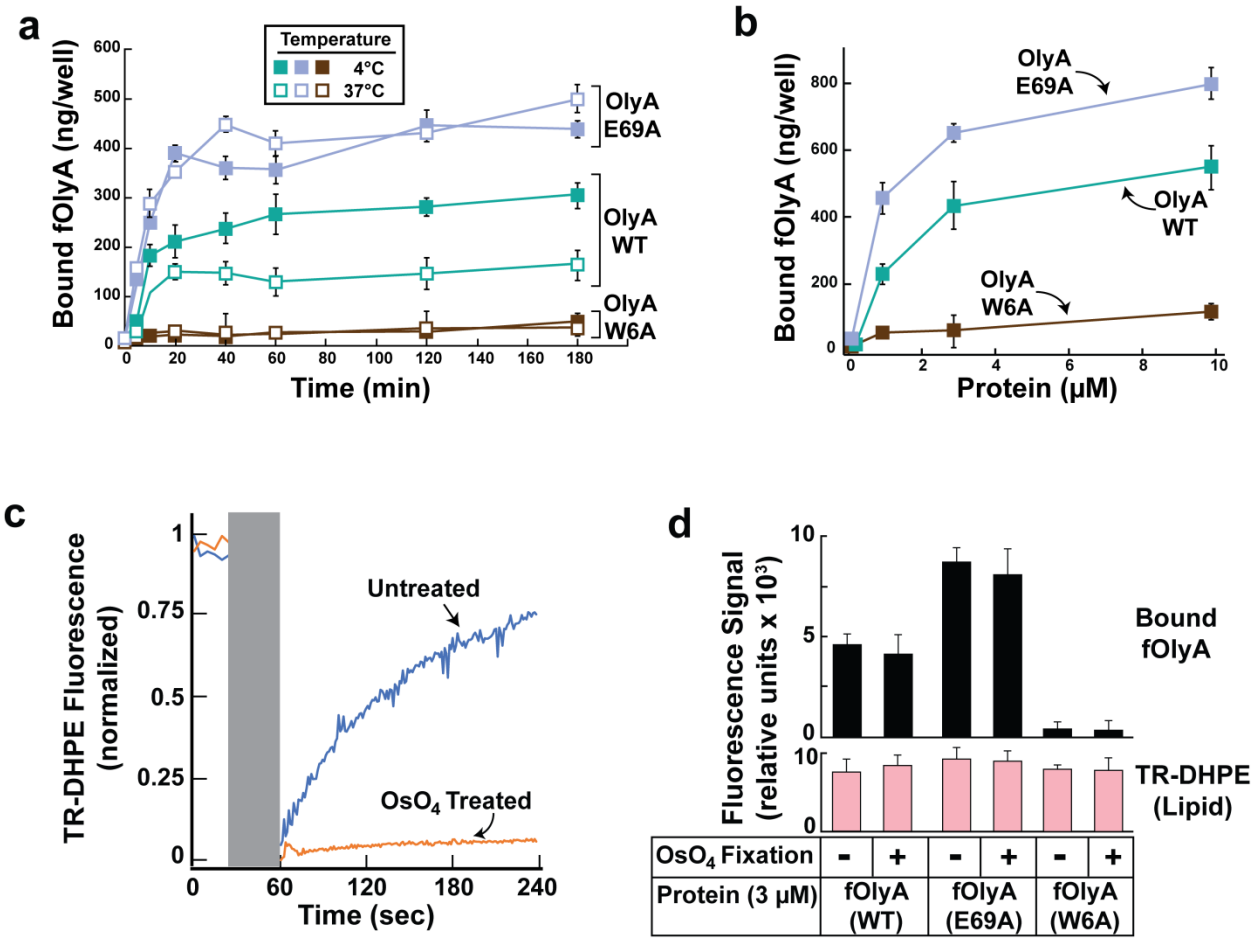

FIGURE 3-2: Time course, dose and lipid mobility dependence of binding of fluorescently-labeled OlyA to CHO-K1 cells. a-b, Recombinant OlyA(WT), OlyA(W6A), and OlyA(E69A) were purified and labeled with Alexa Fluor 488 maleimide as described in **Fig 3-1**. On day 0, CHO-K1 cells were set up in medium B at a density of 6 x 10^4 cells/well of 48-well plates. On day 1, media was removed, and cells were washed with 500 µl of PBS followed by addition of 200 µl of medium C containing either 3 µM (**a**) or varying concentrations (**b**) of the indicated version of OlyA. For quantification purposes, ~5% of OlyA proteins were labeled with Alexa Fluor 488 dyes. After incubation for various times at the indicated temperature (**a**) or 1 h at 4°C (**b**), cells were harvested and subjected to fluorescence analysis of bound OlyA as described in Methods.

Values shown are averages of triplicate assays. **c-d,** Dependence of OlyA binding on membrane lipid mobility. On day 0, CHO-K1 cells were set up in medium B at a density of 5000 cells/well in 96-well glass-bottom plates. On day 2, a fluorescent lipid (TR-DHPE) was incorporated into cell membranes and lateral fluidity of lipid molecules was measured by FRAP before and after fixation with osmium tetroxide (**c**). Gray bar denotes the 30s photobleaching step. Shown are averages of fluorescence values from three different regions in a well. Unfixed and osmium tetroxide-fixed wells were incubated with 3 μM of the indicated fOlyA for 30 min, after which fluorescence of membrane-bound fOlyA and TR-DHPE was measured as described in Methods (**d**). Values shown are averages of binding to four different wells. Chol., cholesterol; Epi., epicholesterol.

FIGURE 3-3

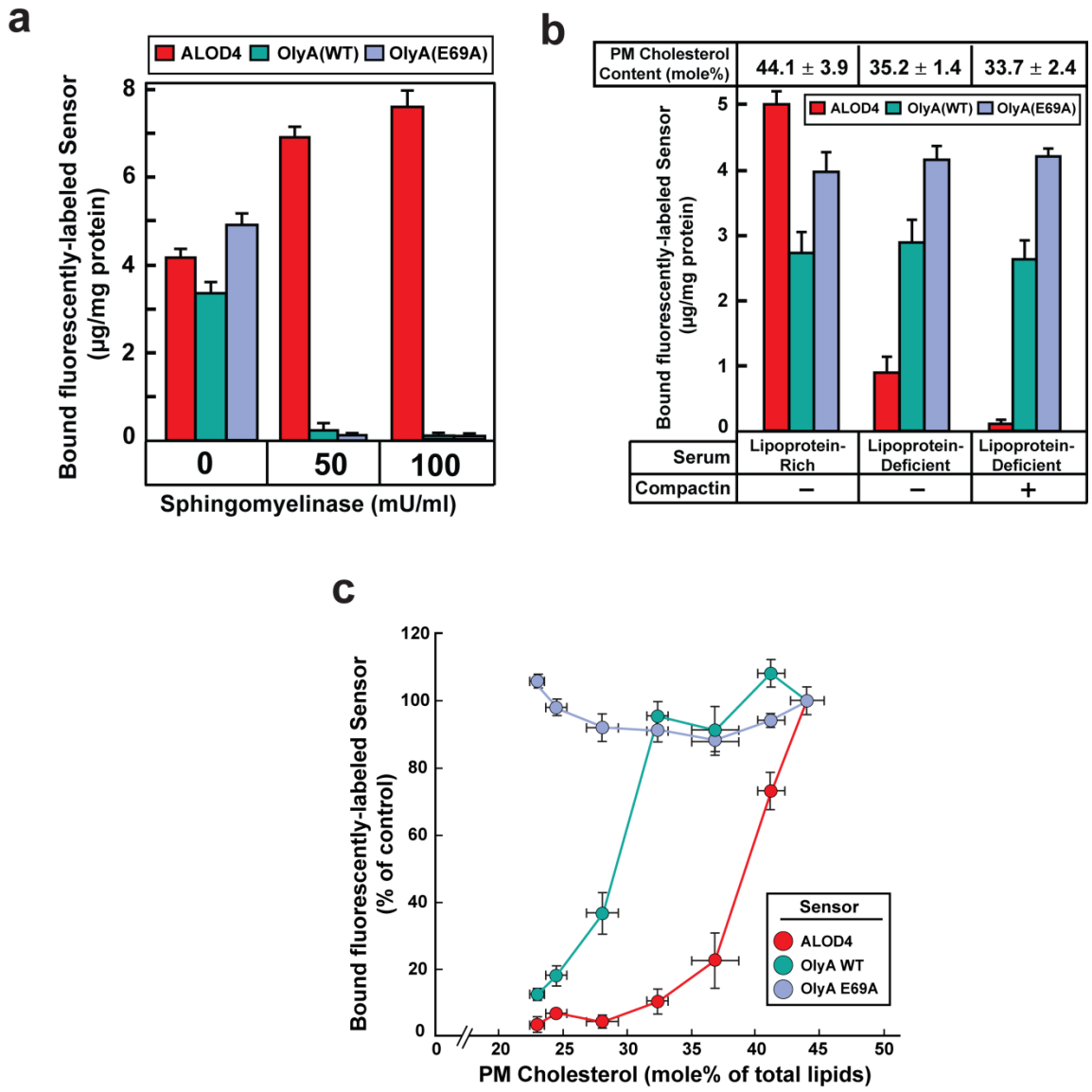

FIGURE 3-3: Organization of SM and cholesterol in PMs of CHO-K1 cells. a-c, On day 0, CHO-K1 cells were set up in medium B at a density of 2.5 x 105 cells/60-mm dish (**a,** 6 dishes/replicate/condition; **b-c**, 12 dishes/replicate/condition). **a,** SMase treatment. On day 2, cells were switched to fresh medium B containing the indicated concentrations of SMase. After incubation for 30 min at 37°C, cells were washed as described in Methods. 2 dishes from each condition were incubated with 2 ml of buffer D containing 3 µM of the indicated sensor protein.

After incubation for 1 h at 4°C, cells were harvested and PM-bound proteins were quantified as described in Methods. **b,** Cholesterol modulation by serum and compactin. On day 1, cells were switched to either fresh medium B, medium C, or medium D containing the indicated serum without or with compactin. On day 2, cells were washed and binding of the indicated sensor proteins was carried out as in b for 6 dishes/replicate/condition. Cells from the remaining 6 dishes were pooled and used for PM purification and cholesterol quantification as described in Methods. **c**, Cholesterol modulation by cyclodextrin. On day 2, cells were switched to fresh medium B (one group) or fresh medium C containing 0.01% - 2% (w/v) HPCD. After incubation for 1 h at 37°C, cells were washed and binding of the indicated sensor proteins and quantification of PM cholesterol was carried out as in **b**. 100% of control values for bound ALOD4, OlyA(WT), and OlyA(E69A) were 5.7, 3.7, and 5.4 μg/mg protein, respectively. Values shown are averages of triplicate assays.

FIGURE 3-4

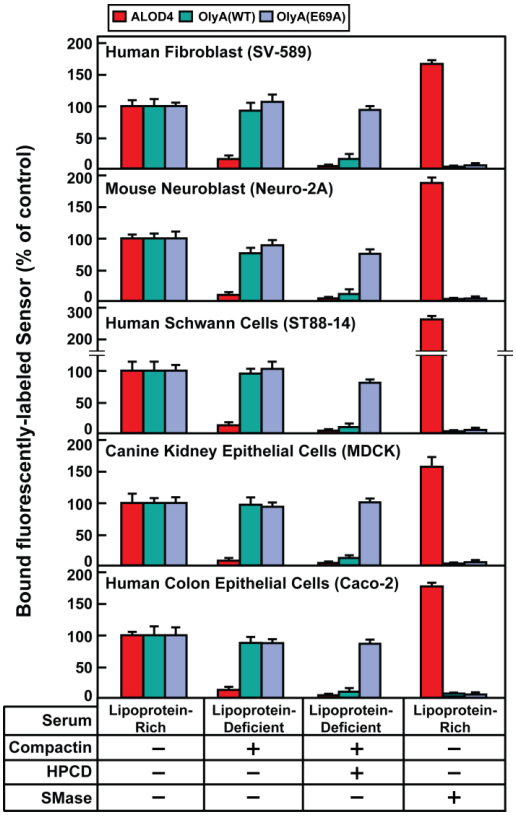

FIGURE 3-4: SM-cholesterol complexes in PMs of different cell lines. On day 0, the indicated cell lines were set up at a density of 2.5 x 10^5 cells/60-mm dish (media described in Methods; 6 dishes/replicate/condition). On day 1, cells were switched to media containing the indicated serum without or with compactin. On day 2, some cells were further treated with SMase (100 mU/mL) or HPCD (1% w/v) as described above, after which all cells were washed and binding of 3 μM of the indicated sensor protein was carried out as described above. 100% of control values for bound ALOD4, OlyA(WT), and OlyA(E69A) for each cell line was as follows: SV-589 (4.9, 3.5, and 6.8 μg/mg protein); Neuro-2A (1.1, 1.8, and 2.6 μg/mg protein); ST88-14 (6.3, 14.3, and 18.2 μg/mg protein); MDCK (4.3, 3.8, and 5.2 μg/mg protein); Caco-2 (4.5, 8.3, and 10.2 μg/mg protein). Values shown are averages of triplicate assays.

DISCUSSION

We used ALOD4 and OlyA to monitor the accessible and SM-sequestered pools of cholesterol in plasma membranes. We find that SM/cholesterol complexes are present in PMs of six different cultured cell lines (Fig 3-3, 3-4). The complexes are present at relatively constant levels even when cholesterol amounts fluctuate by more than 10 mole% (Fig 3-3 c). This invariance is in line with a previous observation that levels of a SM-sequestered pool of cholesterol in PMs of human fibroblasts were maintained at constant levels [31]. Sequestration of a fixed pool of PM cholesterol in complexes with SM could allow for precise, switch-like control over the levels of accessible PM cholesterol that can travel to the ER to ensure cholesterol homeostasis. Quantification of PM lipids in this previous study showed that total SM and SM-sequestered cholesterol constituted ~10 mole% and ~15 mole% of total PM lipids, respectively. This ratio of 1:1.5 is consistent with the SM:cholesterol complex stoichiometries inferred from our current studies (ranging from 1:1 to 1:2 SM:cholesterol in Fig 2-2 h, 2-9 b, 2-10 f,g).

The maintenance of a constant pool of SM/cholesterol complexes in PMs in the face of significant cholesterol depletion raises the possibility of an active mechanism mediated by one or more proteins in the PM. Lipid conformation-specific probes such as OlyA and ALOD4 should allow for the identification of such proteins and shed light on how modulation of distinct conformations of lipids in PMs regulates lipid homeostasis and other cellular signaling events.

CONCLUSION AND PERSPECTIVE

This thesis is focused on developing and characterizing tools to understand cholesterol accessibility in membranes. Interactions of cholesterol with membrane phospholipids determine its accessibility to cholesterol sensing proteins like SCAP and CDCs [48, 100, 130]. As a result, these cholesterol sensing proteins respond to small changes in cholesterol concentrations with a sharp threshold. The work in Chapter 1 is focused on a structural understanding of how accessible cholesterol sensors recognize and bind membrane cholesterol. ALOD4 was used as a proxy for accessible cholesterol sensors. We used NMR spectroscopy and other biophysical techniques to get an insight in to the amino acids that are important for cholesterol sensing. While our efforts to understand the structural basis for accessible membrane cholesterol sensing still continue, we are also working on using CDCs as tools towards other applications.

Cholesterol sensing by SCAP is central to regulation of cholesterol homeostasis in cells. As a result, there is a need for finding inhibitors of SCAP binding. SCAP is a large polytopic membrane protein that is a part of a cellular system with other membrane proteins. Reconstitution of this system and high-throughput screening for potential inhibitors of SCAP is technically challenging. As mentioned in Chapter 1, CDCs and Scap share common sterol structural specificity and identical threshold sensitivity for accessible membrane cholesterol, suggesting that they may be sensing cholesterol in mechanistically-similar ways (Fig C-1) [130]. We reasoned that other non-sterol molecules that bind CDCs might also bind SCAP and lead to inhibition of the SREBP pathway. To that end, we screened a large chemical library (~250,000 compounds) at UT Southwestern's High Throughput Screening Core for molecules that bind ALOFL and prevent its sensing of membrane cholesterol. This screen has yielded several promising hits that bind ALOFL and also have an effect on SCAP-mediated SREBP activation. While the identification of an active

compound that effectively blocks SREBP activation is still ongoing, we are now using these ALOFL-binding molecules towards a yet another potential clinical application.

Listeriolysin O (LLO) is another member of the CDC family of toxins and is secreted by an intracellular gram-positive bacterium, *Listeria monocytogenes* [85]. Pore forming ability of LLO is essential for escape of the bacterium from the host vacuole that is formed upon its initial entry [134]. LLO-negative mutants remain trapped in the vacuole, cannot grow intracellularly or spread from one cell to another making them avirulent in a murine model of listeriosis [46, 49]. LLO shares a common sterol specificity and membrane binding mechanism as PFO and ALO [68]. In collaboration with the lab of Dr. Neal Alto, we are testing ALO binders from the above screen for their ability to block LLO-dependent *Listeria* spread in mammalian cells.

CDCs have previously been used to define three pools of cholesterol in plasma membranes of mammalian cells [31]. One pool is accessible for binding to CDCs, a second pool is SM-sequestered, and the third pool is sequestered by factors yet unknown. The work in Chapter 2 is focused on acquiring a molecular understanding of the SM-sequestered pool of cholesterol. For this purpose, we used OlyA, a protein that binds to membranes only when they contain both sphingomyelin and cholesterol. Structural and biochemical analyses of OlyA binding to membranes revealed that SM adopts two distinct conformations in membranes in the presence of cholesterol. One conformation is induced by stoichiometric, exothermic interactions with cholesterol and is recognized by OlyA. In its second conformation, sphingomyelin is free from cholesterol and is not recognized by OlyA. A point mutation (E69A) abolishes OlyA's ability to discriminate between these two conformations. Cholesterol specificity can be restored to cholesterol-insensitive OlyA(E69A) by making a second point mutation in either of two residues near the SM-binding pocket (Q5A, K99E). These results show proteins can detect distinct

conformations of lipids in an all-or-none fashion and how this specificity can be defined by a single amino acid.

While these basic insights into lipid conformation sensing mechanisms by ALOD4 and OlyA lead to a better understanding of membrane biology, we have also begun to use these two proteins as tools to monitor and modulate the different pools of cholesterol in the PMs of live cells. ALOD4 specifically binds the accessible pool of cholesterol and OlyA specifically binds the SM-sequestered pool (Fig C-2). The work in Chapter 3 is focused on using OlyA and ALOD4 to monitor these pools of cholesterol in plasma membranes of live cells. We found that SM-cholesterol complexes are present in PMs of six different cultured cell lines and these complexes are present at relatively constant levels even when cholesterol amounts fluctuate by more than 10 mole% (Fig 3-3, 3-4).

We are now using ALOD4 and OlyA in cells to modulate levels of cholesterol between the three pools of cholesterol to get better insights into the dynamics of this organization. An example of this kind of modulation is shown in Fig C-2. When CHO-K1 cells are pre-incubated with increasing amounts of OlyA, subsequent binding of ALOD4 decreases (Fig C-3 a). This suggests that OlyA binding to PMs stabilizes SM-cholesterol complexes and drives the reaction between the two lipids towards more complex formation and this leads to a decrease in the pool of accessible cholesterol and ALOD4 binding is reduced. In other words, OlyA can be used be used as a tool to switch cholesterol between accessible and inaccessible states (Fig C-3 b).

OlyA and ALOD4 can potentially be used to answer several other open questions concerning cholesterol regulation. As shown in Chapter 3 (Fig 3-3, 3-4), SM/cholesterol complexes are maintained at a constant level in the face of significant cholesterol depletion. This raises the possibility of an active maintenance mechanism in the PM mediated by one or more

proteins. Also, cells constantly monitor the accessibility of PM cholesterol and relay the information to the ER to shut down or continue cholesterol uptake and synthesis. While mechanisms of transport between PM and ER are still poorly understood, this raises the possibility of an accessible cholesterol sensor in the PM that can sense cholesterol using a mechanism similar to SCAP or CDCs and shut down cholesterol transport to the ER. Proximity-based biotinylation using BioID-labeled versions of ALOD4 and OlyA can allow for identification of any such proteins that are involved in monitoring and maintaining different pools of cholesterol in the PM [109].

FIGURE C-1

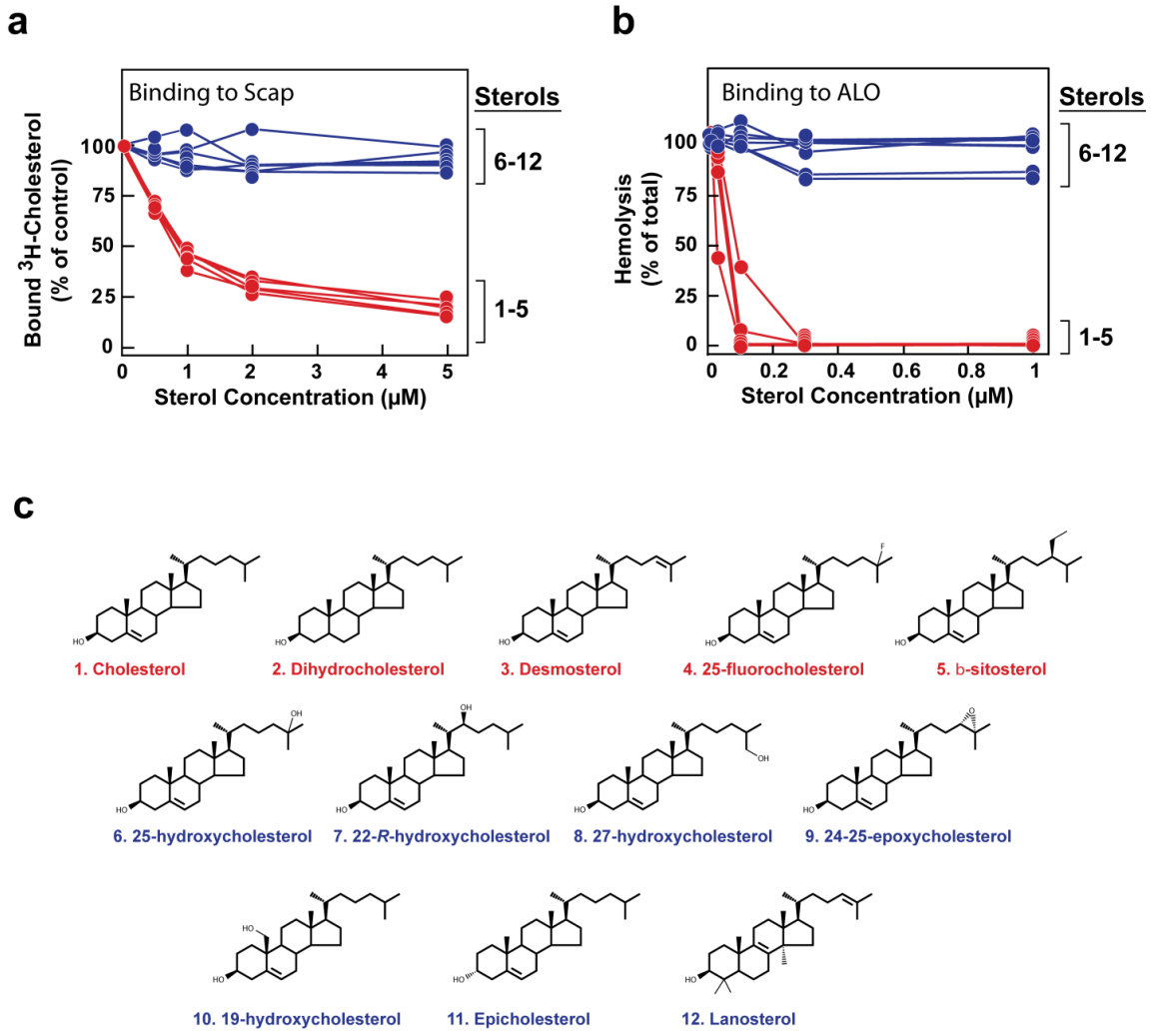

FIGURE C-1: SCAP and ALOFL share identical sterol structural specificity. a, Scap binding to sterols was carried out as in [103]. Purified SCAP (TM 1-8) was incubated ^{3}H-cholesterol in the presence of indicated competitor sterol (unlabeled) and the amount of bound ^{3}H-cholesterol was measured. **b,** Hemolysis competition assays were carried out as in [48]. ALOFL was incubated with indicated amounts sterols for 1 h and this mixture was added to washed rabbit erythrocytes. After incubation for 15 min at room temperature, hemolysis was measured as release of hemoglobin (absorbance at 540 nm). 100% - Hemolysis with 1% (w/v) Triton-X 100. **c,** Chemical structures of sterols used in **a** and **b**.

FIGURE C-2

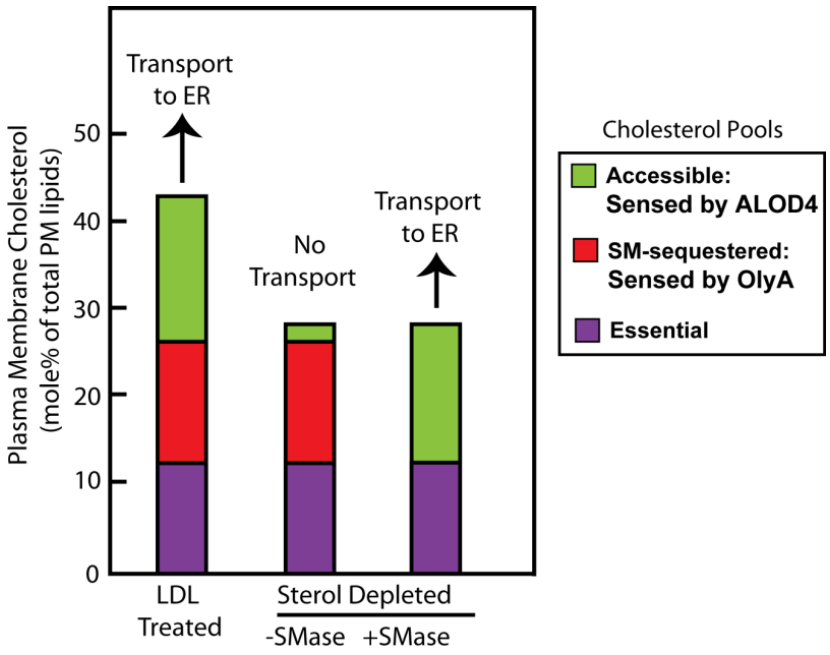

FIGURE C-2: Sensors for different pools of PM cholesterol. Schematic figure illustrating the three pools of cholesterol in the PM of cells under different conditions and their respective sensors. Figure adapted from [31].

FIGURE C-3

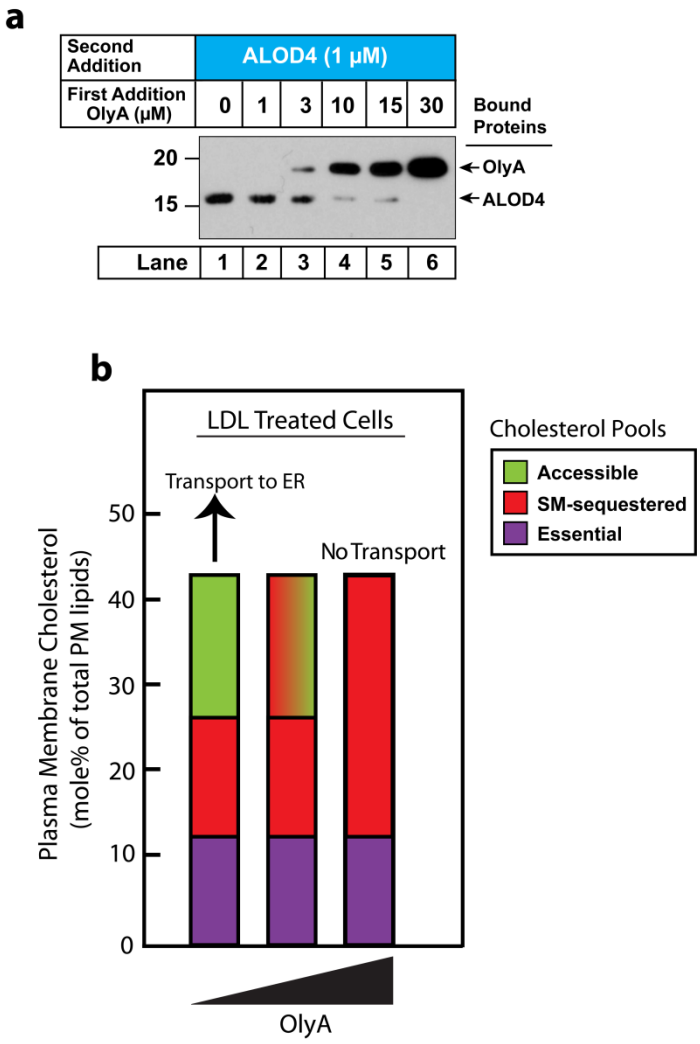

FIGURE C-3: OlyA can be used to switch cholesterol between accessible and inaccessible states. a, On day 0, CHO-K1 cells were set up in medium A at a density of $6x10^4$ cells per well in a 48-well plate. On day 1, media was removed; cells were washed twice with PBS, and treated with 200 µL of medium A with the indicated concentrations of OlyA. After incubation for 1 h at 37 ^{0}C, each well was supplemented with 11 µL of buffer A containing ALOD4 for a final concentration of ~1 µM ALOD4. After further incubation for 30 min at 37 ^{0}C, cells were harvested, and equal aliquots of cell lysates (10% of total) were subjected to immunoblot analysis for bound

OlyA and ALOD4. Medium A is a 1:1 mixture of Ham's F-12 and Dulbecco's modified Eagle's medium (DMEM) supplemented with 5% (v/v) FCS and 100 units/ml penicillin and 100 µg/ml streptomycin sulfate. **b,** Schematic figure illustrating the three pools of cholesterol in the PM of cells after treatment with increasing amounts of OlyA.

BIBILIOGRAPHY

1. Adams, P.D., et al., *PHENIX: a comprehensive Python-based system for macromolecular structure solution.* Acta Crystallogr D Biol Crystallogr, 2010. **66**(Pt 2): p. 213-21.
2. Anderluh, G. and P. Macek, *Cytolytic peptide and protein toxins from sea anemones (Anthozoa: Actiniaria).* Toxicon, 2002. **40**(2): p. 111-24.
3. Anderson, T.G. and H.M. McConnell, *Condensed complexes and the calorimetry of cholesterol-phospholipid bilayers.* Biophys J, 2001. **81**(5): p. 2774-85.
4. Baker, N.A., et al., *Electrostatics of nanosystems: application to microtubules and the ribosome.* Proc Natl Acad Sci U S A, 2001. **98**(18): p. 10037-41.
5. Barrett, P.J., et al., *The amyloid precursor protein has a flexible transmembrane domain and binds cholesterol.* Science, 2012. **336**(6085): p. 1168-71.
6. Beaudet, A.L., et al., *Acid lipase in cultured fibroblasts: cholesterol ester storage disease.* J Lab Clin Med, 1974. **84**(1): p. 54-61.
7. Berg JM, T.J., Stryer L., *Cholesterol Is Synthesized from Acetyl Coenzyme A in Three Stages*, in *Biochemistry*. 2002, W. H. Freeman: New York.
8. Bernheimer, A.W. and L.S. Avigad, *A cytolytic protein from the edible mushroom, Pleurotus ostreatus.* Biochim Biophys Acta, 1979. **585**(3): p. 451-61.
9. Bhat, H.B., et al., *Binding of a pleurotolysin ortholog from Pleurotus eryngii to sphingomyelin and cholesterol-rich membrane domains.* J Lipid Res, 2013. **54**(10): p. 2933-43.
10. Bittman, R., *Has nature designed the cholesterol side chain for optimal interaction with phospholipids?* Subcell Biochem, 1997. **28**: p. 145-71.
11. Bloch, K., *The biological synthesis of cholesterol.* Science, 1965. **150**(3692): p. 19-28.
12. Bloch, K.E., *Sterol structure and membrane function.* CRC Crit Rev Biochem, 1983. **14**(1): p. 47-92.
13. Borek, D., et al., *Diffraction data analysis in the presence of radiation damage.* Acta Crystallogr D Biol Crystallogr, 2010. **66**(Pt 4): p. 426-36.
14. Borek, D., Z. Dauter, and Z. Otwinowski, *Identification of patterns in diffraction intensities affected by radiation exposure.* J Synchrotron Radiat, 2013. **20**(Pt 1): p. 37-48.
15. Borek, D., W. Minor, and Z. Otwinowski, *Measurement errors and their consequences in protein crystallography.* Acta Crystallogr D Biol Crystallogr, 2003. **59**(Pt 11): p. 2031-8.
16. Bourdeau, R.W., et al., *Cellular functions and X-ray structure of anthrolysin O, a cholesterol-dependent cytolysin secreted by Bacillus anthracis.* J Biol Chem, 2009. **284**(21): p. 14645-56.
17. Brewer, K.D., et al., *Reluctance to membrane binding enables accessibility of the synaptobrevin SNARE motif for SNARE complex formation.* Proc Natl Acad Sci U S A, 2011. **108**(31): p. 12723-8.
18. Brown, M.S., et al., *Induction of 3-hydroxy-3-methylglutaryl coenzyme A reductase activity in human fibroblasts incubated with compactin (ML-236B), a competitive inhibitor of the reductase.* J Biol Chem, 1978. **253**(4): p. 1121-8.
19. Brown, M.S. and J.L. Goldstein, *Regulation of the activity of the low density lipoprotein receptor in human fibroblasts.* Cell, 1975. **6**(3): p. 307-16.
20. Brown, M.S. and J.L. Goldstein, *A receptor-mediated pathway for cholesterol homeostasis.* Science, 1986. **232**(4746): p. 34-47.
21. Brown, M.S. and J.L. Goldstein, *The SREBP pathway: regulation of cholesterol metabolism by proteolysis of a membrane-bound transcription factor.* Cell, 1997. **89**(3): p. 331-40.
22. Brown, M.S. and J.L. Goldstein, *Cholesterol feedback: from Schoenheimer's bottle to Scap's MELADL.* J Lipid Res, 2009. **50 Suppl**: p. S15-27.
23. Bucher, N.L., P. Overath, and F. Lynen, *beta-Hydroxy-beta-methyl-glutaryl coenzyme A reductase, cleavage and condensing enzymes in relation to cholesterol formation in rat liver.* Biochim Biophys Acta, 1960. **40**: p. 491-501.

24. Burke, J.A. and W.K. Schubert, *Deficient activity of hepatic acid lipase in cholesterol ester storage disease.* Science, 1972. **176**(4032): p. 309-10.
25. Chakrabarti, R.S., et al., *Variability of cholesterol accessibility in human red blood cells measured using a bacterial cholesterol-binding toxin.* Elife, 2017. **6**.
26. Chen, B., et al., *Protein Lipidation in Cell Signaling and Diseases: Function, Regulation, and Therapeutic Opportunities.* Cell Chem Biol, 2018. **25**(7): p. 817-831.
27. Chen, V.B., et al., *MolProbity: all-atom structure validation for macromolecular crystallography.* Acta Crystallogr D Biol Crystallogr, 2010. **66**(Pt 1): p. 12-21.
28. Cocklin, S., et al., *Real-time monitoring of the membrane-binding and insertion properties of the cholesterol-dependent cytolysin anthrolysin O from Bacillus anthracis.* J Mol Recognit, 2006. **19**(4): p. 354-62.
29. Cooper, R.A., *Influence of increased membrane cholesterol on membrane fluidity and cell function in human red blood cells.* J Supramol Struct, 1978. **8**(4): p. 413-30.
30. Cox, R.A. and M.R. Garcia-Palmieri, *Cholesterol, Triglycerides, and Associated Lipoproteins*, in *Clinical Methods: The History, Physical, and Laboratory Examinations*, rd, et al., Editors. 1990: Boston.
31. Das, A., et al., *Three pools of plasma membrane cholesterol and their relation to cholesterol homeostasis.* Elife, 2014. **3**.
32. Das, A., et al., *Use of mutant 125I-perfringolysin O to probe transport and organization of cholesterol in membranes of animal cells.* Proc Natl Acad Sci U S A, 2013. **110**(26): p. 10580-5.
33. Davies, J.P. and Y.A. Ioannou, *Topological analysis of Niemann-Pick C1 protein reveals that the membrane orientation of the putative sterol-sensing domain is identical to those of 3-hydroxy-3-methylglutaryl-CoA reductase and sterol regulatory element binding protein cleavage-activating protein.* J Biol Chem, 2000. **275**(32): p. 24367-74.
34. De Colibus, L., et al., *Structures of lysenin reveal a shared evolutionary origin for pore-forming proteins and its mode of sphingomyelin recognition.* Structure, 2012. **20**(9): p. 1498-507.
35. de, G. and L. Van Deenen, *Some lipid characteristics of red cell membranes of various animal species.* Biochim Biophys Acta, 1961. **49**: p. 286-96.
36. Delaglio, F., et al., *NMRPipe: a multidimensional spectral processing system based on UNIX pipes.* J Biomol NMR, 1995. **6**(3): p. 277-93.
37. Denisov, I.G., et al., *Directed self-assembly of monodisperse phospholipid bilayer Nanodiscs with controlled size.* J Am Chem Soc, 2004. **126**(11): p. 3477-87.
38. Emsley, P., et al., *Features and development of Coot.* Acta Crystallogr D Biol Crystallogr, 2010. **66**(Pt 4): p. 486-501.
39. Espenshade, P.J., W.P. Li, and D. Yabe, *Sterols block binding of COPII proteins to SCAP, thereby controlling SCAP sorting in ER.* Proc Natl Acad Sci U S A, 2002. **99**(18): p. 11694-9.
40. Evans, W.R. and C.J. Hendriksz, *Niemann-Pick type C disease - the tip of the iceberg? A review of neuropsychiatric presentation, diagnosis and treatment.* BJPsych Bull, 2017. **41**(2): p. 109-114.
41. Farrand, A.J., et al., *Only two amino acids are essential for cytolytic toxin recognition of cholesterol at the membrane surface.* Proc Natl Acad Sci U S A, 2010. **107**(9): p. 4341-6.
42. Fayer, M.D., *Dynamics of liquids, molecules, and proteins measured with ultrafast 2D IR vibrational echo chemical exchange spectroscopy.* Annu Rev Phys Chem, 2009. **60**: p. 21-38.
43. Feil, S.C., et al., *Structural studies of Streptococcus pyogenes streptolysin O provide insights into the early steps of membrane penetration.* J Mol Biol, 2014. **426**(4): p. 785-92.
44. Finean, J.B., *Phospholipid-cholesterol complex in the structure of myelin.* Experientia, 1953. **9**(1): p. 17-9.
45. Flanagan, J.J., et al., *Cholesterol exposure at the membrane surface is necessary and sufficient to trigger perfringolysin O binding.* Biochemistry, 2009. **48**(18): p. 3977-87.
46. Gaillard, J.L., P. Berche, and P. Sansonetti, *Transposon mutagenesis as a tool to study the role of hemolysin in the virulence of Listeria monocytogenes.* Infect Immun, 1986. **52**(1): p. 50-5.
47. Gatt, S. and E.L. Bierman, *Sphingomyelin suppresses the binding and utilization of low density lipoproteins by skin fibroblasts.* J Biol Chem, 1980. **255**(8): p. 3371-6.

48. Gay, A., D. Rye, and A. Radhakrishnan, *Switch-like responses of two cholesterol sensors do not require protein oligomerization in membranes.* Biophys J, 2015. **108**(6): p. 1459-1469.
49. Glomski, I.J., et al., *The Listeria monocytogenes hemolysin has an acidic pH optimum to compartmentalize activity and prevent damage to infected host cells.* J Cell Biol, 2002. **156**(6): p. 1029-38.
50. Gofman, J.W., et al., *The serum lipoprotein transport system in health, metabolic disorders, atherosclerosis and coronary heart disease.* J Clin Lipidol, 2007. **1**(2): p. 104-41.
51. Goldstein, J.L., S.K. Basu, and M.S. Brown, *Receptor-mediated endocytosis of low-density lipoprotein in cultured cells.* Methods Enzymol, 1983. **98**: p. 241-60.
52. Goldstein, J.L. and M.S. Brown, *Familial hypercholesterolemia: identification of a defect in the regulation of 3-hydroxy-3-methylglutaryl coenzyme A reductase activity associated with overproduction of cholesterol.* Proc Natl Acad Sci U S A, 1973. **70**(10): p. 2804-8.
53. Goldstein, J.L. and M.S. Brown, *The low-density lipoprotein pathway and its relation to atherosclerosis.* Annu Rev Biochem, 1977. **46**: p. 897-930.
54. Goldstein, J.L. and M.S. Brown, *Regulation of the mevalonate pathway.* Nature, 1990. **343**(6257): p. 425-30.
55. Goldstein, J.L., et al., *Role of lysosomal acid lipase in the metabolism of plasma low density lipoprotein. Observations in cultured fibroblasts from a patient with cholesteryl ester storage disease.* J Biol Chem, 1975. **250**(21): p. 8487-95.
56. Heberle, F.A., et al., *Fluorescence methods to detect phase boundaries in lipid bilayer mixtures.* Biochim Biophys Acta, 2005. **1746**(3): p. 186-92.
57. Heuck, A.P., et al., *Mechanism of membrane insertion of a multimeric beta-barrel protein: perfringolysin O creates a pore using ordered and coupled conformational changes.* Mol Cell, 2000. **6**(5): p. 1233-42.
58. Heuck, A.P., P.C. Moe, and B.B. Johnson, *The cholesterol-dependent cytolysin family of gram-positive bacterial toxins.* Subcell Biochem, 2010. **51**: p. 551-77.
59. Heuck, A.P., R.K. Tweten, and A.E. Johnson, *Assembly and topography of the prepore complex in cholesterol-dependent cytolysins.* J Biol Chem, 2003. **278**(33): p. 31218-25.
60. Hinz, H.J. and J.M. Sturtevant, *Calorimetric investigation of the influence of cholesterol on the transition properties of bilayers formed from synthetic L- -lecithins in aqueous suspension.* J Biol Chem, 1972. **247**(11): p. 3697-700.
61. Hua, X., et al., *Sterol resistance in CHO cells traced to point mutation in SREBP cleavage-activating protein.* Cell, 1996. **87**(3): p. 415-26.
62. Huang, J., J.T. Buboltz, and G.W. Feigenson, *Maximum solubility of cholesterol in phosphatidylcholine and phosphatidylethanolamine bilayers.* Biochim Biophys Acta, 1999. **1417**(1): p. 89-100.
63. Ikonen, E., *Mechanisms for cellular cholesterol transport: defects and human disease.* Physiol Rev, 2006. **86**(4): p. 1237-61.
64. Infante, R.E. and A. Radhakrishnan, *Continuous transport of a small fraction of plasma membrane cholesterol to endoplasmic reticulum regulates total cellular cholesterol.* Elife, 2017. **6**.
65. Johnson, B.A. and R.A. Blevins, *NMR View: A computer program for the visualization and analysis of NMR data.* J Biomol NMR, 1994. **4**(5): p. 603-14.
66. Johnson, B.B. and A.P. Heuck, *Perfringolysin O structure and mechanism of pore formation as a paradigm for cholesterol-dependent cytolysins.* Subcell Biochem, 2014. **80**: p. 63-81.
67. Jost, P., U.J. Brooks, and O.H. Griffith, *Fluidity of phospholipid bilayers and membranes after exposure to osmium tetroxide and gluteraldehyde.* J Mol Biol, 1973. **76**(2): p. 313-8.
68. Koster, S., et al., *Crystallization and X-ray crystallographic analysis of the cholesterol-dependent cytolysin listeriolysin O from Listeria monocytogenes.* Acta Crystallogr Sect F Struct Biol Cryst Commun, 2013. **69**(Pt 11): p. 1212-5.
69. Kwon, H.J., et al., *Structure of N-terminal domain of NPC1 reveals distinct subdomains for binding and transfer of cholesterol.* Cell, 2009. **137**(7): p. 1213-24.

70. Ladokhin, A.S., *Measuring membrane penetration with depth-dependent fluorescence quenching: distribution analysis is coming of age.* Biochim Biophys Acta, 2014. **1838**(9): p. 2289-95.
71. Lange, Y. and B.V. Ramos, *Analysis of the distribution of cholesterol in the intact cell.* J Biol Chem, 1983. **258**(24): p. 15130-4.
72. Lange, Y. and T.L. Steck, *Quantitation of the pool of cholesterol associated with acyl-CoA:cholesterol acyltransferase in human fibroblasts.* J Biol Chem, 1997. **272**(20): p. 13103-8.
73. Lange, Y., et al., *Plasma membranes contain half the phospholipid and 90% of the cholesterol and sphingomyelin in cultured human fibroblasts.* J Biol Chem, 1989. **264**(7): p. 3786-93.
74. Lange, Y., J. Ye, and J. Chin, *The fate of cholesterol exiting lysosomes.* J Biol Chem, 1997. **272**(27): p. 17018-22.
75. Le Gall, S., A. Neuhof, and T. Rapoport, *The endoplasmic reticulum membrane is permeable to small molecules.* Mol Biol Cell, 2004. **15**(2): p. 447-55.
76. Liscum, L., et al., *Regulation of 3-hydroxy-3-methylglutaryl coenzyme A reductase and its mRNA in rat liver as studied with a monoclonal antibody and a cDNA probe.* J Biol Chem, 1983. **258**(13): p. 8450-5.
77. Lu, Z., et al., *Bicelles at low concentrations.* Mol Pharm, 2012. **9**(4): p. 752-61.
78. Lukoyanova, N., et al., *Conformational changes during pore formation by the perforin-related protein pleurotolysin.* PLoS Biol, 2015. **13**(2): p. e1002049.
79. Makino, A., et al., *A novel sphingomyelin/cholesterol domain-specific probe reveals the dynamics of the membrane domains during virus release and in Niemann-Pick type C.* FASEB J, 2017. **31**(4): p. 1301-1322.
80. Mancheno, J.M., et al., *Crystal and electron microscopy structures of sticholysin II actinoporin reveal insights into the mechanism of membrane pore formation.* Structure, 2003. **11**(11): p. 1319-28.
81. Mattjus, P. and J.P. Slotte, *Does cholesterol discriminate between sphingomyelin and phosphatidylcholine in mixed monolayers containing both phospholipids?* Chem Phys Lipids, 1996. **81**(1): p. 69-80.
82. McConnell, H.M. and A. Radhakrishnan, *Condensed complexes of cholesterol and phospholipids.* Biochim Biophys Acta, 2003. **1610**(2): p. 159-73.
83. McCoy, A.J., et al., *Phaser crystallographic software.* J Appl Crystallogr, 2007. **40**(Pt 4): p. 658-674.
84. McMullen, T.P., R.N. Lewis, and R.N. McElhaney, *Differential scanning calorimetric study of the effect of cholesterol on the thermotropic phase behavior of a homologous series of linear saturated phosphatidylcholines.* Biochemistry, 1993. **32**(2): p. 516-22.
85. Mengaud, J., et al., *Expression in Escherichia coli and sequence analysis of the listeriolysin O determinant of Listeria monocytogenes.* Infect Immun, 1988. **56**(4): p. 766-72.
86. Miao, L., et al., *From lanosterol to cholesterol: structural evolution and differential effects on lipid bilayers.* Biophys J, 2002. **82**(3): p. 1429-44.
87. Minor, W., et al., *HKL-3000: the integration of data reduction and structure solution--from diffraction images to an initial model in minutes.* Acta Crystallogr D Biol Crystallogr, 2006. **62**(Pt 8): p. 859-66.
88. MuhandiramD.R.KayL.E., *Gradient-Enhanced Triple-Resonance Three-Dimensional NMR Experiments with Improved Sensitivity.* Journal of Magnetic Resonance, Series B, 1994. **103**.
89. Naureckiene, S., et al., *Identification of HE1 as the second gene of Niemann-Pick C disease.* Science, 2000. **290**(5500): p. 2298-301.
90. Neufeld, E.B., et al., *Intracellular trafficking of cholesterol monitored with a cyclodextrin.* J Biol Chem, 1996. **271**(35): p. 21604-13.
91. Nohturfft, A., M.S. Brown, and J.L. Goldstein, *Topology of SREBP cleavage-activating protein, a polytopic membrane protein with a sterol-sensing domain.* J Biol Chem, 1998. **273**(27): p. 17243-50.
92. Otwinowski, Z., et al., *Multiparametric scaling of diffraction intensities.* Acta Crystallogr A, 2003. **59**(Pt 3): p. 228-34.

93. Payne, A.H. and D.B. Hales, *Overview of steroidogenic enzymes in the pathway from cholesterol to active steroid hormones.* Endocr Rev, 2004. **25**(6): p. 947-70.
94. Pervushin, K., et al., *Attenuated T2 relaxation by mutual cancellation of dipole-dipole coupling and chemical shift anisotropy indicates an avenue to NMR structures of very large biological macromolecules in solution.* Proc Natl Acad Sci U S A, 1997. **94**(23): p. 12366-71.
95. Peters, C., et al., *The cholesterol membrane anchor of the Hedgehog protein confers stable membrane association to lipid-modified proteins.* Proc Natl Acad Sci U S A, 2004. **101**(23): p. 8531-6.
96. Phillips, M.C., W.J. Johnson, and G.H. Rothblat, *Mechanisms and consequences of cellular cholesterol exchange and transfer.* Biochim Biophys Acta, 1987. **906**(2): p. 223-76.
97. Polekhina, G., et al., *Insights into the action of the superfamily of cholesterol-dependent cytolysins from studies of intermedilysin.* Proc Natl Acad Sci U S A, 2005. **102**(3): p. 600-5.
98. Prosser, R.S., et al., *Current applications of bicelles in NMR studies of membrane-associated amphiphiles and proteins.* Biochemistry, 2006. **45**(28): p. 8453-65.
99. Puthenveetil, R., K. Nguyen, and O. Vinogradova, *Nanodiscs and Solution NMR: preparation, application and challenges.* Nanotechnol Rev, 2017. **6**(1): p. 111-126.
100. Radhakrishnan, A., et al., *Switch-like control of SREBP-2 transport triggered by small changes in ER cholesterol: a delicate balance.* Cell Metab, 2008. **8**(6): p. 512-21.
101. Radhakrishnan, A., et al., *Sterol-regulated transport of SREBPs from endoplasmic reticulum to Golgi: oxysterols block transport by binding to Insig.* Proc Natl Acad Sci U S A, 2007. **104**(16): p. 6511-8.
102. Radhakrishnan, A. and H.M. McConnell, *Thermal Dissociation of Condensed Complexes of Cholesterol and Phospholipid.* The Journal of Physical Chemistry B, 2002. **106**(18): p. 4755-4762.
103. Radhakrishnan, A., et al., *Direct binding of cholesterol to the purified membrane region of SCAP: mechanism for a sterol-sensing domain.* Mol Cell, 2004. **15**(2): p. 259-68.
104. Raffy, S. and J. Teissie, *Control of lipid membrane stability by cholesterol content.* Biophys J, 1999. **76**(4): p. 2072-80.
105. Ramachandran, R., et al., *Structural insights into the membrane-anchoring mechanism of a cholesterol-dependent cytolysin.* Nat Struct Biol, 2002. **9**(11): p. 823-7.
106. Ramachandran, R., R.K. Tweten, and A.E. Johnson, *The domains of a cholesterol-dependent cytolysin undergo a major FRET-detected rearrangement during pore formation.* Proc Natl Acad Sci U S A, 2005. **102**(20): p. 7139-44.
107. Riobo, N.A., *Cholesterol and its derivatives in Sonic Hedgehog signaling and cancer.* Curr Opin Pharmacol, 2012. **12**(6): p. 736-41.
108. Rossjohn, J., et al., *Structure of a cholesterol-binding, thiol-activated cytolysin and a model of its membrane form.* Cell, 1997. **89**(5): p. 685-92.
109. Roux, K.J., D.I. Kim, and B. Burke, *BioID: a screen for protein-protein interactions.* Curr Protoc Protein Sci, 2013. **74**: p. Unit 19 23.
110. Russell, D.W., *Fifty years of advances in bile acid synthesis and metabolism.* J Lipid Res, 2009. **50** Suppl: p. S120-5.
111. Sakai, J., et al., *Sterol-regulated release of SREBP-2 from cell membranes requires two sequential cleavages, one within a transmembrane segment.* Cell, 1996. **85**(7): p. 1037-46.
112. Sakai, J., et al., *Identification of complexes between the COOH-terminal domains of sterol regulatory element-binding proteins (SREBPs) and SREBP cleavage-activating protein.* J Biol Chem, 1997. **272**(32): p. 20213-21.
113. Sanders, C.R., 2nd and G.C. Landis, *Reconstitution of membrane proteins into lipid-rich bilayered mixed micelles for NMR studies.* Biochemistry, 1995. **34**(12): p. 4030-40.
114. Scheek, S., M.S. Brown, and J.L. Goldstein, *Sphingomyelin depletion in cultured cells blocks proteolysis of sterol regulatory element binding proteins at site 1.* Proc Natl Acad Sci U S A, 1997. **94**(21): p. 11179-83.
115. Schoenheimer, R. and F. Breusch, *SYNTHESIS AND DESTRUCTION OF CHOLESTEROL IN THE ORGANISM.* 1933. **103**(2): p. 439-448.

116. Schrank, E., G.E. Wagner, and K. Zangger, *Solution NMR studies on the orientation of membrane-bound peptides and proteins by paramagnetic probes.* Molecules, 2013. **18**(7): p. 7407-35.
117. Sezgin, E., et al., *The mystery of membrane organization: composition, regulation and roles of lipid rafts.* Nat Rev Mol Cell Biol, 2017. **18**(6): p. 361-374.
118. Shannon, J.G., et al., *Characterization of anthrolysin O, the Bacillus anthracis cholesterol-dependent cytolysin.* Infect Immun, 2003. **71**(6): p. 3183-9.
119. Shepard, L.A., et al., *Identification of a membrane-spanning domain of the thiol-activated pore-forming toxin Clostridium perfringens perfringolysin O: an alpha-helical to beta-sheet transition identified by fluorescence spectroscopy.* Biochemistry, 1998. **37**(41): p. 14563-74.
120. Shepard, L.A., et al., *The mechanism of pore assembly for a cholesterol-dependent cytolysin: formation of a large prepore complex precedes the insertion of the transmembrane beta-hairpins.* Biochemistry, 2000. **39**(33): p. 10284-93.
121. Simons, K., *Cell membranes: A subjective perspective.* Biochim Biophys Acta, 2016. **1858**(10): p. 2569-2572.
122. Simons, K. and E. Ikonen, *Functional rafts in cell membranes.* Nature, 1997. **387**(6633): p. 569-72.
123. Simons, K. and E. Ikonen, *How cells handle cholesterol.* Science, 2000. **290**(5497): p. 1721-6.
124. Skocaj, M., et al., *Tracking cholesterol/sphingomyelin-rich membrane domains with the ostreolysin A-mCherry protein.* PLoS One, 2014. **9**(3): p. e92783.
125. Slotte, J.P., *Enzyme-catalyzed oxidation of cholesterol in mixed phospholipid monolayers reveals the stoichiometry at which free cholesterol clusters disappear.* Biochemistry, 1992. **31**(24): p. 5472-7.
126. Slotte, J.P., *The importance of hydrogen bonding in sphingomyelin's membrane interactions with co-lipids.* Biochim Biophys Acta, 2016. **1858**(2): p. 304-10.
127. Slotte, J.P. and E.L. Bierman, *Depletion of plasma-membrane sphingomyelin rapidly alters the distribution of cholesterol between plasma membranes and intracellular cholesterol pools in cultured fibroblasts.* Biochem J, 1988. **250**(3): p. 653-8.
128. Slotte, J.P., et al., *Rapid turn-over of plasma membrane sphingomyelin and cholesterol in baby hamster kidney cells after exposure to sphingomyelinase.* Biochim Biophys Acta, 1990. **1030**(2): p. 251-7.
129. Sokol, J., et al., *Type C Niemann-Pick disease. Lysosomal accumulation and defective intracellular mobilization of low density lipoprotein cholesterol.* J Biol Chem, 1988. **263**(7): p. 3411-7.
130. Sokolov, A. and A. Radhakrishnan, *Accessibility of cholesterol in endoplasmic reticulum membranes and activation of SREBP-2 switch abruptly at a common cholesterol threshold.* J Biol Chem, 2010. **285**(38): p. 29480-90.
131. Song, Y., A.K. Kenworthy, and C.R. Sanders, *Cholesterol as a co-solvent and a ligand for membrane proteins.* Protein Sci, 2014. **23**(1): p. 1-22.
132. Sun, L.P., et al., *Insig required for sterol-mediated inhibition of Scap/SREBP binding to COPII proteins in vitro.* J Biol Chem, 2005. **280**(28): p. 26483-90.
133. Sun, L.P., et al., *Sterol-regulated transport of SREBPs from endoplasmic reticulum to Golgi: Insig renders sorting signal in Scap inaccessible to COPII proteins.* Proc Natl Acad Sci U S A, 2007. **104**(16): p. 6519-26.
134. Tilney, L.G. and D.A. Portnoy, *Actin filaments and the growth, movement, and spread of the intracellular bacterial parasite, Listeria monocytogenes.* J Cell Biol, 1989. **109**(4 Pt 1): p. 1597-608.
135. Tomita, T., et al., *Pleurotolysin, a novel sphingomyelin-specific two-component cytolysin from the edible mushroom Pleurotus ostreatus, assembles into a transmembrane pore complex.* J Biol Chem, 2004. **279**(26): p. 26975-82.
136. Tweten, R.K., *Nucleotide sequence of the gene for perfringolysin O (theta-toxin) from Clostridium perfringens: significant homology with the genes for streptolysin O and pneumolysin.* Infect Immun, 1988. **56**(12): p. 3235-40.

137. Tweten, R.K., *Cholesterol-dependent cytolysins, a family of versatile pore-forming toxins.* Infect Immun, 2005. **73**(10): p. 6199-209.
138. Valcarcel, C.A., et al., *Effects of lipid composition on membrane permeabilization by sticholysin I and II, two cytolysins of the sea anemone Stichodactyla helianthus.* Biophys J, 2001. **80**(6): p. 2761-74.
139. Wang, M.L., et al., *Identification of surface residues on Niemann-Pick C2 essential for hydrophobic handoff of cholesterol to NPC1 in lysosomes.* Cell Metab, 2010. **12**(2): p. 166-73.
140. Wang, X., et al., *Nuclear protein that binds sterol regulatory element of low density lipoprotein receptor promoter. II. Purification and characterization.* J Biol Chem, 1993. **268**(19): p. 14497-504.
141. Wang, X., et al., *SREBP-1, a membrane-bound transcription factor released by sterol-regulated proteolysis.* Cell, 1994. **77**(1): p. 53-62.
142. Wishart, D.S. and B.D. Sykes, *The 13C chemical-shift index: a simple method for the identification of protein secondary structure using 13C chemical-shift data.* J Biomol NMR, 1994. **4**(2): p. 171-80.
143. Xu, L., et al., *Crystal structure of cytotoxin protein suilysin from Streptococcus suis.* Protein Cell, 2010. **1**(1): p. 96-105.
144. Xu, X.X. and I. Tabas, *Lipoproteins activate acyl-coenzyme A:cholesterol acyltransferase in macrophages only after cellular cholesterol pools are expanded to a critical threshold level.* J Biol Chem, 1991. **266**(26): p. 17040-8.
145. Yamaji, A., et al., *Lysenin, a novel sphingomyelin-specific binding protein.* J Biol Chem, 1998. **273**(9): p. 5300-6.
146. Yang, T., et al., *Crucial step in cholesterol homeostasis: sterols promote binding of SCAP to INSIG-1, a membrane protein that facilitates retention of SREBPs in ER.* Cell, 2002. **110**(4): p. 489-500.
147. Yokoyama, C., et al., *SREBP-1, a basic-helix-loop-helix-leucine zipper protein that controls transcription of the low density lipoprotein receptor gene.* Cell, 1993. **75**(1): p. 187-97.